OAK RIDGE NATIONAL LABORATORY LIBRARY
3 4456 0004624 2

ORNL/TM-9655

OAK RIDGE NATIONAL LABORATORY

MARTIN MARIETTA

# Kinematics and Duty Cycles of the SM-229 Force-Reflecting Servomanipulator

R. S. Stoughton

OAK RIDGE NATIONAL LABORATORY
CENTRAL RESEARCH LIBRARY
CIRCULATION SECTION
4500N ROOM 175
LIBRARY LOAN COPY
DO NOT TRANSFER TO ANOTHER PERSON
If you wish someone else to see this report, send in name with report and the library will arrange a loan.

OPERATED BY
MARTIN MARIETTA ENERGY SYSTEMS, INC.
FOR THE UNITED STATES
DEPARTMENT OF ENERGY

Printed in the United States of America. Available from
National Technical Information Service
U.S. Department of Commerce
5285 Port Royal Road, Springfield, Virginia 22161
NTIS price codes—Printed Copy: [illegible] Microfiche: A01

[illegible]

ORNL/TM-9655
Dist. Category UC-86

Consolidated Fuel Reprocessing Program

# KINEMATICS AND DUTY CYCLES OF THE SM-229 FORCE-REFLECTING SERVOMANIPULATOR*

R. S. Stoughton†
Instrumentation and Controls Division

*Thesis presented for the Master of Science Degree, University of Tennessee, Knoxville, 1985.

†The University of Tennessee, Knoxville.

Date Published: February 1986

Prepared by the
OAK RIDGE NATIONAL LABORATORY
Oak Ridge, Tennessee 37831
operated by
MARTIN MARIETTA ENERGY SYSTEMS, INC.
for the
U.S. DEPARTMENT OF ENERGY
under Contract No. DE-AC05-84OR21400

OAK RIDGE NATIONAL LABORATORY LIBRARY
3 4456 0004624 2

TABLE OF CONTENTS


| | PAGE |
|---|---|
| LIST OF FIGURES | v |
| LIST OF TABLES | vi |
| ABSTRACT | vii |
| 1. INTRODUCTION | 1 |
| 1.1 Background | 5 |
| 1.1.1 Remote-Handling Systems | 5 |
| 1.1.2 Servomanipulators | 6 |
| 1.1.3 Standard Design Practices | 7 |
| 1.2 Purpose and Approach | 8 |
| 2. EXPERIMENTAL SYSTEM DESCRIPTION | 10 |
| 2.1 The Remote Systems Development Facility (RSDF) | 10 |
| 2.1.1 The Remote Cell | 10 |
| 2.1.2 The Control Station | 11 |
| 2.2 The TOS Model SM-229 Servomanipulator | 13 |
| 2.2.1 Master-Slave Motions | 14 |
| 2.2.2 Gear Reductions | 17 |
| 2.2.3 Actuators | 17 |
| 2.2.4 Control System | 17 |
| 2.2.5 Tuning the Controls | 19 |
| 2.3 Experimental Tasks | 20 |
| 2.3.1 The Instrument Package Task | 20 |
| 2.3.2 The Motor Mount Task | 21 |
| 2.3.3 The Tubing Service Jumper Task | 21 |
| 2.3.4 The 30-in. Flange Task | 25 |
| 2.3.5 The 6-in. Flange Task | 25 |
| 2.4 Data Acquisition | 25 |
| 2.4.1 Hardware | 26 |
| 2.4.2 Software | 27 |
| 2.4.3 Procedures | 29 |
| 2.5 Data Reduction | 30 |
| 3. DUTY CYCLE EXPERIMENTAL RESULTS | 34 |
| 3.1 Preliminary Observations | 34 |
| 3.2 Kinematic Ranges | 37 |
| 3.2.1 Individual Joints | 37 |
| 3.2.2 Wrist Positions and Orientations | 44 |
| 3.2.3 Mean Positions | 50 |
| 3.3 Motor Currents and Energy | 51 |
| 3.4 Joint Velocities | 57 |
| 3.5 Mechanical Power and Energy | 61 |
| 3.6 Position-Torque Relationships | 70 |

TABLE OF CONTENTS (continued)

PAGE

4. APPLICATIONS TO MANIPULATOR DESIGN . . . . . 79

4.1 Motion Ranges . . . . . 79
4.2 Gear Reductions . . . . . 81
4.3 Actuator Sizings . . . . . 84
4.4 Differential Drive Load Sharing . . . . . 86
4.5 Additional Applications . . . . . 88

CONCLUSIONS . . . . . 89

REFERENCES . . . . . 90

APPENDIX A. UNCERTAINTY ANALYSIS . . . . . 91

APPENDIX B. CALIBRATIONS AND TESTS . . . . . 103

APPENDIX C. SELECTION OF VELOCITY ALGORITHM . . . . . 115

APPENDIX D. KINEMATICS . . . . . 121

LIST OF FIGURES


| FIGURE | | PAGE |
|---|---|---|
| 1. | Slave manipulator arms and remote cell | 2 |
| 2. | Manipulator coordinate frames and modeling parameters | 3 |
| 3. | Operator control station | 12 |
| 4. | Instrument package | 22 |
| 5. | Motor mount and 30-inch flange | 23 |
| 6. | Tubing service jumper | 24 |
| 7. | Range of shoulder pitch position usage | 38 |
| 8. | Range of shoulder roll position usage | 39 |
| 9. | Range of elbow pitch position usage | 40 |
| 10. | Range of elbow roll position usage | 41 |
| 11. | Range of wrist pitch position usage | 42 |
| 12. | Range of wrist roll position usage | 43 |
| 13. | Wrist position grid--top view | 46 |
| 14. | Wrist position grid--right side view | 47 |
| 15. | Wrist position grid--back view | 48 |
| 16. | Wrist orientation grid | 49 |
| 17. | Current histogram for upper shoulder motor | 52 |
| 18. | Current histogram for lower shoulder motor | 52 |
| 19. | Current histogram for elbow pitch motor | 53 |
| 20. | Current histogram for elbow roll (yaw) motor | 53 |
| 21. | Current histogram for left wrist motor | 54 |
| 22. | Current histogram for right wrist motor | 54 |
| 23. | Current histogram for tong motor | 55 |
| 24. | Velocity histogram for shoulder pitch | 58 |
| 25. | Velocity histogram for shoulder roll | 58 |
| 26. | Velocity histogram for elbow pitch | 59 |
| 27. | Velocity histogram for elbow roll | 59 |
| 28. | Velocity histogram for wrist pitch | 60 |
| 29. | Velocity histogram for wrist roll | 60 |
| 30. | Ideal mechanical power grid | 62 |
| 31. | Mechanical power grid for shoulder pitch | 63 |
| 32. | Mechanical power grid for shoulder roll | 64 |
| 33. | Mechanical power grid for elbow pitch | 65 |
| 34. | Mechanical power grid for elbow roll | 66 |
| 35. | Mechanical power grid for wrist pitch | 67 |
| 36. | Mechanical power grid for wrist roll | 68 |
| 37. | Position-torque grid for shoulder pitch | 72 |
| 38. | Position-torque grid for shoulder roll | 73 |
| 39. | Position-torque grid for elbow pitch | 74 |
| 40. | Position-torque grid for elbow roll | 75 |
| 41. | Position-torque grid for wrist pitch | 76 |
| 42. | Position-Torque grid for wrist roll | 77 |

LIST OF TABLES


| TABLE | | PAGE |
|---|---|---|
| 1. | Weights and dimensions of Model SM-229 | 14 |
| 2. | Dynamic characteristics of Model SM-229 | 15 |
| 3. | Approximate gear reductions | 18 |
| 4. | Motor specifications | 19 |
| 5. | Static maximum currents per motor, amperes | 37 |
| 6. | DOF position end ratios and unused ranges | 45 |
| 7. | Mean positions | 51 |
| 8. | Average energy and peak current per motor per task | 56 |
| 9. | Average and maximum continuous time above 60% current | 57 |
| 10. | Average peak velocities and accelerations per task | 61 |
| 11. | Average mechanical energy and peak power per task | 71 |
| 12. | Improved motion ranges | 81 |
| 13. | Improved gear reductions | 83 |
| 14. | Joint torque distribution in the mean configuration | 84 |
| 15. | Improved actuator sizes | 87 |
| A.1. | Approximate DOF gearing backlash | 95 |
| A.2. | Probable position uncertainties | 96 |
| A.3. | Probable velocity uncertainties | 98 |
| A.4. | Torque calibration uncertainty parameters | 100 |
| A.5. | Mechanical energy uncertainty | 102 |
| B.1. | Slave arm shoulder position calibration data (January 5, 1984) | 106 |
| B.2. | Slave arm elbow position calibration data (January 5, 1984) | 107 |
| B.3. | Slave arm wrist calibration data (January 5, 1984) | 108 |
| B.4. | Joint torque calibration | 109 |
| B.5. | Applied torque calibration data | 111 |
| B.6. | Motor resistance measurement parameters | 112 |
| C.1. | Velocity uncertainty and truncation error | 120 |
| D.1. | Transformation parameters | 124 |

ABSTRACT

This report describes the first known experimental study of servomanipulator duty cycles to appear in the literature. The servomanipulator used was TeleOperator Systems Model SM-229. The experimental approach used was to record the joint positions and motor currents of the right slave arm at a rate of 10 Hz over about 50 h of typical remote manipulation operations. The results are presented as position usage patterns in joint and real-world coordinates, time-use histograms of joint velocities and motor currents, and three-dimensional mechanical power histograms for each joint. All results are presented in dimensionless form, scaled to the design ranges of the manipulator and the total operation time recorded. Applications of this study include improvements in kinematic ranges, gear reductions, motor sizings, drive configurations, and stress relief. Included in appendices are an uncertainty analysis, calibration procedures, and analysis of the kinematics of the manipulator.

# 1. INTRODUCTION

Servomanipulators are used for remote maintenance and repair work in hazardous and/or inaccessible environments such as high radiation, subsea, or outer space. These systems usually consist of similar master and slave manipulators. Each manipulator has two multidegree of freedom arms with end effectors. The operator moves the master arms and the slave arms follow the motions of the master in real time. Remote closed circuit television (CCTV) cameras send pictures of the working environment back to television screens for the operator to view. The slave arms of the servomanipulator used in this study are shown in Fig. 1.

Most modern servomanipulators have arms that resemble human arms in their configuration and kinematic range. Typically, each arm has six degrees of freedom (DOFs) to allow arbitrary positioning and orientation of the end effector. Manipulators with more DOFs can have control problems as the manipulator configuration often becomes degenerate (two or more DOFs produce the same motion of the end effector). The six DOFs of the servomanipulator in Fig. 1 are shown schematically in Fig. 2 as rotations about the six z axes.

The humanlike servomanipulator arms are mounted on a base ("body") in one of two basic configurations: the "elbows-up" and "elbows-down" (anthropormorphic) stances. Figures 1 and 2 show the elbows-up stance, in which the reference position of the manipulator has the upper arm extending horizontally outward, the lower arm dropping vertically downward, and the end effector extending horizontally outward. The anthopormorphic stance is that of the human arm. The upper arm drops vertically, and the lower arm and end effector axes are aligned, extending forward horizontally.

Another stance, which has been used in a Japanese design,[1] lies between the above mentioned stances and has been referred to as "elbows sideways."

There are two advantages of the elbows-up stance. The master arm does not interfere with the movements of the operator's arm as it can in the elbows-down stance. Also, in the reference position, the wrist

ORNL Photo 2058-84

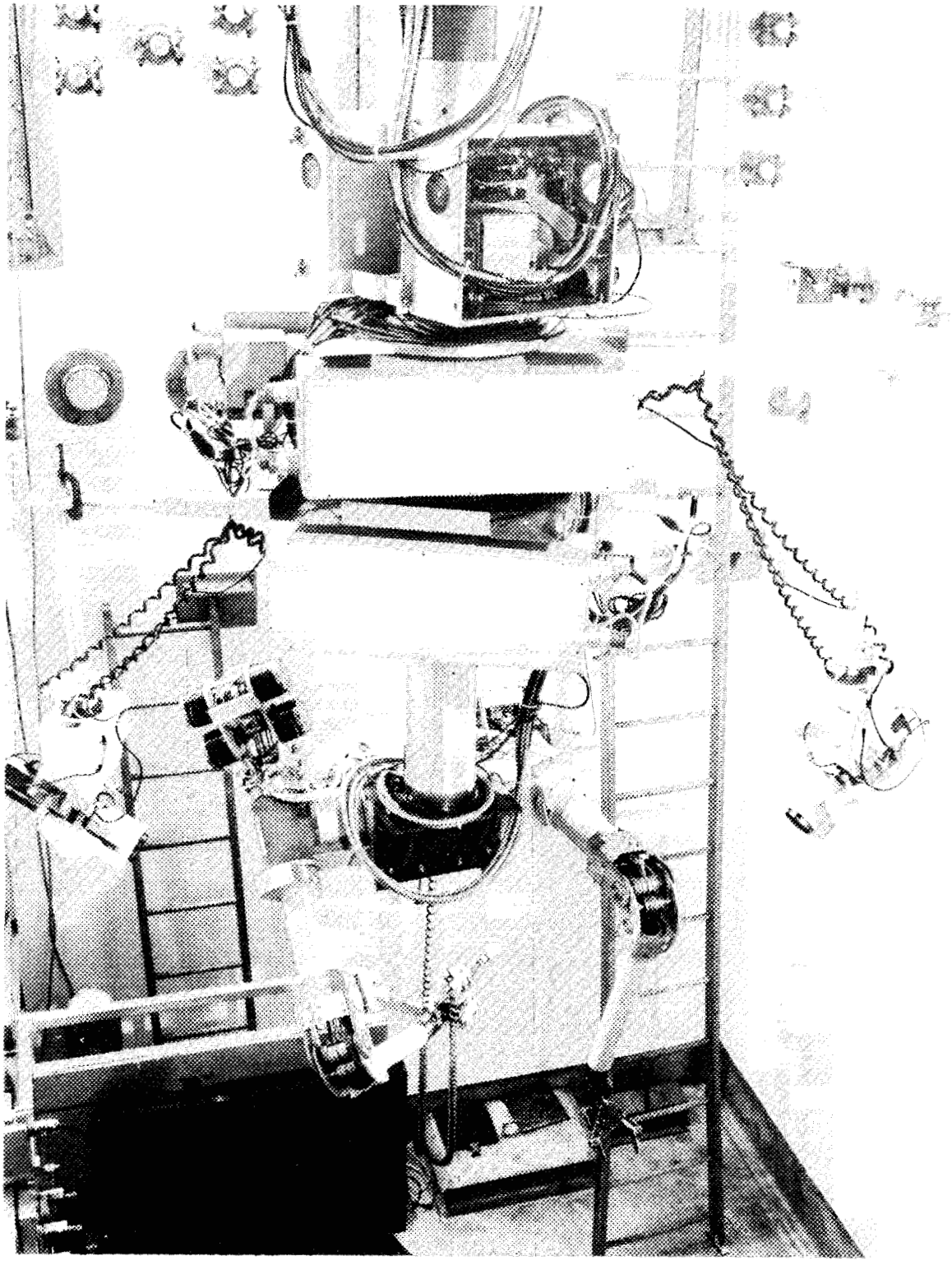

Fig. 1. Slave manipulator arms and remote cell.

ORNL-DWG 83-10771

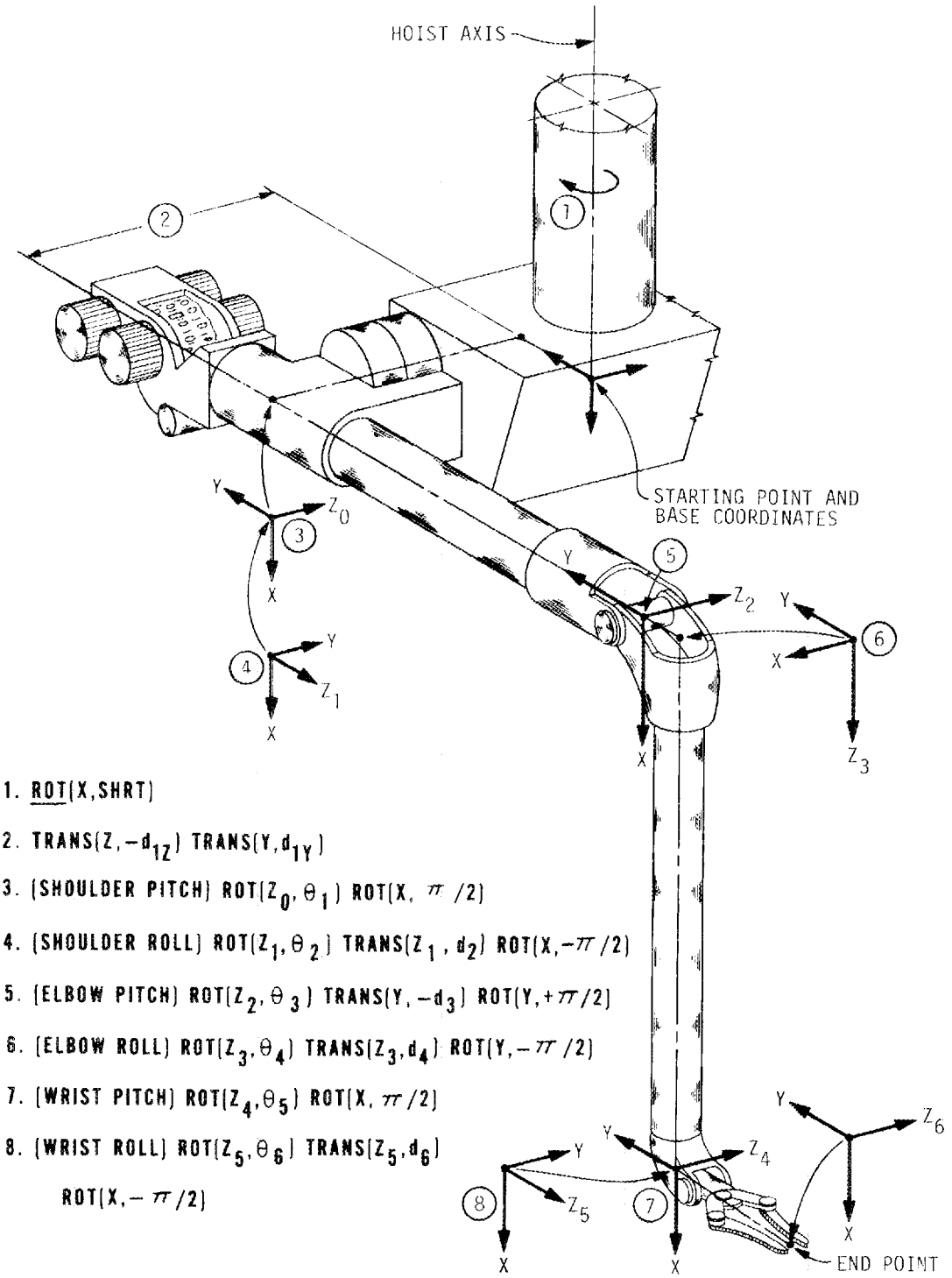


Fig. 2. Manipulator coordinate frames and modeling parameters.

yaw motion can be achieved with an elbow roll motion. This allows two independent motions to be placed in each mechanical joint (shoulder, elbow, and wrist) rather than having all three wrist orientation DOFs in the wrist. This simplifies the design because the yaw drive need not be transferred as far down the arm.

The TeleOperator Systems (TOS) Model SM-229* (shown in Fig. 1) is a force-reflecting servomanipulator using the elbows-up stance. Forces in the slave manipulator (such as pushing against a wall or inertia of a load) are reflected back to the operator at the master, creating a better sense of operator presence in the working environment. The slave/master force ratio is logarithmic, automatically adjusting from 1:1 for light loads to 2.2:1 for heavy loads (above 10 $lb_f$).

The SM-229 manipulator system used in this study was installed at the Remote Systems Development Facility (RSDF) located at Oak Ridge National Laboratory (ORNL). This facility has been set up for the express purpose of developing and testing remote repair and maintenance systems in an actual working environment. The experimental cell contains the equipment for a variety of experimental tasks considered representative of those anticipated in the Consolidated Fuel Reprocessing Facility under development at ORNL. These experimental tasks have been continually performed and upgraded for many purposes, including special tooling design and human factors studies. This thesis presents an experimental analysis of the duty cycles of the SM-229 manipulator system at RSDF. Applications of the results to manipulator design are discussed. Kinematic relationships between real world and manipulator joint coordinates are presented in an appendix.

It should be noted that modern remote-handling systems include many subsystems such as the support or transporter system, and the viewing and communications systems. This report will be restricted to the manipulator system.

---

*Designed and built by TeleOperator Systems Corp., Bohemia, N.Y.

## 1.1 BACKGROUND

### 1.1.1 Remote-Handling Systems

The rise of nuclear energy in the 1940s spawned a technology dedicated to removing the need for humans to enter hazardous environments to perform manipulations. The design objective of this remote-handling technology has been to project the control motions of the human operator into the remote environment in such a way that as many types of manipulations can be performed remotely as could be done directly with the hands and power tools. While this objective has never been completely realized, modern remote-handling systems are capable of performing many tasks more effectively than could be performed directly. A famous example of this is the space shuttle's remote manipulator system used to deploy and retrieve satellites.

The early work in remote-handling systems was led by a group at Argonne National Laboratory (ANL) under the direction of Ray Goertz. This group, formed in 1947, has developed several generations of remote handling systems.[2]

The first manipulators developed were velocity-controlled unilateral (nonforce-reflecting) manipulators. These consisted of a mechanical arm with seven (or more) independent motions (including tong grip motion), a pair of tongs for gripping objects, a support system, and a control box. Electric motors were used to actuate all motions. The motor speeds were controlled by switches or joysticks moved by a human operator.

The primary disadvantages of this type of manipulator were that the operator had no way of sensing the forces that the manipulator was applying in the remote environment, and that only one motion of the arm could be readily moved at a time. Modern improvements in sensory capabilities and control technology have allowed unilateral manipulators to find useful applications (such as the space shuttle remote manipulator system), but, at that time, the lack of force control was a major limitation.

The next manipulator system developed by ANL was a master-slave type of manipulator consisting of a slave arm (working arm) for performing the work in the hostile environment and a similarly shaped

master arm (control arm) controlled by the human operator. Each motion of the master and slave arms was mechanically connected by metallic bands so that the slave arm followed the motions of the master arm, and the load forces in the slave arm were reflected back to the master arm and handle. Thus the operator had an excellent feel for the forces being generated by the slave manipulator, and movement of the manipulator was easily achieved.

The mechanical master-slave manipulator was very successful. Many such manipulators are still used in commercial operation today. However, there are disadvantages to this type of manipulator. Since the master and slave are directly connected, the operator is required to remain in close proximity to the working environment, and the volumetric coverage of the slave arms is limited because the system must be mounted on a fixed base. The ratio of slave to master forces is fixed at about 1:1, so the slave can apply forces only within the range of human capabilities.

### 1.1.2 Servomanipulators

Servomanipulators were developed to overcome the limitations of mechanical master-slave manipulators. These systems consist again of similar master and slave manipulators, but the connections between the motions of the master and slave are electrical rather than mechanical. This results in several advantages. First and foremost, the slave manipulator can be mounted on a mobile transporter system, resulting in a greatly increased volumetric coverage. Thus, while the unit cost of an electric servomanipulator system is greater than that of a similar mechanical system, the decreased number of manipulators needed in a large-volume facility may well result in a lower total cost for the electric servomanipulators.

Another important advantage of the electric servomanipulator is that it is quite easy to change the force feedback ratio from slave to master. Thus, the master manipulator can be designed to operate with a range of forces that is both useful in terms of force sensing and comfortable in terms of ease of operation to the human operator, while the slave manipulator can be designed to operate with a force range

appropriate to the tasks it will perform.[3] The master and slave manipulators need not be located in close proximity to one another. This has resulted in additional applications for servomanipulators including undersea and outer space.

### 1.1.3 Standard Design Practices

Servomanipulators can be driven with electric motors or hydraulic actuators. Hydraulics are most favorably applied in underwater or extremely heavy-duty applications. Electromechanical drive systems offer 1% of peak load force sensitivity through backdrivable gear trains, and are used on most modern servomanipulator systems.[4]

As an object in space has six DOFs, a general-purpose manipulator must have at least six DOFs plus end-effector actuation. Additional DOFs are rarely used on servomanipulator systems as they are redundant, increase the system complexity, are difficult to operate, and are only rarely useful. As mentioned earlier, modern servomanipulators usually have a configuration similar to the human arm. The joints are almost always rotary. Prismatic joints, though common in robots and mechanical master-slave manipulators, are rarely used in servomanipulators.

The general-purpose two-fingered tong gripper is the most used end effector. Considerable research has been directed toward improved general-purpose end effectors, but the simplicity and reliability of the two-fingered tong maintained its popularity.

Only two American companies currently market complete master-slave servomanipulator systems commercially. These are Central Research Laboratories (CRL) of Red Wing, Minn., and TeleOperator Systems Corp., (TOS) of Bohemia, N.Y.[4]

The CRL Model M-2 servomanipulator installed at the Integrated Equipment Test Facility at ORNL represents the first successful implementation of an entirely digitally controlled servomanipulator. This results in an inherently flexible control system by virtue of its software implementation. Advanced control features include selective robotic operations, slave to master force ratios, and indexing between

master and slave. The slave manipulator has a peak load capacity of 100 pounds and a continuous load capacity of 50 pounds.[5]

The TOS Model SM-229 is the servomanipulator used in this study, and will be discussed in detail later.

Servomanipulators have been designed, built, and operated in many foreign countries, most notably France.[6,7]

## 1.2 PURPOSE AND APPROACH

The experimental objective was to determine the kinematic usage and duty cycles of the SM-229 right slave arm in the actual work environment. The slave arms are more critical than the master arms because they have greater duty cycles (force reflection is not 1:1) and reliability is much more critical. The master arms, located outside the hot cell, can readily be accessed for repair, while the slave arms cannot.

A review of the literature revealed no work in the area of determining servomanipulator duty cycles in the actual work environment. This type of analysis has applications in design optimization of motion ranges, actuator sizing, gear reductions, and drive configurations; in pinpointing areas of high stress and wear; and in projecting expected component life and system reliability.

As this study is the first of its kind, a comprehensive definition of servomanipulator duty cycles used in this study will be presented as a reference for future comparative studies.

The duty cycles are subdivided into two main groups--joint duty cycles and motor duty cycles. The joint duty cycles are defined as the periodic usage of positions, velocities, torques, and mechanical power and energy. Position and velocity will be expressed on a scale of their corresponding design ranges (per DOF) in histogram form as percentage time (0 to 2, 2 to 4, 4 to 6%, etc.). Mechanical power will be presented as a 3-D image with velocity and torque (scaled to the design ranges) the independent variables and log of percentages of total operating time the dependent variable. Mechanical energy will be expressed as a total per DOF per task (averaged). The motor duty cycles are defined as the periodic usage of electrical current and

energy. Again, the current will be expressed in histogram form, scaled to the motor design range. As all seven motors are identical, the scaling will not be done individually. The energy will be expressed as a total per task (average). Average peak values per task of velocity, acceleration, mechanical power, and motor current will be presented.

The joint duty cycles are expressed in joint (or DOF) coordinates. The six joints are referred to as pitch and roll of the shoulder, elbow, and wrist. The motor duty cycles are expressed in motor coordinates. The elbow pitch and roll motor coordinates correspond directly to the joint coordinates, but the shoulder and wrist are driven by differentials, so that the pitch is proportional to the sum of the two motor coordinates and the roll proportional to the difference.

The experimental approach used to determine the duty cycles was to select five different representative remote-handling tasks to be performed by four experienced manipulator operators. The tasks were selected on the basis of being generic and representative of operations with servomanipulator systems. Each operator performed each task from 10 to 50 times. While these tasks were being performed, the seven manipulator positions and seven motor currents (including tong) for the right slave arm were recorded at a rate of 10 Hz. A total of 47 1/2 h of manipulator operational data were recorded.

The above-mentioned duty-cycle data were calculated for each experiment and then composited for each task (a given task was performed the same number of times by each operator). The overall composite results were obtained from the composite results for each task with equal weighting on each task. The final results have thus been composited over a wide range of manipulator usage, and should be highly repeatable for any similar set of trials.

Data were sampled for the right arm only due to data-logging limitations. It has been determined[8] that the right arm is used more often in operation than the left. Thus, this limitation was not considered to restrict the results obtained.

## 2. EXPERIMENTAL SYSTEM DESCRIPTION

The system used in the experimental investigation will now be described. This includes the manipulator system, the transporter, the remote environment, the operator (control) station, the experimental tasks, the data acquisition system, and the data reduction techniques.

### 2.1 THE REMOTE SYSTEMS DEVELOPMENT FACILITY (RSDF)

The experimental work was carried out at the RSDF located at ORNL. This facility has been set up for the specific purpose of developing and testing remote maintenance concepts and equipment, both hardware and software. Included are a mock-up remote cell to simulate the working environment, a separate control station, and a Digital Equipment Corp. (DEC) PDP 11/34 data aquisition system.

#### 2.1.1 The Remote Cell

The remote cell contains the slave manipulators (to be discussed later) mounted on a telescoping hoist of an overhead three-axis transporter system (see Fig. 1). This transporter system has three translational DOFs, allowing the slave manipulators to be positioned anywhere in the remote cell. Additionally, the slave manipulators can be rotated about the hoist axis to achieve the desired angle of approach to the work site. The manipulator arms are mounted parallel, with each shoulder pivot point (intersection of the shoulder pitch and roll axes) located 13 7/8 in. out from and 6 in. behind the hoist axis. Thus, the total separation of the arms is 2 × 13 7/8 in. = 27 3/4 in.

Two cameras, each mounted on four DOF-positioning systems, are mounted on the hoist just above the manipulators. These cameras can be rotated about the hoist axis, extended or retracted from the hoist axis, and panned and tilted to achieve a range of viewing angles. The cameras feature remotely controlled zoom lenses, aperture, and focusing.

Two facility cameras are mounted in fixed locations in the top corners of the cell. These cameras also feature remotely controlled zoom lenses, aperture, and focusing. These cameras are used primarily

when moving the transporter to ensure that obstacles are avoided and to locate objects (such as tools) which may be out of sight of the on-board cameras.

A variety of special tools including wrenches and screwdrivers are located in a tool bin. These tools have been equipped with attachments for use with two-fingered tong grippers. The most used special tool is an impact wrench which has a mount on the hoist between the two slave arms. In Fig. 1, the right slave arm is shown reaching for the impact wrench. The wrench holder is located 28 1/2 in. below, 18 1/2 in. to the left of, and 3 in. behind the right arm shoulder pivot. The holder is oriented in the horizontal plane, 30° right of the forward direction. In this position and orientation, the wrench and holder do not interfere with the movements of the manipulator, yet the wrench is easily grabbed by the right arm gripper. When grabbing the wrench, the right arm configuration is:

shoulder pitch = +40° (down)
shoulder roll = +28° (left or in)
elbow pitch = +12° (in)
elbow roll (yaw) = -114° (in or left)
wrist pitch = +14° (down)
wrist roll = 0°

Several remote-handling tasks have been modeled in the cell. These will be discussed in detail later.

### 2.1.2 The Control Station

The operator is located away from the remote cell at the control station (see Fig. 3). Central to the control station are the master manipulator arms mounted on a fixed support. The arms are mounted parallel, with the same separation distance as the slave arms (27 3/4 in.).

Directly in front of the operator are four 7-in. black and white television monitors dedicated to the four cameras in the remote cell. Two large-screen color monitors are located above and to the right of

ORNL Photo 4920-82AR

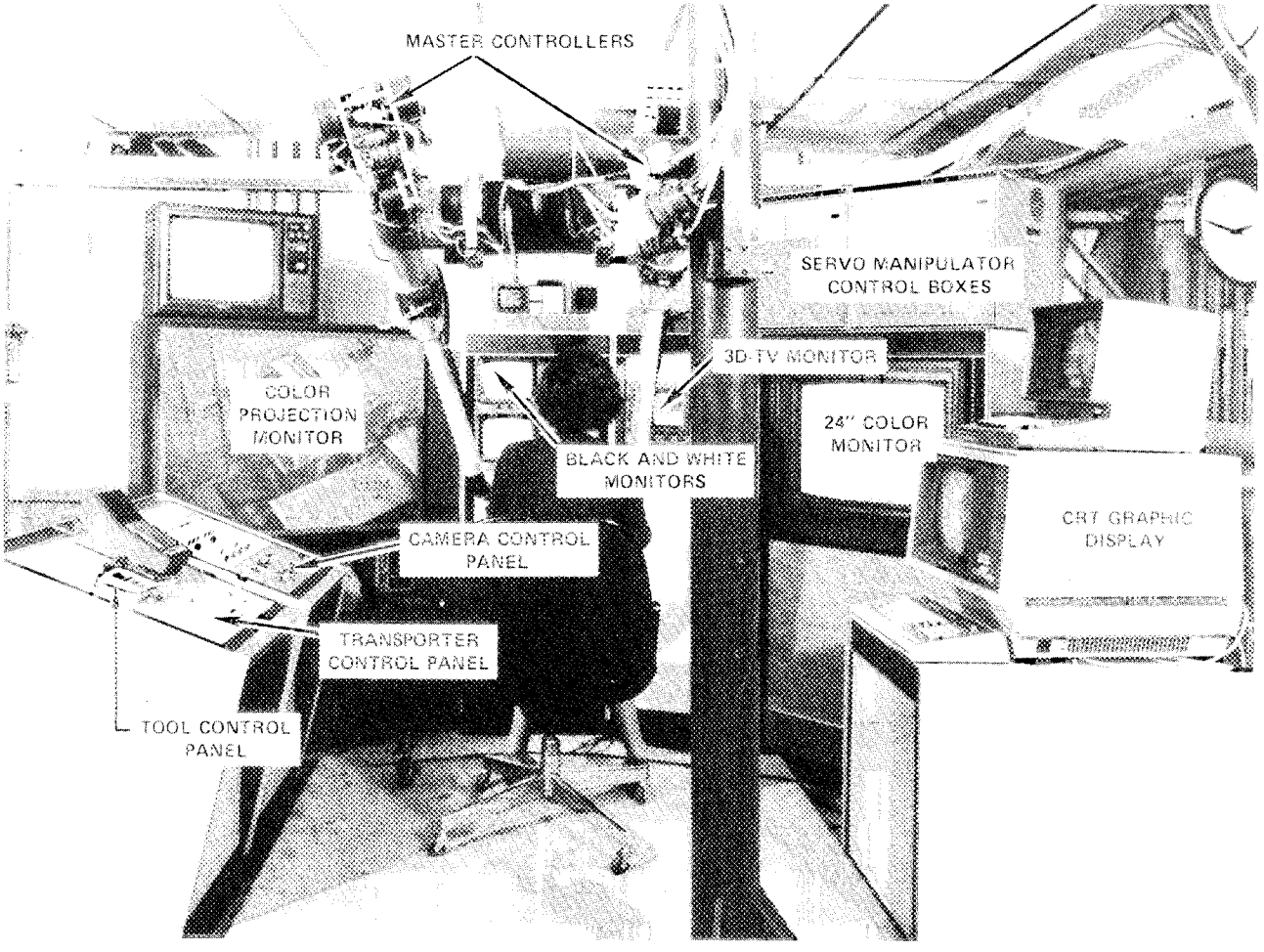


Fig. 3. Operator control station.

the small monitors. These large monitors can be switched to display the views of any of the cameras or the display of a computer terminal.

Above the right large-screen monitor are boxes containing the analog controls for each of the arms. Light-emitting diodes (LEDs) on the front panel of these boxes indicate the arm and tong brake status. If misalignment of the master and slave causes the brakes to energize, the misaligned DOF is indicated by an appropriate LED.

Controls for the cameras, monitors, impact wrench, and transporter system are located on the operator's left. Joysticks control camera position (pan, tilt, rotate, and extend as well as pan and tilt of the facility cameras) and lenses (aperature, focus, and zoom of on-board and facility cameras). Switches control on-board camera lights and monitor selection. Another switch will cause the on-board cameras to automatically follow the right arm tong gripper. A special three-axis joystick controls the movement of the transporter. Three switches cut off the power to each of the transporter DOFs as an added safety precaution. Toggle switches control the power to and direction of the on-board impact wrench. Pushing a spring-loaded switch energizes the impact wrench. Another switch actuates a chain-driven hoist used in two of the tasks.

On a graphics terminal to the operator's right is a top view map of the remote cell showing the relative location of the manipulator and obstacles within the cell. The map continually updates itself as the operator moves the transporter through the cell.

## 2.2 THE TOS MODEL SM-229 SERVOMANIPULATOR

The servomanipulator used in the RSDF system is the TOS Model SM-229. The manipulator system was on loan to ORNL from the Princeton University Plasma Physics Laboratory. The manipulator configuration is elbows up, and the master and slave manipulators are identical except that the tong gripper of the slave is replaced with the master handle.

Weights and dimensions are given in Table 1, and dynamic characteristics are given in Table 2.

Table 1. Weights and dimensions of Model SM-229

| | |
|---|---|
| Upper arm | 22 in. |
| Lower arm | 27 in. |
| Terminal device | 7.5 in. (to tip) |
| Total reach | 49 in. (at wrist joint) |
| Weight (master or slave) | 105 $lb_f$. |
| Handling capacity | 20 $lb_f$. |
| Counterbalance | X, Y & Z motions |

### 2.2.1 Master-Slave Motions

Master-slave motions are developed by various combinations of gears, links, tapes, and cables.[9] The descriptions refer to the slave, although master motions are identical except that they are initiated at the master handle. These are individually described as follows.

The wrist pitch and roll (WP, WR) are generated through the same drive train by two motors located at the counterbalance. These motors drive two pairs of tape pulleys through a gear reduction. Tapes fastened to these pulleys travel through the arms, over a series of idlers, to the wrist where they drive a similar set of pulleys in the wrist. These pulleys, through gearing, drive a pair of bevel gears which act as input to a differential. The wrist is rigidly attached to the pinion of the differential. When both pulleys move in the same direction, a pitch motion of the wrist is developed. Opposite rotation provides a roll motion, and differential velocities provide a combination of pitch and roll.

The elbow roll (ER or yaw) is equivalent to a wrist yaw and is developed by rotation of the forearm at the elbow joint. As with the wrist motions, a motor at the counterbalance drives a pair of tape pulleys through a gear reduction. Tapes attached to these pulleys pass through the upper arm and are attached to a similar set of

Table 2. Dynamic characteristics of Model SM-229.

| | x (Shoulder roll) | y (Elbow pitch) | z (Shoulder pitch) | Yaw | Pitch | Roll | Terminal device |
|---|---|---|---|---|---|---|---|
| Maximum moment arm | 33 in. | 33 in. | 55 in. | 7 in. | 6 in. | 4.5 in. | N/A |
| Maximum available torque or force at slave (in.-lb) | 900 | 700 | 1390 | 127 | 118 | 100 | 30 lb |
| Typical apparent no-load mass of inertia | 6.0 lb | 6.0 lb | 13.5 lb | 200 lb-in.$^2$ | 135 lb-in.$^2$ | 90 lb-in.$^2$ | |
| Typical maximum no-load linear or angular velocity[a] | 65 in./s | 40 in./s | 70 in./s | 7.1 rad/s | 14.4 rad/s | 23.1 rad/s | 32 in./s |
| Typical compliance of complete system rad/in.-lb.[b] | $15 \times 10^{-5}$ | $18 \times 10^{-5}$ | $12 \times 10^{-5}$ | $12 \times 10^{-4}$ | $14 \times 10^{-4}$ | $20 \times 10^{-4}$ | N/A |
| Typical motion range[c] | ±45° | -45°, +140° | -50°, +100° | 340 | -120°, +45° | 320° | 3.25 in. |

[a]For x, y, and z motions perceived friction, velocity and apparent mass are a function of the angle that the lower arm makes with respect to the upper arm. The numbers given are for the maximum velocity.

[b]At maximum load.

[c]References from a vertical position of the forearm and horizontal position of upper arm and terminal device (+) = up or forward; (-) = down or to rear.

pulleys at the elbow. These pulleys drive a bevel gear attached to the forearm tube.

The elbow pitch (EP) is a pitch motion of the forearm at the elbow joint. A motor at the counterbalance drives a longitudinal shaft coaxial with the upper arm through a dual gear reduction and a mitre gear pair. Gearing at the elbow transfers this motion to a spur gear rigidly attached to the forearm, providing the desired motion.

The shoulder pitch and roll (SP, SR) are combined motions and are derived similarly to the pitch and roll motions of the wrist. A pair of motors at the shoulder drive differential input bevel gears through suitable gearing. A pinion attached to the output bevel gear of the differential thus moves about the center of the input gears if both inputs are moving in the same direction and rotates about its own axis when the inputs are in the opposite direction. These motions are transferred to the upper arm through an idler to a gear fixed to the outer diameter of the upper tube.

The terminal device (tong) is driven closed by a motor on the counterbalance. It is released by springs contained in the terminal device. The drive motor, through a double gear reduction, drives a pulley to which is fixed a steel cable. This cable passes through the arms over suitable idlers and is terminated in a threaded ferrule which engages the threaded actuator in the terminal device. A cam action in the terminal device closes the clamp fingers.

The counterbalance is moved in relation to the forearm (elbow pitch) to maintain balance in different forearm positions. This motion is accomplished by moving the counterbalance relative to the forearm with the same motor that drives the elbow. A pair of idler gears transmits this motion to a gear fixed on the counterbalance.

The upper three DOFs (shoulder pitch and roll and elbow pitch) place the wrist in the desired position, while the lower three DOFs (yaw or elbow roll, wrist pitch and roll) provide the desired orientation.

### 2.2.2 Gear Reductions

The manufacturer's specifications on exact gear reductions were not available. The gear reductions were measured approximately using the procedure described below.

Angles were measured on the right slave arm with the power off. The selected DOF was pushed against its mechanical stop. The DOF angle was measured with a bubble balance protractor. The accuracy was ±0.5° for the shoulder DOFs, ±2.0° on the elbow pitch, and ±3.0° on the lower DOFs (absolute). The motor angles were measured by placing a red mark on the armature and housing when the DOF was at one limit and counting the revolutions before the DOF reached its second limit. The remaining angle was estimated by eye: accuracy = ±10° on the elbow DOFs, ±20° on the shoulder (differential) drives, and ±15° on wrist drives. The gear reductions (GR) are expressed as

$$GR = \frac{\text{revolution of motor(s)}}{\text{revolution of DOF}}$$

For the differential drives, the motor revolutions given are the revolutions that <u>each motor</u> travels--it is not the sum (or difference) of the two. Gear reductions and uncertainties are given in Table 3.

### 2.2.3 Actuators

Both master and slave arms are driven by seven (per arm) identical electric motors, Model OT-2919-2923 manufactured by Inland Motors Division of Kollmorgen Corp. These motors are compact (~4 in. diam, 3 in. height) and light weight (about 2.5 $lb_f$). They are brush type dc servomotors and feature semarium/cobalt magnets for improved flux density. Friction is low, typically about 0.02·ft $lb_f$. Motor specifications are presented in Table 4.

### 2.2.4 Control System

The control system used with the manipulators is that supplied by the manufacturer. The system is entirely analog. Since master and slave are kinematically identical, each motor can be controlled individually. The slave drive is the output of a proportional plus

differential (PD) controller. Input to the controller is the position error between master and slave. The proportional gain is set by adjusting potentiometers located in the power amplifier cards of each motor. Unfortunately, these potentiometers tend to drift considerably and are also rather difficult to adjust precisely. The velocity gain cannot be readily adjusted. Master drive is proportional to the log of the slave drive so that the force reflection ratio varies from 1:1 at light loads to about 2.2:1 at maximum loads.

The brake control is triggered by any one of the position error signals exceeding a fixed value. This enables the brakes and

Table 3. Approximate gear reductions

| | DOF travel | Motor travel[a] | Gear reduction[b] (± probable error) |
|---|---|---|---|
| SP | 165° ±1 1/2° | 18 6/20 ±3/20 | 39.93 ±1.1% |
| SR | 90° ±1 1/2° | 7 7/20 ±3/20 | 29.4 ±2.2% |
| EP | 176° ±2 1/2° | 21 1/4 ±1/8 | 43.47 ±1.5% |
| ER | 349° ±3° | 7 9/11 ±3/22 | 8.065 ±2.0% |
| WP | 173° ±4° | 1 22/25 ±1/25 | 3.912 ±3.1% |
| WR | 335° ±4° | 3 1/25 ±1/25 | 3.267 ±1.8% |
| Tong | 3.5" ±1/16" | 1 8/20 ±1/20 | 0.4 rev/in ±4% |

[a]Travel of both motors on shoulder and wrist.

[b]Gear reduction = $\frac{\text{revolution of motor}}{\text{revolution of joint}}$ .

disables the drive on all of the slave motors except the tong (which has a separate brake on/off switch).

Another potentiometer in the power amplifier cards can be used to limit the current to the motors. Note that there are two ways to limit the maximum current that can be generated by a given motor:

decreasing the current limit to provide saturation, or increasing the current limit to where the proportional gain determines the maximum current when the brakes energize at maximum position error.

### 2.2.5 Tuning the Controls

The procedure used for tuning the controls for optimum performance was the same for each of the six DOF motors. At the master station, a voltmeter was connected across one of two zener diodes located on each of the power amplifier cards (there are two gain

Table 4. Motor specifications

| | |
|---|---|
| **Motor Size Constants** | |
| Peak torque | 20.4 in•$lb_f$ |
| Motor constant | 1.92 in•$lb_f$/W |
| Electrical time constant | 2.3 ms |
| Mechanical time constant | 9.2 ms |
| Power input, stalled at peak torque (25°C) | 112 W |
| Viscous damping | 0.432 in•$lb_f$•s/rad |
| Motor friction torque | 0.312 in•$lb_f$ |
| Maximum permissible winding temperature | 155°C |
| Rotor moment of inertia | $3.96 \times 10^{-3}$ $lb_f$•in/$s^2$ |
| Maximum power rate | $1.056 \times 10^5$ $lb_f$•in/$s^2$ |
| Maximum theoretical accel | $5.2 \times 10^3$ rad/$s^2$ |
| No-load speed | 48 rad/s |
| Weight | 2.5 $lb_f$ |
| **Winding Constants** | |
| Dc resistance (25°C) | 5.5 ohms |
| Volts at peak torque (25°C) | 24.8 V |
| Amperes at peak torque | 4.5 A |
| Torque sensitivity | 4.56 in•$lb_f$/A |
| Back electronative force | 0.52 V•s/rad |
| Inductance | 13.6 mHz |

potentiometers and two corresponding zener diodes on each power amplifier card--one for each direction). The system was turned on, and the master and slave were synchronized. The slave brakes were left on, and the appropriate master motion was pushed until the error

signal exceeded the limit. The voltage across the diode just before the error signal was exceeded (indicated by illumination of an LED on the front panel of the control cabinet) was proportional to the position gain of the controller. This voltage was adjusted to 5.6 to 5.8 V. It had been observed that adjusting the gain any higher than this resulted in a high risk of damaging electrical components in the control system. This adjustment was made twice for each motor motion (once in each direction) for all six motors, and once for the tong motor. Thus, these cards were adjusted to provide the highest current limit attainable (still below the design limit of 4.5 A as will be discussed later). This type of adjustment was desirable for the slave arms in order to be able to generate the highest possible forces. A somewhat "softer" tuning was desirable for the master to reduce stiffness and ease operation. Thus, these cards were then exchanged with the slave cards. The (former) slave cards (now the master cards) were then adjusted in the same way, but the goal was to attain a good "feel" with the arms. This usually resulted with a voltage of about 4.6 to 5.2 V across the zener diodes.

## 2.3 EXPERIMENTAL TASKS

Following is a description of the tasks used in the experiments. These tasks were selected on the basis of their being representative of tasks to be performed in remote maintenance activities, and containing aspects of generic maintenance tasks as demonstrated on a manipulator test stand.[10] During the three-year history of the RSDF these tasks have been continually performed and upgraded for man/machine interface and special tooling design studies.

### 2.3.1 The Instrument Package Task

The purpose of this task was to demonstrate removal and reinstallation of a simulated in-line instrument package. A mounting block was fixed on a test stand, and a horizontal nut-operated clamp was used to engage the bottom block of the instrument package with the mounting block. The bottom block was attached to a simulated

instrumentation package. A simulated instrument jumper to the instrument package consisted of a horizontally engaged pin connected on the top of the instrument package, a length of cable, and a vertically engaged pin connected to the test stand frame. (The task setup can be seen in Fig. 4.) The approach to the work site was both from above and from the side. The task essentially had two small-volume work sites, the instrument package and the vertical pin connector. Thus, only two transporter movements were required.

### 2.3.2 The Motor Mount Task

The purpose of this task was to demonstrate removal and reinstallation of a medium-sized motor with a horizontal shaft. The motor and mount assembly are shown Fig. 5. Removal of this motor required the use of an overhead hoist, which was mounted on a manually movable jib positioned by the manipulator arm. A control for hoist up-and-down was provided in the control room, and the approach to the work site was entirely from above. The task covered a small volume except for reaching for the hoist.

### 2.3.3 The Tubing Service Jumper Task

The purpose of this task was to demonstrate removal of a simulated remote tubing service jumper as depicted in Fig. 6. The setup had three horizontal connectors (in a line separated by 4 in. and 7 in.) that required the use of the on-board impact wrench. The setup was mounted with the connectors on the right side to emphasize the use of the right arm. This task covered a medium-size volume, and the approach to the work site was strictly from the side.

Reinstallation of the jumper was not done because the jumper was dropped frequently in disassembly, causing it to bend slightly. It would then not fit precisely into the connectors, making remote reassembly difficult or impossible. Assembly of ill-fitting parts was not considered to be representative of remote maintenance activities because an actual failed jumper would be replaced with a new part that would fit precisely.

ORNL Photo 2059-84

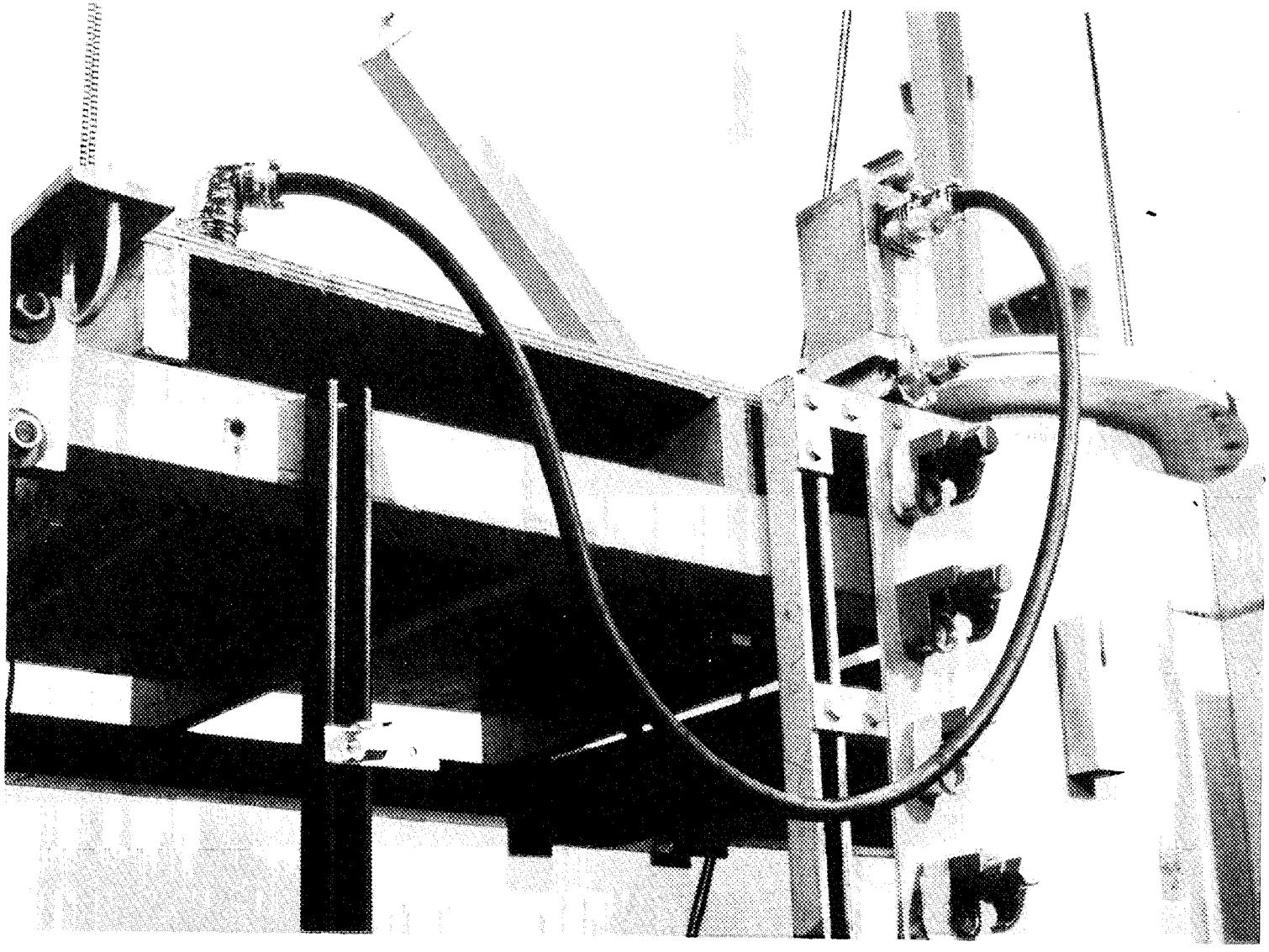

Fig. 4. Instrument package.

ORNL Photo 2061-84

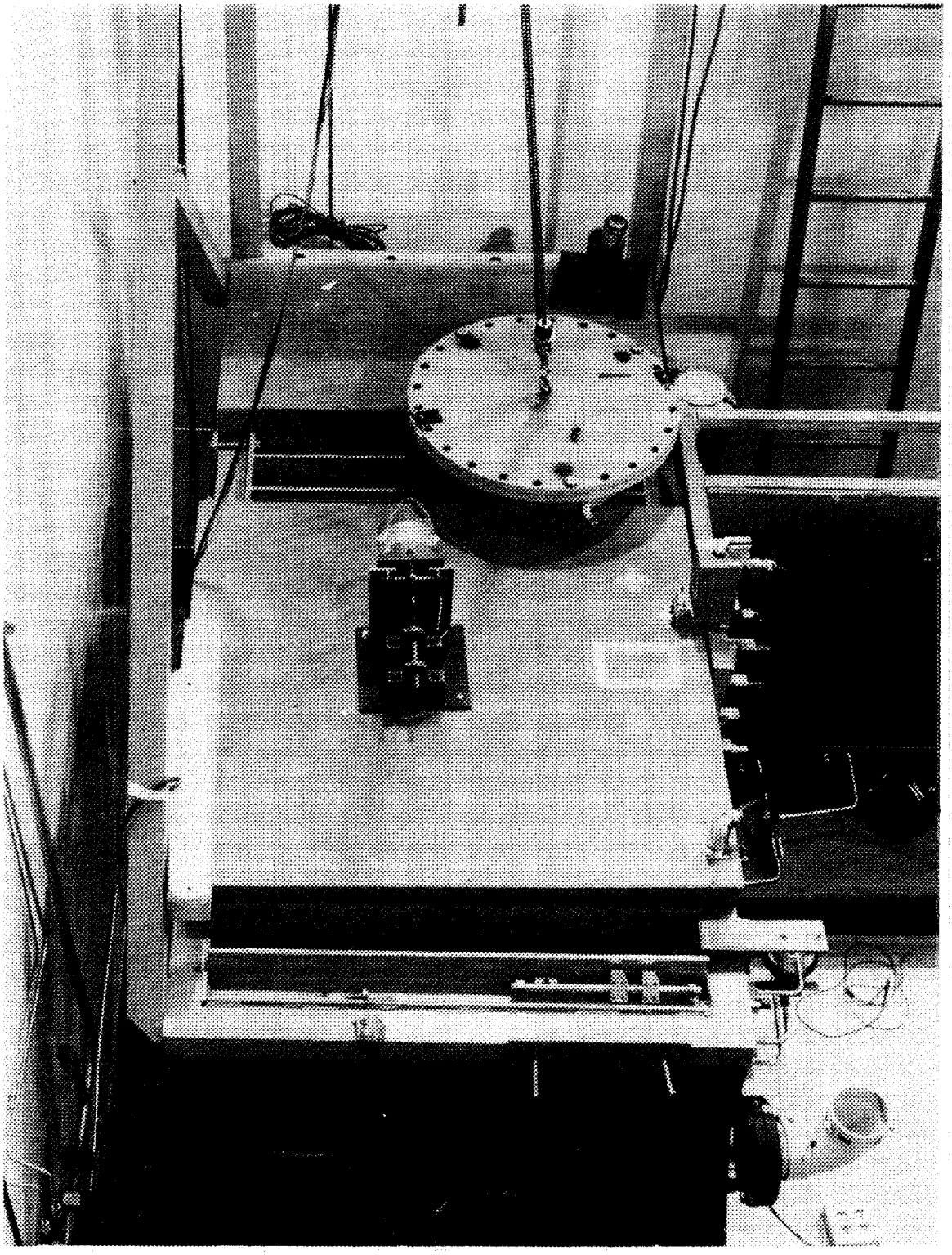

Fig. 5. Motor mount and 30-inch flange.

ORNL Photo 2057-84

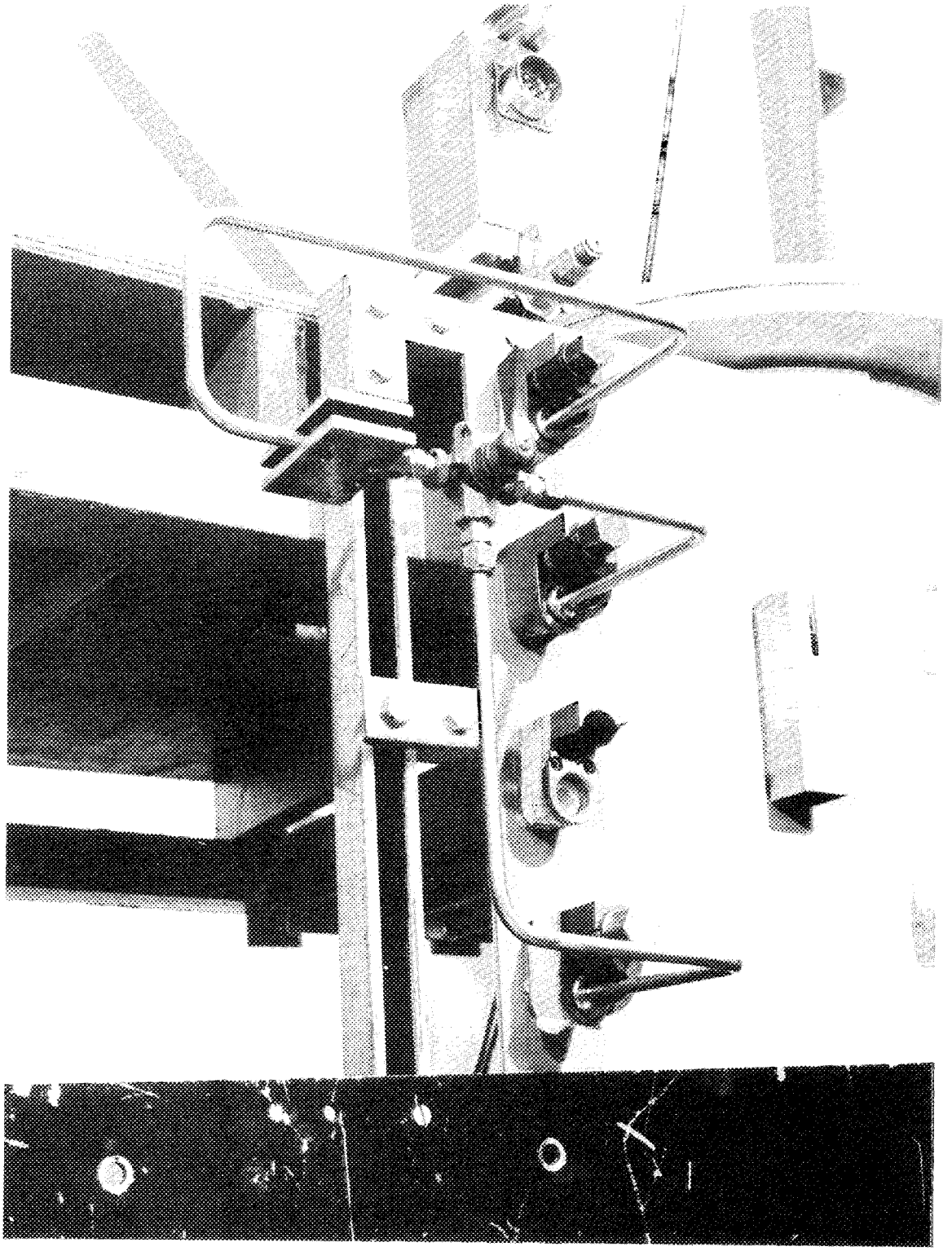

Fig. 6. Tubing service jumper.

### 2.3.4 The 30-in. Flange Task

This task involved the removal and reinstallation of a 30-in. pipe flange (shown with the motor mount in Fig. 5). The actual flange has about 30 3/4-in. bolts. To reduce the time required, only three of the bolts were used. The on-board impact wrench was required to remove and reinstall the bolts. The overhead hoist used with the motor mount was used to lift the flange.

The approach to the work site was strictly from above, and the volumetric coverage of this task was the largest of the five tasks. The flange itself was large, and the operator had to reach several feet to grab the hoist hook. Thus, the transporter was used often to reposition the manipulator.

### 2.3.5 The 6-in. Flange Task

The purpose of this task was to demonstrate removal of a 6-in. pipe flange. The flange was provided with guide pins and two horizontal captured bolts, and was oriented with the pipe axes in the horizontal plane. The on-board impact wrench was required to remove the bolts. To emphasize the right arm, the captured bolts were placed on the right side of the flange. The volumetric coverage was relatively small. The approach to the work site was strictly from the side. Reinstallation of the flange was omitted because it was found that holding the flange required very high wrist torques, resulting in marginal stability and making the precise positioning required for reinstallation very difficult.

Due to the similarities between the tubing service jumper removal task and the 6-in. flange removal task, it was decided to average the results from these two tasks and consider the results to be from one task.

## 2.4 DATA ACQUISITION

The duty cycles were determined experimentally by measuring the position and current signals for the slave right arm while operators performed the selected maintenance tasks. The signals were available

as analog voltages and were read by the host PDP 11/34 computer at a rate of 10 Hz. The estimated measurement uncertainties are presented in Appendix A.

### 2.4.1 Hardware

The positions of all motions of master and slave manipulators are sensed by precision potentiometers* driven through suitable gearing from either the motion drive or the motion itself. Relative positions of the master and slave potentiometers provide the error signal to drive both master and slave. All potentiometers are located within the arms.

The wrist pitch and roll potentiometers are located on the casting supporting the wrist tapes in the counterbalance. The elbow roll (yaw) potentiometer is located in the lower half of the elbow joint; the elbow pitch is located in the upper half of the elbow joint; the shoulder pitch and roll are located in the casting where the motion drive motors are mounted; and the tong position is sensed on the structure mounting the cable drive pulley.

The signal range is ±15 V, and the manufacturer's specifications indicate linearity to within 0.5% within this range. Calibration procedures and data are presented in Appendix B.

Motor-current data were available as the voltage drop across 0.1-Ω shunt resistors located in the slave electronics boxes. These are precision resistors, accurate to ±1%. As the maximum motor current is 4.5 A, the signal range is ±450 mV.

The variable end of each signal is taken through 200 ft of shielded cable to a relay box located in the RSDF control room. All signals have a common ground, and ground reference is picked up on the relay box. Master and slave grounds are connected via a 200-ft-long, 3/8-in.-thick copper welding cable. From the relay box, the signals are sent to the PDP 11/34 analog input cards through 150 ft of shielded, twisted pair cabling.

Noise was detected on the input signals at the relay box in the control room. Using an oscilloscope, noise of magnitude up to 200 mV

*Bourns Corp., Model 7934BZ, supplied with the SM-229 system.

(with spikes up to 500 mV) and primary frequency of about 500 Hz was seen. To eliminate this, first-order resistor-capacitor (RC) filters with a cutoff frequency of 11 Hz were added to each channel of the analog inputs. This effectively eliminated the noise from the signal as seen by the PDP 11/34. The real signal remained essentially unaffected by the filters as it had been determined[11] that the response of the slave arms to the sinusoidal motions of the master drops sharply at frequencies above 3 Hz.

Unfortunately, master and slave grounds vary randomly. The average deviation is about 10 mV with a maximum observed difference of 16 mV. This has little effect on the position signals (±15 V) but contributes significantly to current signal uncertainty.

Analog signals are converted to digital signals by a DEC AD01-D converter.[12] This is a high-speed converter capable of handling up to 10,000 samples/s with a settling time of only 25 μs. The range of the converter is ±10 V, with optional gains of 2, 4, and 8. As the position signal range is ±15 V, voltage dividers were added to the position signals to prevent saturation. The signals were put across 5- and 10-KΩ resistors in series, with the PDP 11/34 reading the voltage across the 10-KΩ resistor. These resistors were off-the-shelf items accurate only to ±5%. Their values were measured precisely with a Tektronix DM 5013 (IC #043154) ohmmeter, and the exact ratio for each channel was incorporated into the calibration. The current signals were read with a gain factor of eight (i.e., a full-scale reading of 1.25 V = 2000 counts).

### 2.4.2 Software

Two tasks, running in real time, were coordinated using system global event flags to log the data precisely and reliably. These tasks were written in FORTRAN Four Plus. The operating system used was Version 3.2 of RSX-11M.[12]

The first task, ANAIN, was the system analog input scanning task. It scanned all 24 analog input channels and placed the data in a dynamic memory common. It ran on its own software timer at 10 Hz, with negligible timestep variation (see Appendix B). The channel

numbers (including gains) and time between scans were also elements of the dynamic common. These ordinarily remain at 0 through 23 and 0.1 s, respectively, but could be changed readily if desired.

The dynamic common had room for 4096 two-byte words, most of which (3900) were used as two 1950-word data buffers. Each time it scanned the data, ANAIN placed incrementally in one of the buffers the 15 channels of interest (there is one blank channel between the 7 position signals and 7 current signals). When a buffer was filled, ANAIN checked to see whether the data-logging global event flag was set, indicating that data logging was active. If it was not, ANAIN simply reset its buffer index and repeated. If the flag was set, several checks were processed. The buffer index was reset. The buffer identification flag, the 3091st element of the common, was flipped (its value is +1 or -1) so that further scanning could continue loading the second buffer while LOGDAT (the writing task) wrote the first buffer to disk. The "buffer dumped" flag was checked. This flag was set by LOGDAT when it finished dumping a buffer. If this flag was not set, then LOGDAT had not finished dumping the buffer that ANAIN was preparing to write to. If this occurred, ANAIN cleared the data-logging flags and sent a message to the terminal stating that data logging had been aborted. (Note: this condition never occurred; it took ANAIN 13 s to fill a buffer, while LOGDAT could dump it in about 3.5 s.) If this flag was set, ANAIN cleared the flag, set the "buffer full" flag, and proceeded with scanning and loading the second buffer. This technique is referred to as "double buffering." Note that there is no "window" open for a scan to go by without the previous scan being logged.

The function of the second task, LOGDAT, should now be clear. This task first opened a disk file and requested the operator to input a record number for the data. This number was written to disk, and was also recorded by the operator in a data-logging notebook along with all pertinent information about the task. After a 13-s delay (to allow the operator to begin the task), the data-logging flag was set and LOGDAT waited for the "buffer full" flag to be set. When this occurred, this flag was immediately cleared. LOGDAT then checked the

data-logging flag. If it was clear, the disk file was closed, and a message was sent to the terminal (DATA LOGGING ENDING). If the flag was set, one of the buffers (determined by the 3901st element of the common) was dumped to disk (unformatted) in 15-word records. When the entire buffer had been dumped, LOGDAT set the "buffer dumped" flag and went back to wait for the "buffer full" flag. Data-logging was terminated by running another task, STPLOG, which simply cleared the data-logging flag.

### 2.4.3 Procedures

The operators were allowed to perform each task twice to become familiar with the system. While all four operators were experienced with mechanical manipulators and a different servomanipulator system, only two of the operators were familiar with the RSDF system.

When performing the tasks for data logging, the operators were told to complete the task as rapidly as could be done safely and effectively. A given task--including transporter movements, camera adjustments, and all manipulator work--was performed entirely by one operator. The data logger was started when the operator began the task, but from 0 to 13 s of data were not recorded because the first buffer was not dumped. The logger was stopped when the operator completed the task, but again 0 to 13 s of data were not recorded because the last buffer was not dumped. Thus, all of the data were taken during operation--there were no long periods of data-logging with the arms not in use, which would have biased the data with zero motor current and constant position. Note that there were short periods when the arm was not in operation, such as when the operators were moving the transporter or adjusting the cameras.

Each operator performed tasks for about 1 h per day for about eight weeks. The operators could typically complete one to eight tasks in a session.

The instrument package task was performed 23 times, the motor mount task 117 times, and the 30-in. flange task 112 times. Each task included both assembly and disassembly. Assembly and disassembly data were recorded separately so that the operators could relax and release

the manipulator for about 20 to 30 s after completing the assembly or disassembly. The 6-in. flange and tubing service jumper disassembly tasks were performed 75 and 76 times respectively.

Counting assembly and disassembly as separate tasks, there were a total of 653 trials totaling 47.56 h of operation.

## 2.5 DATA REDUCTION

All data reduction except graphic display was done on the RSDF PDP 11/34 computing system. Data were logged at 10 Hz, and each data sample consisted of seven integer-valued position signals and seven integer-valued motor-current signals each from the slave right arm. As a typical task required about 5 min, there were about 45,000 words of raw data per task.

The first reducing program read the record number from the raw data file and tagged output data files with the record number, associating the data with the task from which it was generated. After initializing all arrays, the first five data samples were read into memory for a five-point differentiation scheme. The first two current samples were skipped so that velocity and current data would remain synchronized. The first five position signals were calibrated to DOF radians, completing the set up for the "working loop" of data reduction.

In the working loop, the DOF velocities were first determined by a five-point central difference algorithm. The five-point algorithm allowed for a better trade-off truncation error and uncertainty due to position signal uncertainty over a three-point algorithm (see Appendix C). Accelerations were determined by a three-point central difference algorithm. A five-point second derivative algorithm would yield a higher uncertainty than the three-point algorithm due to position signal uncertainty. Acceleration data were used only for estimating peak accelerations, due to the high uncertainty.

The peak velocities, accelerations, and mechanical power for each DOF and current for each motor were determined by averaging the five highest values of each for the entire experiment. This allowed for some smoothing of this peak value data.

The current data were then calibrated to amperes. The electrical power was determined by $P = I^2R$ and integrated (rectangular rule) to find the total energy per motor. The positions and velocities were scaled to the kinematic ranges specified in the Operation and Maintenance Manual for the SM-229.[9] The joint torques were calibrated to motor currents (See Appendix B). Since the maximum motor current was 4.5 A, the maximum torque to use in scaling was determined by extrapolating the calibration to this value. The maximum mechanical power to scale each joint to was determined as $1/4\ T_{mx}\Omega_{mx}$, using the maximum torque and velocity values previously determined.

Since all of the seven motors were identical, the currents were scaled equally for each. As stated before, the maximum current was 4.5 A. The resistance of the motors was measured and recorded (See Appendix B). The power was calculated by $P = I^2R$.

Histogram current data in increments of 2% of the maximum were generated using an array of counters. The maximum number of data samples in which each motor stayed above 60% of maximum current was counted, with allowance for up to ten counts (1 s) below the 60% level before counting was rezeroed. The applied torque per DOF was calibrated to the motor currents and the DOF power was determined by torque times velocity. The total mechanical energy transferred per DOF was found by rectangular rule integration of power data. The power, position, velocity, and torque were then individually scaled to the DOFs. Histogram data were generated for each DOF in the same manner as current histogram data were generated.

The five-point position signal array and three-point current signal array were then incremented one timestep, and the new data sample was read in. The new position data were calibrated. This ended the working loop of data reduction.

After the last data sample was processed, separate data files were opened for each of the following:

1. peak value of velocity and acceleration,
2. position histogram data,
3. velocity histogram data,

4. transferred mechanical energy,
5. maximum time above 60% of maximum current,
6. current histogram data,
7. mechanical power histogram data,
8. total electrical energy, and
9. DOF torque histogram data.

As mentioned, the record number of the experiment was written to each data file. The total number of data samples for the experiment was written to each data file so that composite data could be readily obtained. Upon exit, the program flagged either successful completion or an appropriate error message.

Composite results were determined by another task (there were five compositing tasks--one for each experimental task). This task opened a histogram data file and its corresponding old composite histogram data file as input files and a new composite histogram file as an output file. The task skipped over the record number in the new file, and read the number of data samples in each of the input files. The sum was written to the output file. Each histogram data value was updated as

$$(N_1 \times Value_1 + N_2 \times Value_2)/(N_1 + N_2)$$

where

$N_1$ = number of data samples in the new histogram file,

$Value_1$ = histogram data value in the new histogram file,

$N_2$, $Value_2$ = number and value for the old composite histogram file.

The total energy data files were updated similarly. The peak value data files wrote the highest values to the new output file and updated the average peak value per task.

When all files were successfully composited, an indirect command file renamed the raw data file and the individual experiment data files to identify them as having been crunched and composited. The

new composite data files were renamed as new versions of composite data files, and the composited files were then purged.

Another compositing task updated the mean and variance of the peak values per experiment per task of velocity, acceleration, mechanical power, and motor current.

It was later decided to go back through the data to extract more information. Additional data reduction tasks based on the above tasks were written to obtain histogram data in 2% increments (the original task used 5% increments), and to obtain three dimensional histograms of mechanical power (velocity versus torque), position versus torque, and position versus velocity per DOF. Another task was written to obtain 3-D plots of the front, top, and side views of wrist position in base frame coordinates and a 3-D plot of elbow roll (yaw) versus wrist pitch. As with the 2-D histogram plots, the dependent variable for all 3-D plots was the percentage of total time.

All composite results were obtained per experimental task. The results for the tubing service jumper-removal task and the 6-in. flange-removal task were then averaged with equal weighting and considered to be one task. These results and the results for the other three tasks were then averaged with equal weighting to obtain the final composited results.

# 3. DUTY CYCLE EXPERIMENTAL RESULTS

The results of the experimental study will now be presented. Unless specifically stated, all results presented were obtained by compositing, over time, the results for each experimental task, and then compositing with equal weighting the results for the four tasks (recall that each task is actually the average of two tasks).

Preliminary observations of the experiments will first be presented. The position data will be presented from the perspective of the individual DOFs, and the "base frame" perspective of wrist position and orientation. Velocity and torque data will be presented per DOF as average and overall peak values per task. Motor-current data will be presented similarly per motor. Histograms of the percentage of maximum versus the percentage of time will be presented for velocities, torques, and currents. Torque and velocity data will be combined per DOF in 3-D histogram mechanical power plots with the percentage of maximum velocity and percent of maximum torque as the independent axis, and log of the percentage of total time as the dependent axis. Average total electrical energy per motor per task and average total mechanical energy per DOF per task will be presented.

Finally, 3-D position-torque plots will be presented per DOF which will be similar to the 3-D mechanical power plots.

## 3.1 PRELIMINARY OBSERVATIONS

It should be noted that individual variations among human operators can be considered to represent a stochastic input to system. The use of only four operators does not then represent a sufficient sample size. Thus, the quantitative results may be expected to change for larger samples, but the qualitative results are believed to be valid.

The transporter system allowed the operator to approach the work site from any direction and to get as close as desired. This eliminated any variations due to the locations of the work sites within the remote cell.

It was apparent from all of the tasks that the wrist torque capacity was a significant limitation to the overall manipulator capability. At times it was difficult to hold the impact wrench horizontally, as the torque required was near capacity. The stability margin was greatly reduced at high torques, and disturbances in the master wrist position could cause oscillations in the slave wrist. This was also apparent with the 6-in. flange, which had to be held with its center of gravity well out from the tong. Reassembly of the flange was nearly impossible because of this and was therefore omitted from the testing. No other joint experienced such problems.

Since disassembly was done only on the tubing jumper and 6-in. flange tasks, the data for these tasks were primarily representative of tool changing in picking and replacing the impact wrench in its holder and horizontal bolt removal with the impact wrench. The position range used in these tasks was expected to be rather small. The motor-current range was expected to be representative of very often repeated tasks such as tool changing and horizontal bolt removal. It was the similarity between these tasks that caused them to be considered one task.

Since the transporter system was mounted overhead with the manipulator on a telescoping hoist, it was never necessary to reach upward to perform tasks. Thus, the upper range of the shoulder pitch (arm reaching up) was not expected to be used very much. It is important to note that this probably is not the case for a vehicle type transporter system and that reducing the kinematic range of this motion could be restrictive if the manipulators were mounted on a ground-based transporter system.

The instrument package task had the greatest increase in difficulty between actual "hands on" work and remote work with the manipulators. This was because the pin connectors and attached cabling were round, causing them to slip in the tong. This made it difficult to properly orient and engage the connectors. Thus, this task was representative of unforeseen tasks for which special tooling has not been developed, and of work in areas using old equipment without modern remote tooling adaptations.

The elbow pitch appeared to have the slowest response of any of the joints. The operators would often move the master elbow at a rate that appeared to be very near the design limit. This resulted in decreased force sensitivity in this motion. The friction in moving the elbow pitch was also considerably greater than in any other joint. This was because the elbow pitch is driven entirely by gears and has more gears in its drive train than any other DOF. This also results in a greater inertia than in any other DOF. Thus, high currents in the elbow pitch motor may be caused more by accelerating the considerable inertia and by friction torques than by static loading.

The manipulators were tuned at intervals of about two weeks during the testing period. (The tuning procedure was presented earlier.) About halfway through the testing period, it was discovered that the maximum current that could be generated in the slave motors could be checked easily by switching the slave to computer drive and applying a 10-V drive signal. This is the maximum value the position error signal can attain before the brakes are locked. This was done before and after the manipulators were tuned to get an idea of the actual maximum static current attainable for each motor. Note that for short periods of time the actual current could exceed this limit due to an additional voltage--the back emf--being "applied" to the motor. This can occur only when the acceleration and velocity are in opposite directions.

It was expected that the operators would not often take the manipulator very close to the current limit. Close to this limit, it becomes very easy to pass the position error limit with only a slight movement of the master, and thus lock the brakes. When this occurs, the operator must turn his attention from the task being performed to realign the master with the slave and release the brakes. This is inconvenient, and the operators naturally tend to avoid this possibility.

The data on maximum (static) current attainable are presented in Table 5. The averaged values probably represent a more appropriate maximum current per motor than does the design value of 4.5 A. Note that the values for the maximum static current are not the maximum

static current attainable at any time during the testing--they are the average values just after retuning for two different retunings and two directions per motor. The manipulators were retuned twice before the measurement technique was discovered. Note that the lowest currents attainable were for the shoulder motors. It was not felt that this provided a serious limitation, since the shoulder position error signals caused the brakes to energize only a very few times during the entire testing period and, when they did, the manipulators were retuned within the next two days.

Picking up and replacing the impact wrench required considerable skill, which all of the operators acquired fairly quickly. By the end of the testing period, the operators could pick up or replace the wrench in about 5 s.

Table 5. Static maximum currents per motor, amperes

| Motor | Before tuning[a] | After tuning[a] | Average percentage of maximum |
|---|---|---|---|
| Upper shoulder | 2.11 | 2.93 | 2.52 (56%) |
| Elbow pitch | 2.39 | 3.75 | 3.07 (68%) |
| Lower shoulder | 2.60 | 2.93 | 2.77 (62%) |
| Right wrist | 3.56 | 3.70 | 3.63 (81%) |
| Left wrist | 4.03 | 4.03 | 4.03 (90%) |
| Elbow roll | 3.78 | 3.93 | 3.86 (86%) |
| Tong | 2.59 | 3.49 | 3.04 (68%) |

[a]Average of four values--two retunings times two directions.

## 3.2 KINEMATIC RANGES

The usage patterns of the kinematic ranges will now be presented.

### 3.2.1 Individual Joints

Figures 7 through 12 represent the use of the design motion range of each joint. Each plot is drawn with a front, side, or top view of

ORNL-DWG 84-16665

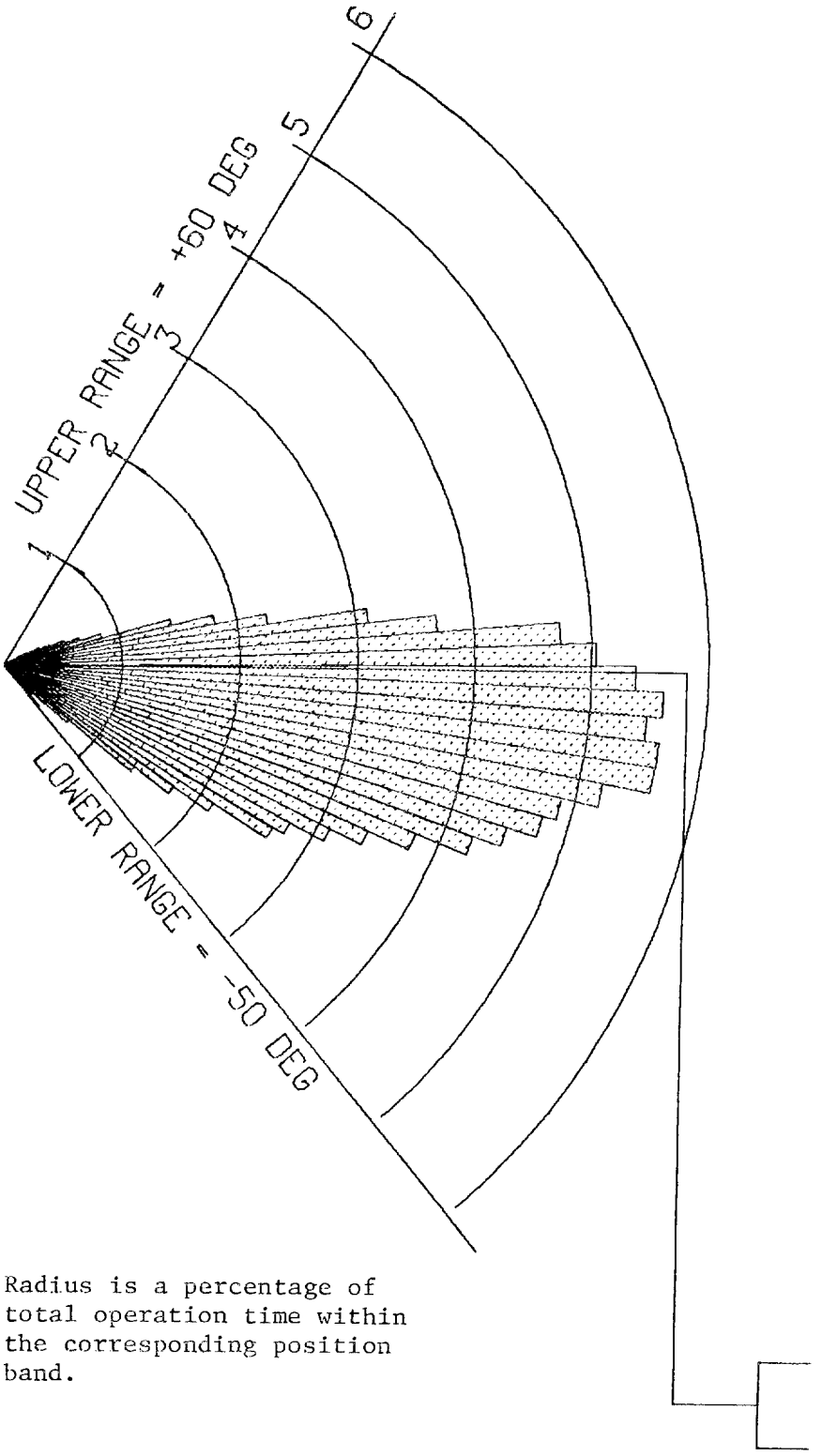


Radius is a percentage of total operation time within the corresponding position band.

Fig. 7. Range of shoulder pitch position usage.

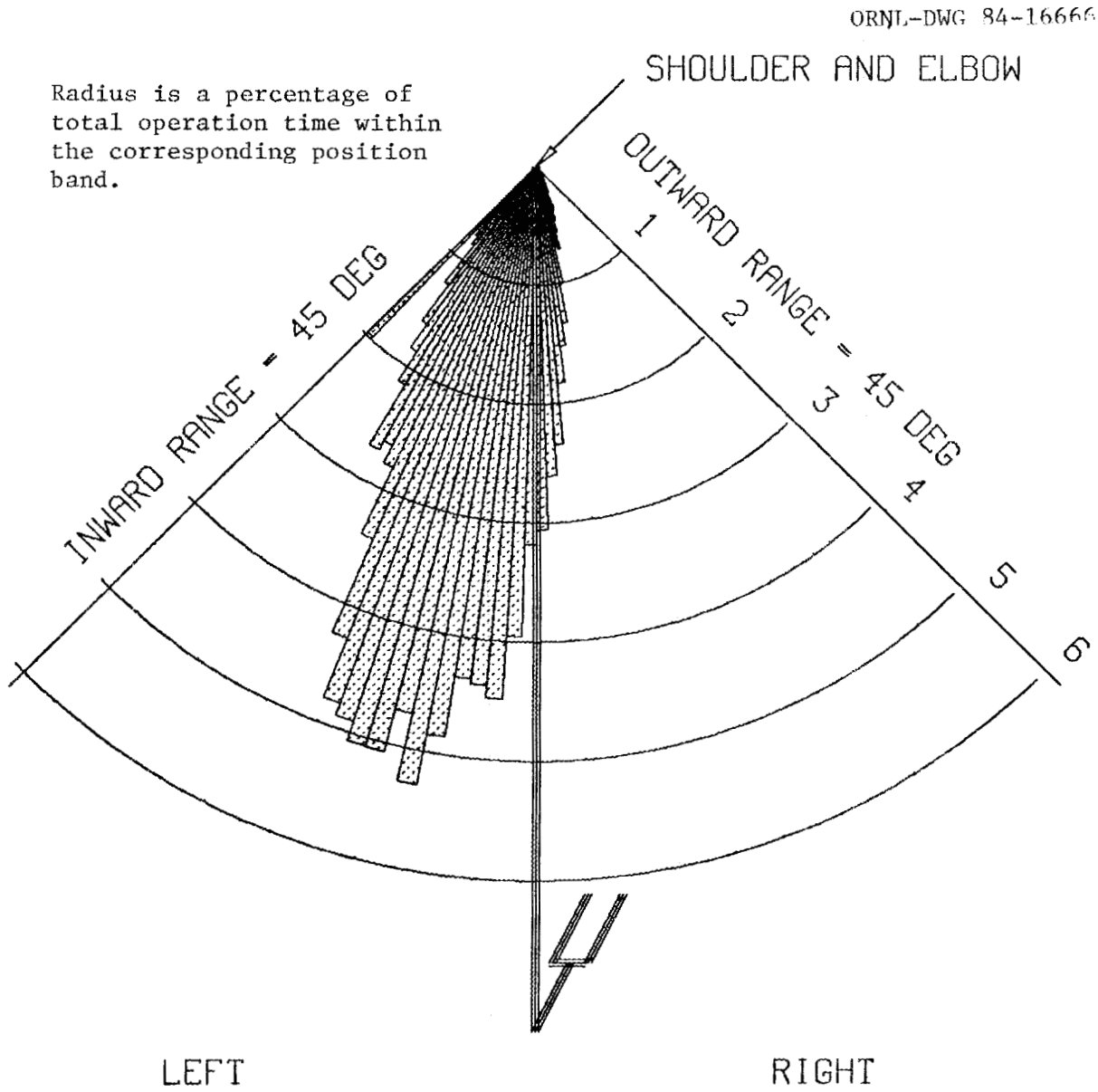


Fig. 8. Range of shoulder roll position usage.

ORNL-DWG 84-16667

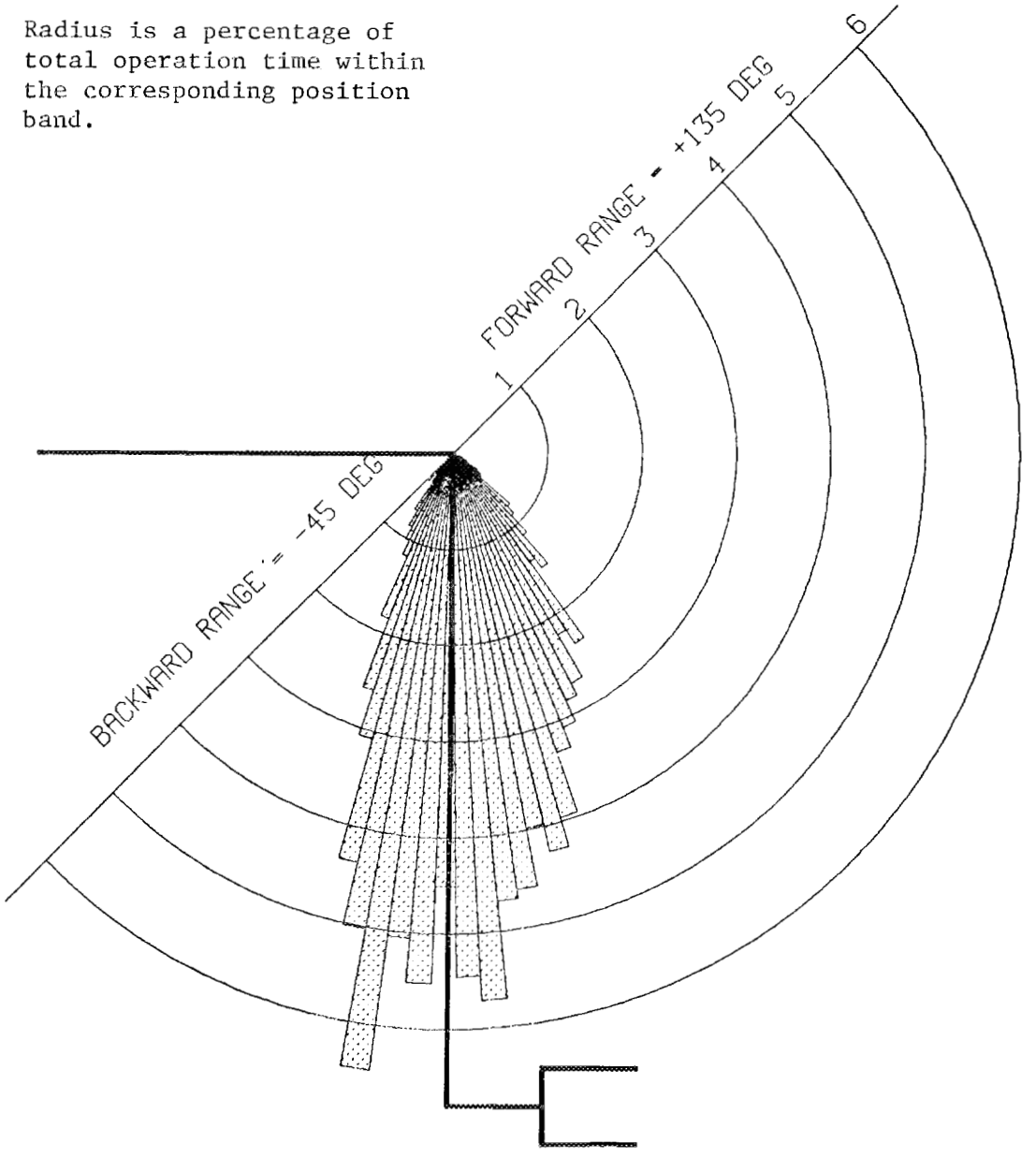


Fig. 9. Range of elbow pitch position usage.

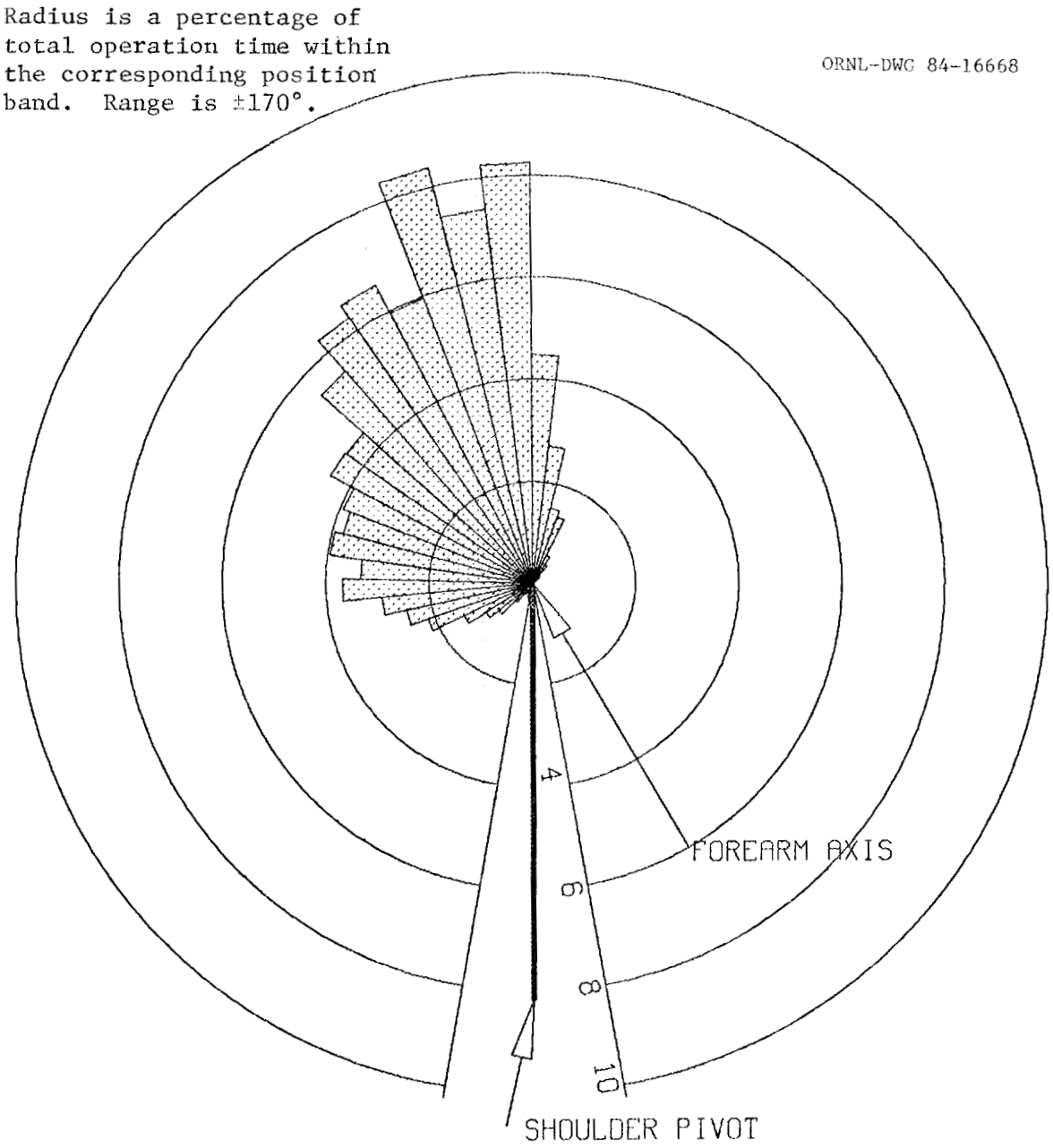


Fig. 10. Range of elbow roll position usage.

ORNL-DWG 84-16669

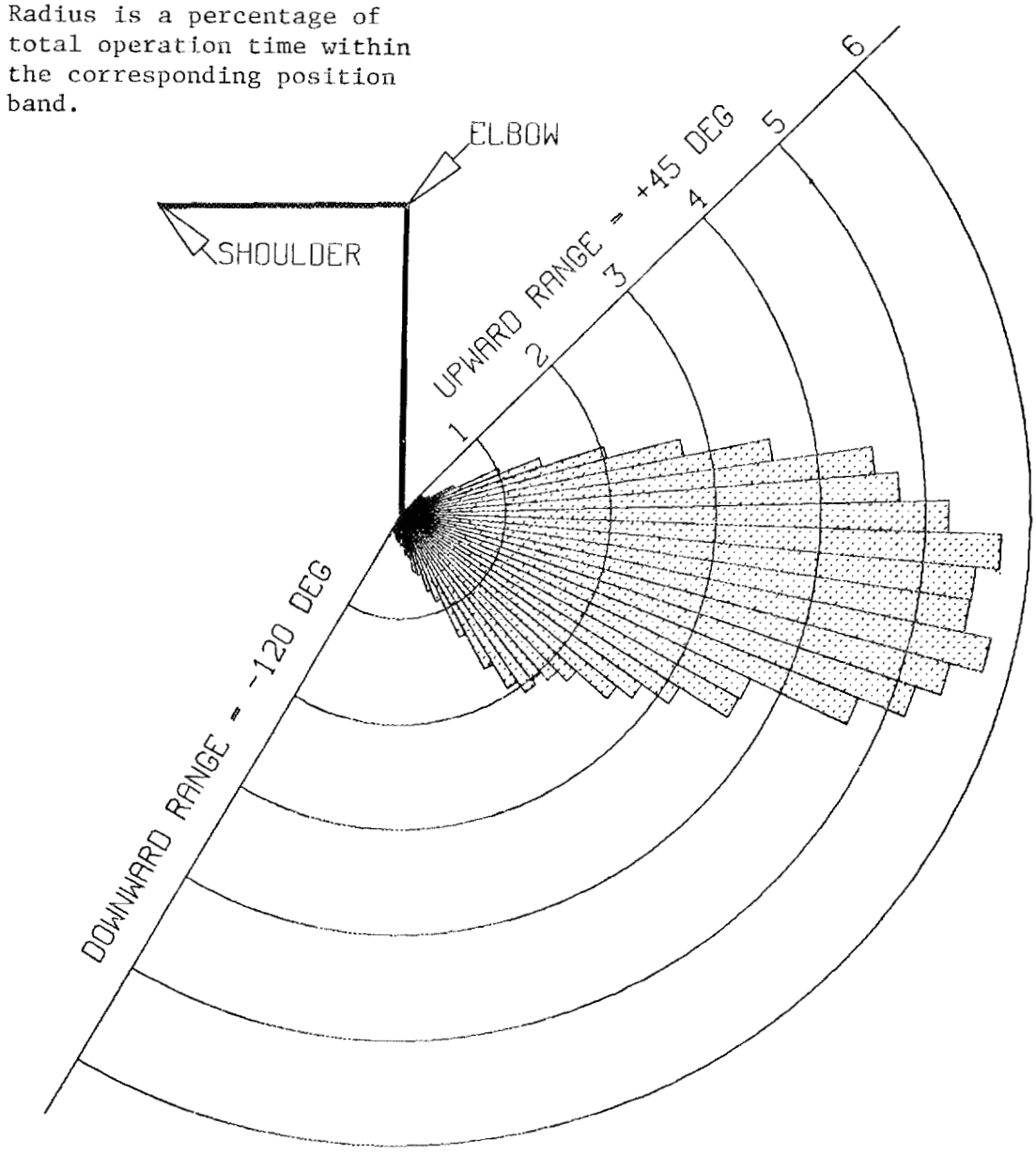


Fig. 11. Range of wrist pitch position usage.

ORNL-DWG 84-16670

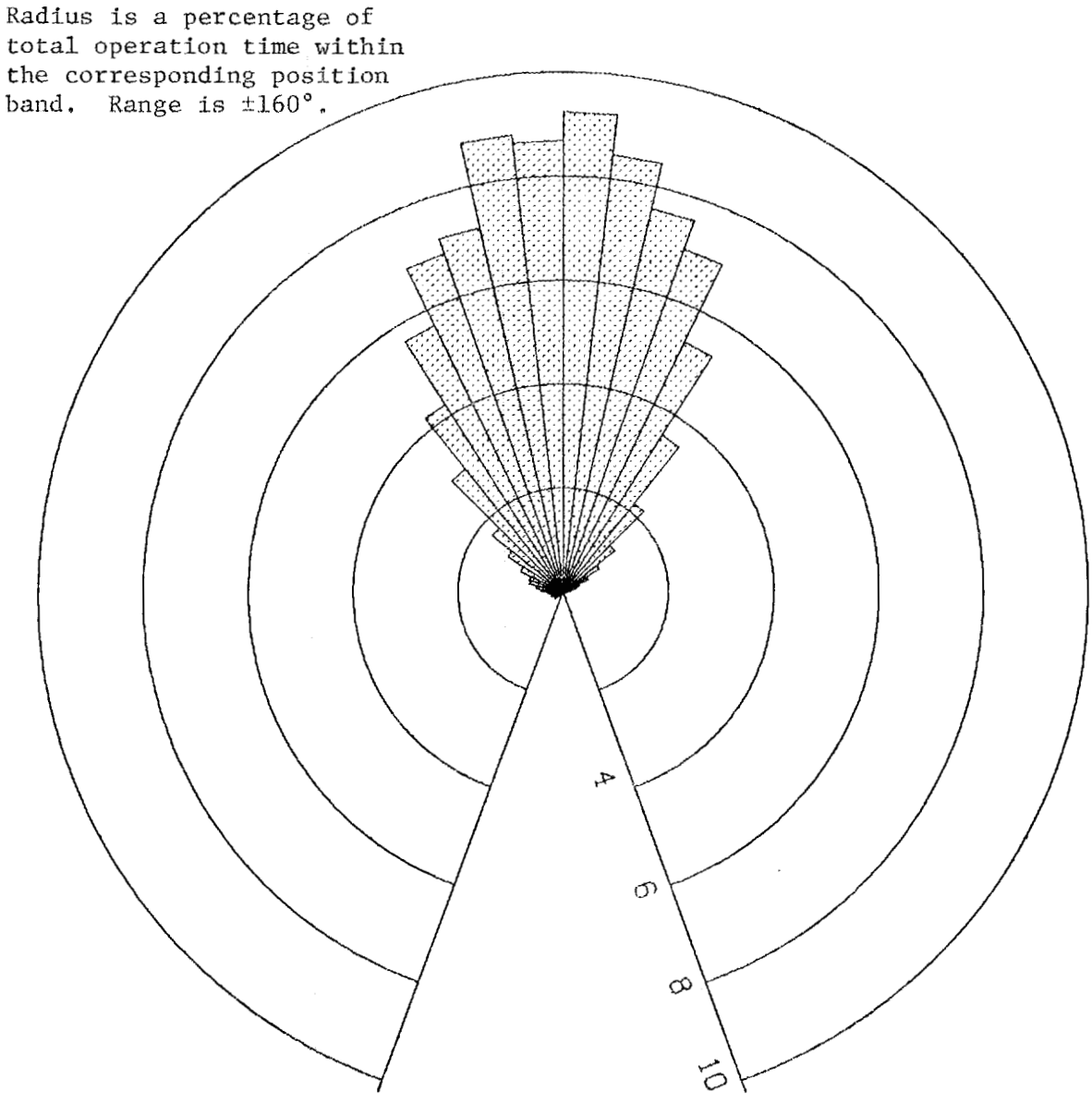


Fig. 12. Range of wrist roll position usage.

the manipulator, depending on which view clearly presents the specific joint motion in the reference position. The manipulator is sketched in as it would appear from the specific view when in the reference position. The angular range of each polar plot corresponds to the motion range of the DOF that is plotted. The radius of each "pie slice" is proportional to the percentage of total time spent, within that range of motion. A note is in order concerning Fig. 12 wrist roll position usage. To picture what is being represented, consider the tong to be holding a pin or bar such that it is vertical in the reference position. The figure represents the histogram of the orientation of that bar with respect to the wrist.

An interesting aspect of these plots is the ratio of the percentage time in 0 to 2% (98 to 100%) of range to the percentage time in 2 to 4% (96 to 98%) of range. This will be referred to as the lower (upper) "end ratio." If this end ratio is greater than one, it is an indication that the operators are taking the manipulator to its limit and holding it there. This suggests that extending this particular limit would be appropriate. Another noteworthy aspect of these plots is the percentage of range not used. This represents a range of motion that could be eliminated if any savings would be obtained. These parameters are summarized in Table 6.

### 3.2.2 Wrist Positions and Orientations

The histograms presented in the previous section, while very useful design aids, do not adequately present the location and orientation of the wrist. That is, nothing is said of where the shoulder roll and elbow pitch are when the shoulder pitch, for example, is at 28 to 30% of its range. For this reason, the 3-D histogram plots of Figures 13 through 16 are presented. Figures 13, 14, and 15 represent the position of the wrist as seen from top, right side, and back respectively; Fig. 16 plots the elbow roll versus the wrist pitch. In each of these plots, the darkest areas are those used the most. The single most used block is entirely black. The next shade (which appears black) represents those areas whose time use was 60 to 100% that of the most used block, the next shade represents 36 to 60%, the

next 21.6 to 36%, and so on. This geometric scale with a ratio of 0.6 was chosen so that the lightest of the ten shades represents 1% of the time use of the most used block. Areas that were used, but for a time less than 1% of the maximum are indicated by light dots.

Table 6. DOF position end ratios and unused ranges

| DOF | Positive | | | Negative | | |
|---|---|---|---|---|---|---|
| | Percentage time at end | End ratio | Unused range (deg) | Percentage time at end | End ratio | Unused range (deg) |
| SP(+ ≡ up)[a] | 0 | 0 | 2.2 | 0.38 | 2.42 | 0 |
| SR(+ ≡ right)[a] | 0.01 | 0.94 | 0 | 1.81 | 3.23 | 0 |
| EP(+ ≡ forward)[a] | 0 | - | 45 | 0.33 | 1.53 | 0 |
| ER(+ ≡ left)[a] | 0.27 | 1.23 | 0 | 0 | - | 48 |
| WP(+ ≡ up)[a] | >.01 | .14 | 0 | 0.20 | 1.87 | 0 |
| WR(+ ≡ CCW)[b] | 0.08 | 0.89 | 0 | 0.17 | 17.1 | 0 |

[a]For each DOF, positive is that rotation which would cause the tong to move in the defined direction when the arm is in the reference position.

[b]For the wrist roll, positive is a counterclockwise (CCW) rotation when viewed from behind the manipulator.

The reference position of each of the joints is indicated by the clear round symbols. It should be clear which symbol represents the wrist.

Note that the position of the wrist when accessing the wrench holder shows up clearly on each of the position grids, but the orientation of the wrist when accessing the wrench holder (elbow roll ≈ 114 in. left, wrist pitch ≈ 14° down) does not show up. This indicates that when picking up or replacing the wrench, the operators first place the wrist near the holder, then orient the wrist. When moving away from the holder, the wrist is almost immediately oriented forward. Thus, the tool-changing configuration will significantly

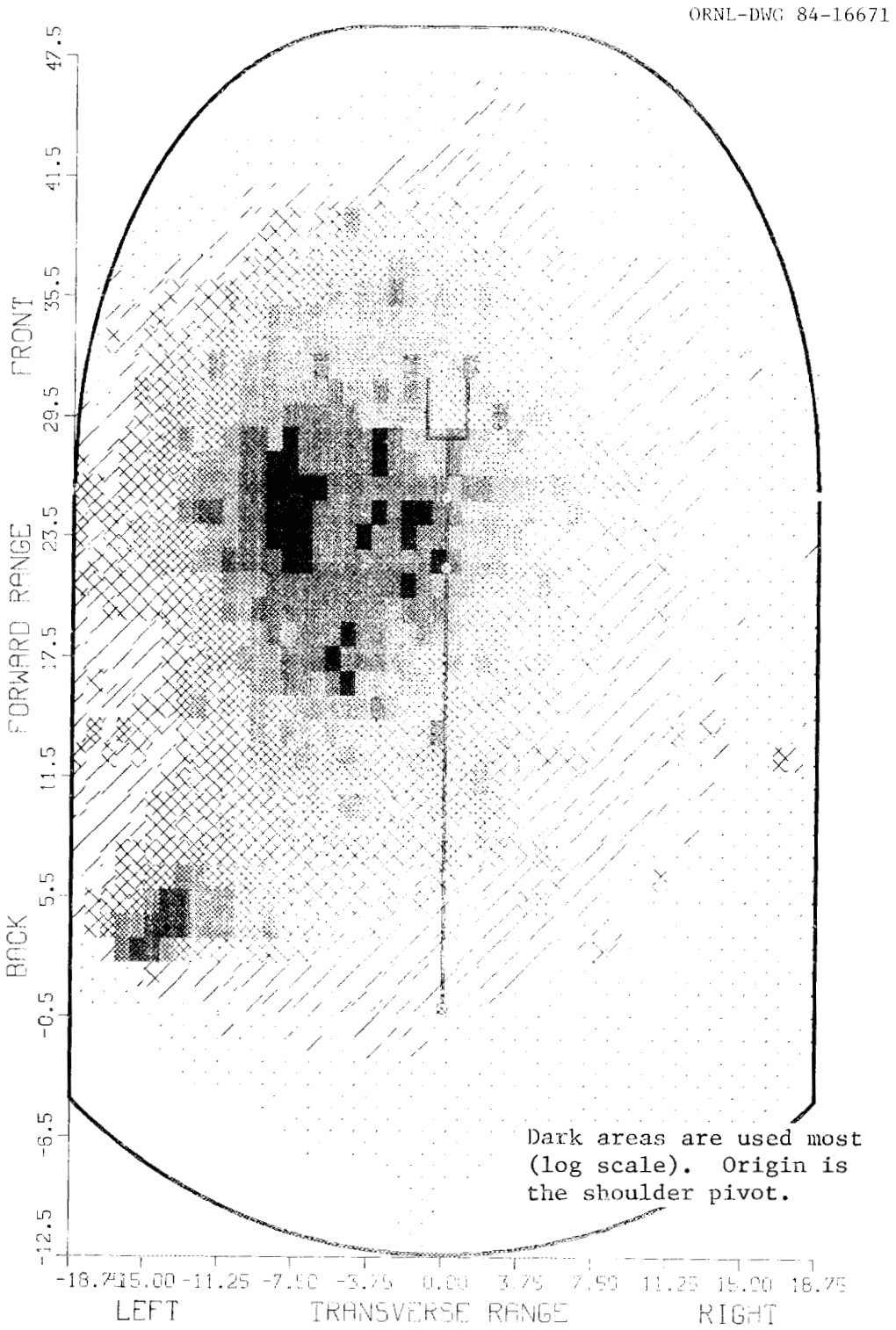


Fig. 13. Wrist position grid--top view.

ORNL-DWG 84-16672

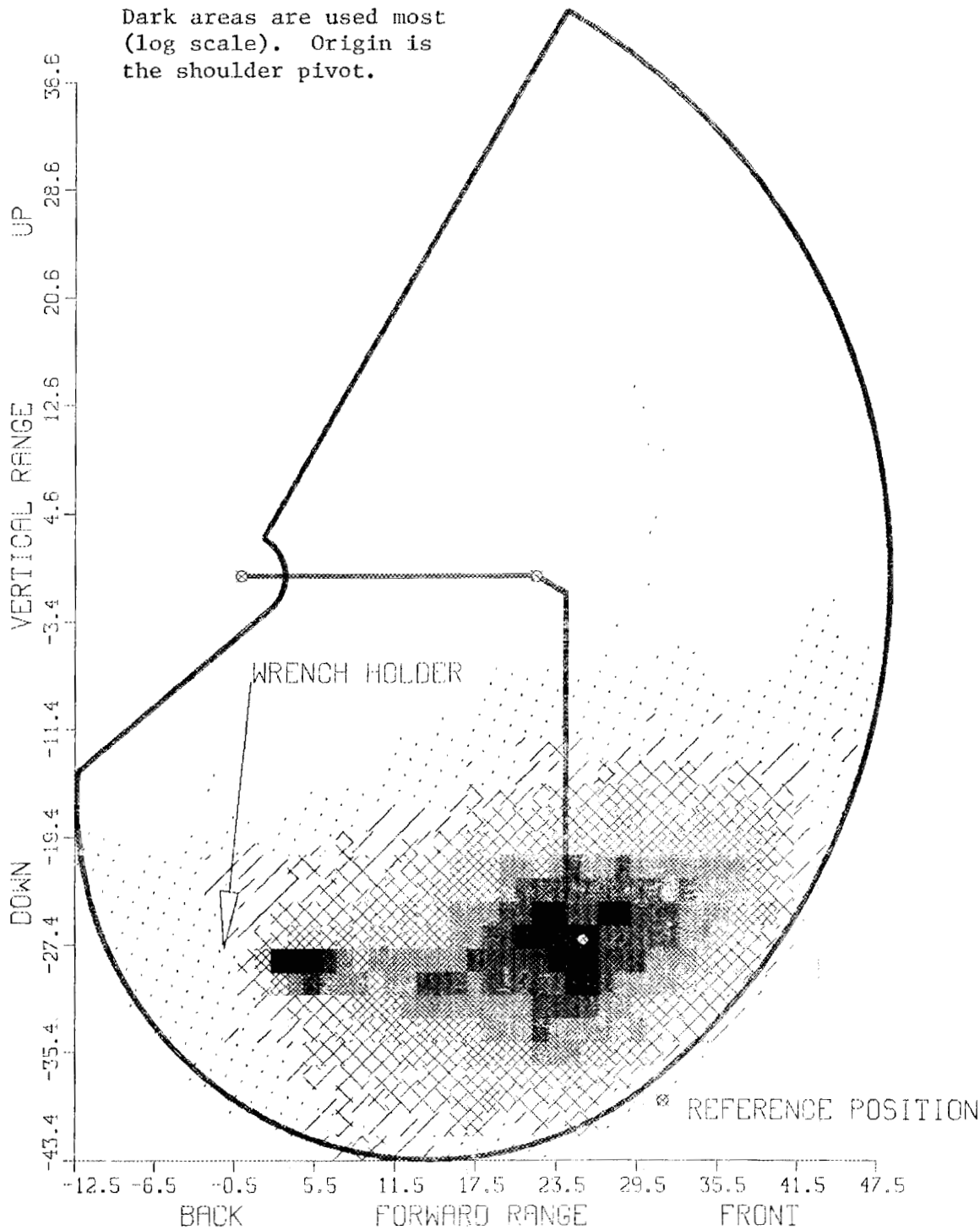


Fig. 14. Wrist position grid--right side view.

ORNL-DWG 84-16673

Fig. 15. Wrist position grid--back view.

ORNL-DWG 84-16674

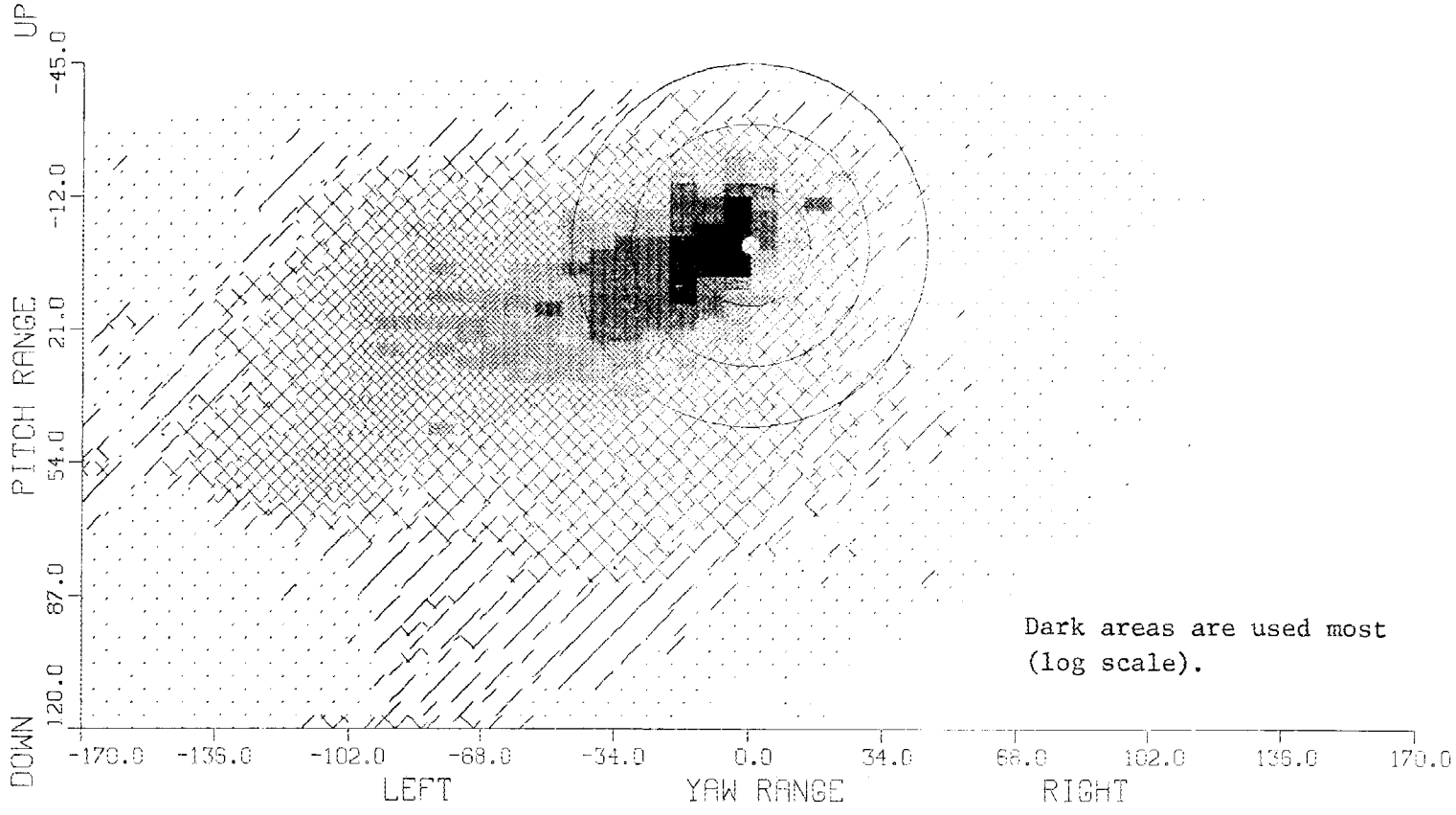


Fig. 16. Wrist orientation grid.

affect the main positions of the upper three (positioning) angles (shoulder pitch and roll, and elbow pitch) but will have only a small effect on the mean positions of the lower three (orientation) angles. As noted earlier, the operators quickly became very skilled at picking up and replacing the impact wrench and could do it in 5 s.

The top and back views clearly indicate that the wrist is taken inward toward the operator from the reference position most of the time. The top and side views indicate that except for tool changing, the wrist is used with approximate symmetry about the reference position in the forward direction, perhaps behind the reference position slightly more than in front of it. The back and side views indicate that the wrist is located slightly below the reference position most of the time, and that nearly all of the upper range of motion is never used. Note that in the top view, almost the entire range is used.

The wrist orientation grid indicates that most of the time the wrist is pitched down slightly (-5°) and yawed inward about 10 to 15°. Each of these motions is used asymmetrically about their most used positions; the wrist is pitched down more than up and yawed in more than out about the most used orientation, and even more so about the reference orientation. It is interesting to note that if one orients one's own wrist about a curve described by the centroids of each of the shaded regions, it appears to be the most natural path for the wrist to follow.

### 3.2.3 Mean Positions

It is of interest to know the mean position for the individual joints and for the absolute wrist position. These data are presented in Table 7. For the individual joints, the mean position is referenced to the reference configuration of the manipulator. For the absolute wrist positions the x, y, and z positions are referenced to the wrist position in the reference configuration.

The mean position of the individual joints was found by averaging all of the sampled data. The mean absolute wrist positions were found by finding the "centroid" of the histogram blocks, associating all of the time in a given block with the center of that block.

Table 7. Mean positions

| Location | Mean Position |
|---|---|
| Individual Joints | |
| Shoulder pitch | -9.8° (down) |
| Shoulder pitch | -13.0° (left) |
| Elbow pitch | 5.1° (forward) |
| Elbow roll | 42.5° (left) |
| Wrist pitch | -17.7° (down) |
| Wrist roll | 4.0° (CCW) |
| Base Frame wrist positions | |
| Vertical (x) | 27.36 in. (down)[a] |
| | 0.86 in. (down)[b] |
| Forward (y) | 22.21 in. (forward)[a] |
| | 3.29 in. (backward)[b] |
| Transverse (z) | 4.77 in. (left)[a] |
| | 4.77 in. (left)[b] |

[a]Relative to the shoulder pivot.

[b]Relative to the wrist position in the reference configuration.

## 3.3 MOTOR CURRENTS AND ENERGY

The periodic usage of motor currents and energy consumption will now be presented. Recall that the elbow pitch and roll are driven directly by separate motors so that normalized histogram plots of motor current and joint torque correspond exactly. This is not true of the shoulder and wrist pitches and rolls, which are driven by differentials. For these DOFs, the pitch torque is proportional to the sum of the two motor currents, and the roll torque is proportional to the difference of the two. Figures 17 through 23 present the current usage of the motors. A log scale was used so that the very short times at which the motors operated at high currents could be seen. It is important to bear in mind that the data presented earlier in Table 5, which indicated that the maximum current attainable varied with time and from

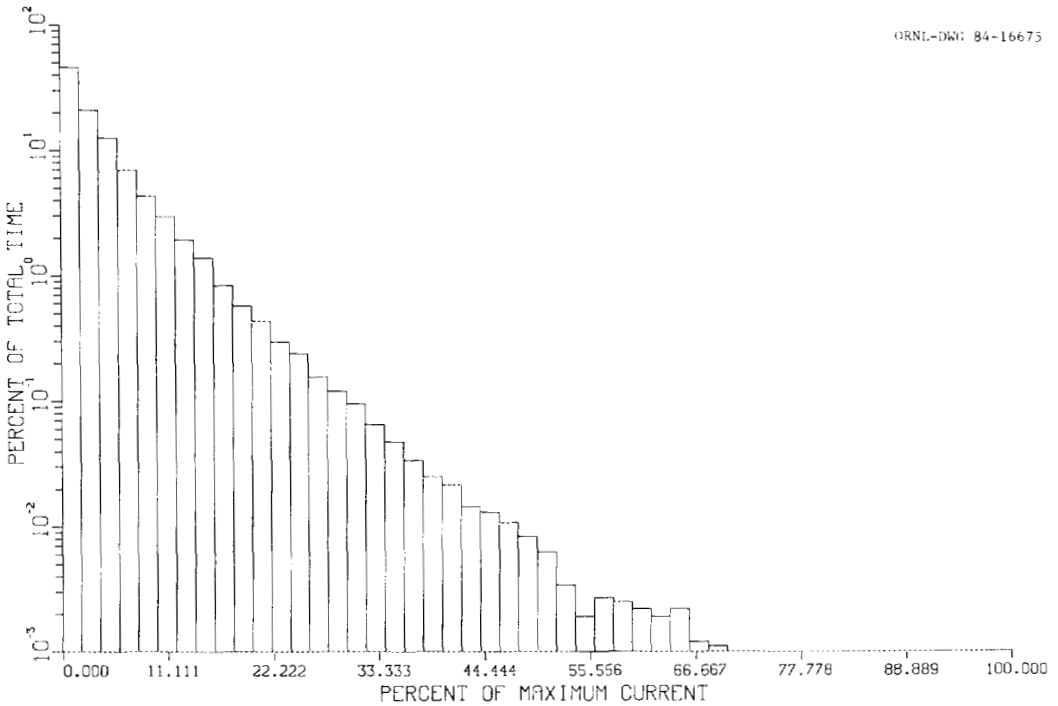


Fig. 17. Current histogram for upper shoulder motor.

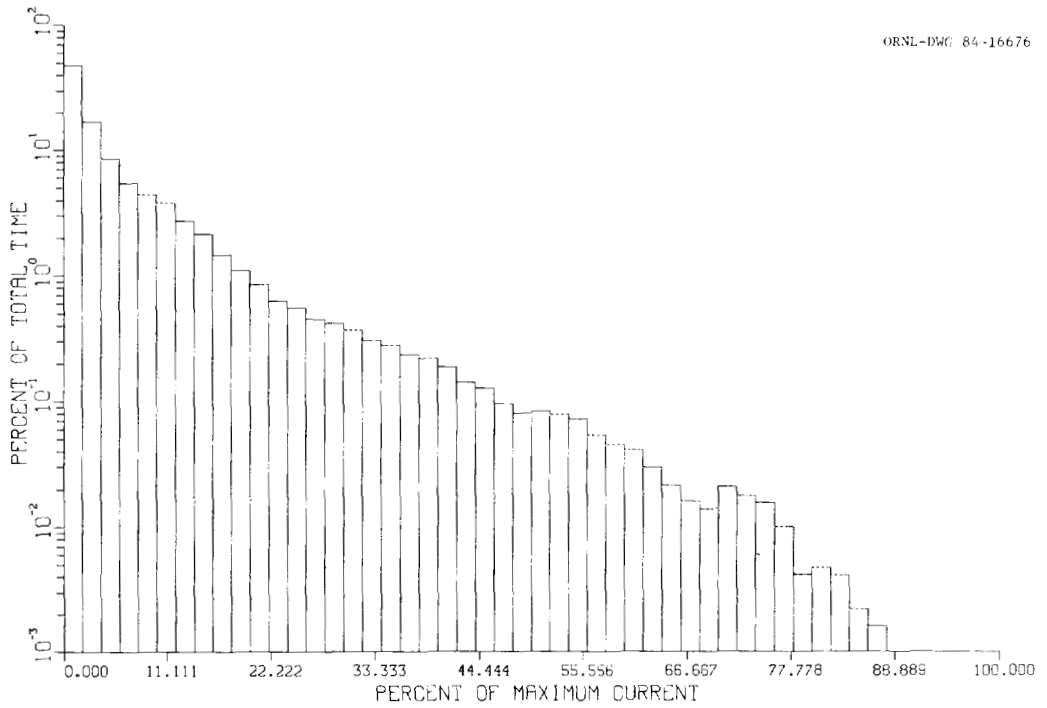


Fig. 18. Current histogram for lower shoulder motor.

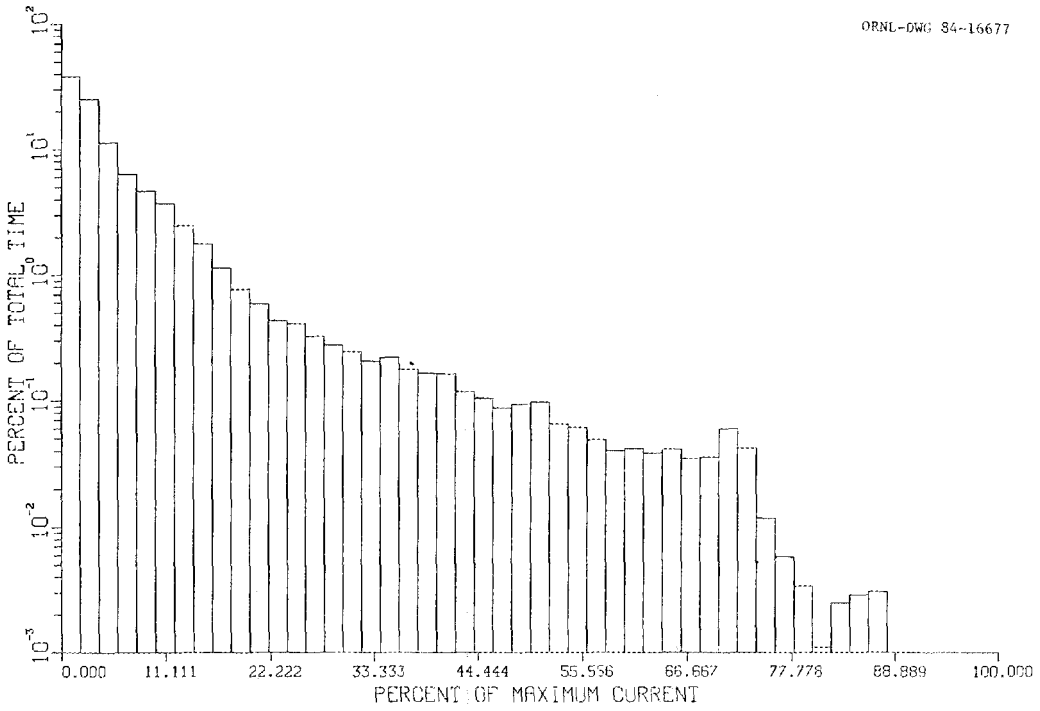


Fig. 19. Current histogram for elbow pitch motor.

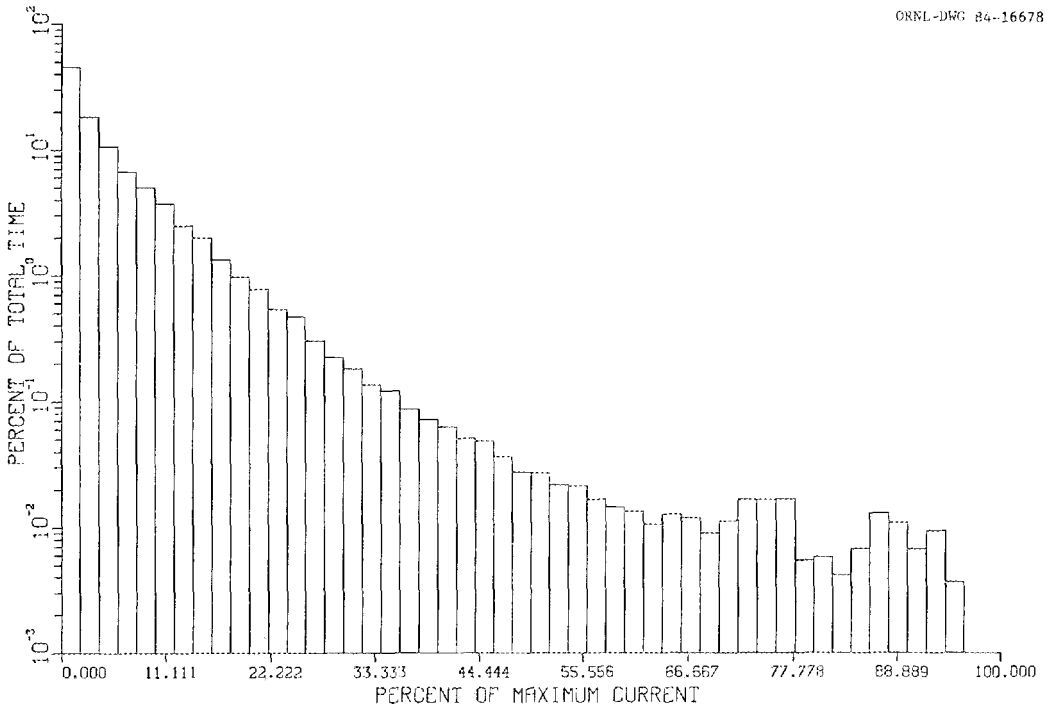


Fig. 20. Current histogram for elbow roll (yaw) motor.

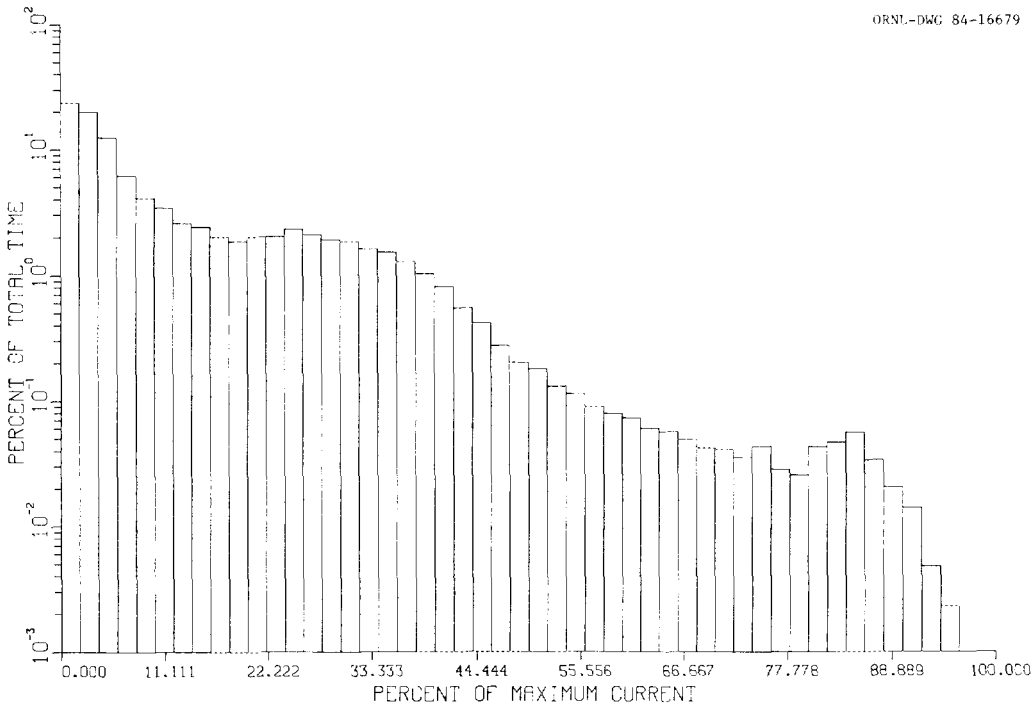


Fig. 21. Current histogram for left wrist motor.

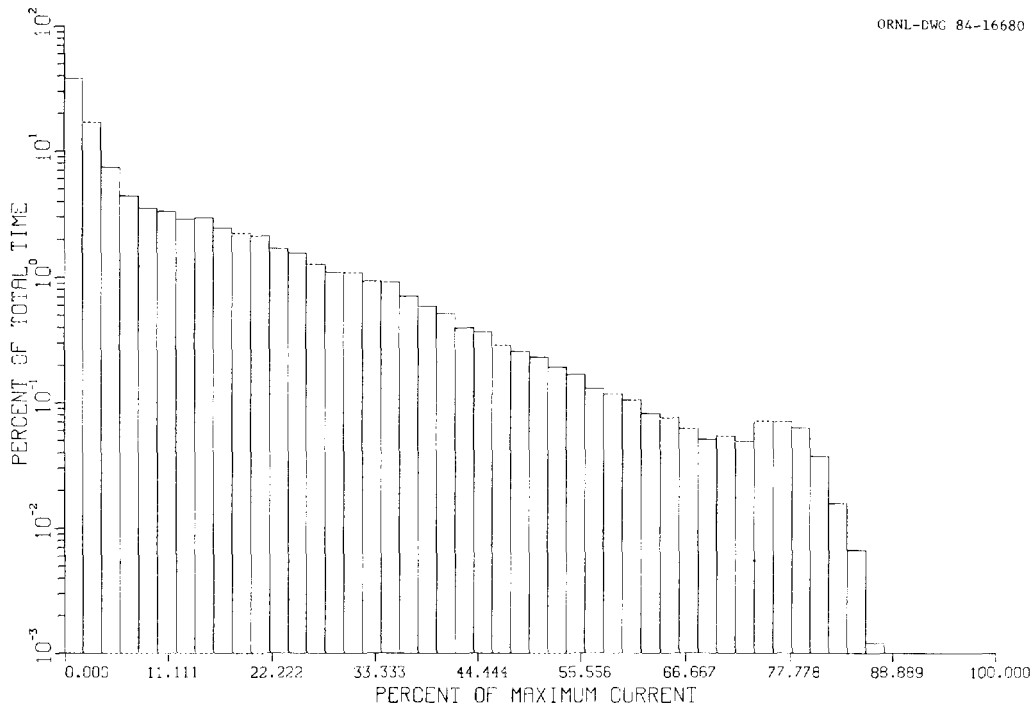


Fig. 22. Current histogram for right wrist motor.

motor to motor, was below the design limit of 4.5 A for all of the motors.

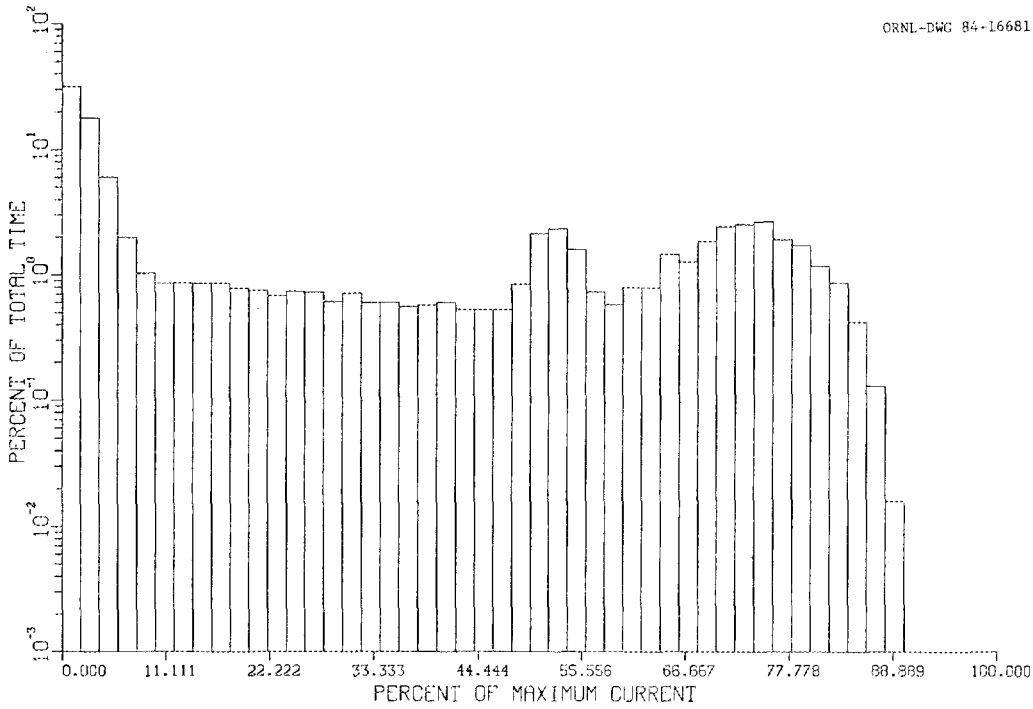


Fig. 23. Current histogram for tong motor.

Table 8 presents the average energy consumed by each motor per task. The data in this table are not the actual energy consumed by the motors but are the integrals of $I^2R$, where I is the measured current and R is the nominal value of the winding resistance for each motor supplied by the manufacturer (5.5 Ω). The actual resistances of the motors were measured, and they deviated significantly from the nominal value (data in Appendix B). Since the aim of this study is to present generic duty cycles, it was felt that the values of interest were the relative values of the integral of the current squared over time for each of the motors and that using the actual resistance values would only obscure these data. The interested reader can easily calculate the actual energies per motor if he or she desires them.

Figures 17 and 18 and Table 8 clearly show that the two shoulder motors had considerably different duty cycles. The lower shoulder motor consumed more than twice the energy consumed by the upper

shoulder motor. The histogram blocks above 33% (1.5 A) average about a decade larger on the lower shoulder motor plot than on the upper shoulder motor plot. This significant difference is related to the fact that the shoulder is rolled inward most of the time. This will be a subject of discussion in the next chapter.

Table 8. Average energy and peak current per motor per task

| Motor | Energy, W-s (percentage of tong) | | Average peak current, A (percentage of maximum) | |
|---|---|---|---|---|
| Upper shoulder | 123 | (2.7%) | 1.11 | (24.7%) |
| Lower shoulder | 273 | (6.0%) | 1.58 | (35.1%) |
| Elbow pitch | 258 | (5.7%) | 1.66 | (36.9%) |
| Elbow roll | 220 | (4.9%) | 1.74 | (38.7%) |
| Left wrist | 708 | (15.7%) | 2.45 | (54.4%) |
| Right wrist | 877 | (19.4%) | 2.63 | (58.4%) |
| Tong | 4522 | (100%) | 3.23 | (71.8%) |

Comparing the lower shoulder and elbow pitch motor data indicates comparable duty cycles in both current distribution and total energy.

The elbow roll histogram data (Fig. 20) indicates a smooth drop up to about 70% of peak current but rises slightly above this value. This rise is an indication that the motor and/or gear reduction is undersized.

The high wrist torques alluded to earlier can be seen clearly by comparing Figs. 21 and 22 to Figs. 17 through 20. For the wrist motors, the histogram blocks above about 20% are considerably higher than those of the other DOFs. Additionally, each wrist motor consumed more than three times the energy consumed by any other motor, with the exception of the tong motor.

The duty cycles of the tong motor were surprising. This motor, which performed practically no mechanical work, consumed about twice the energy of all six of the other motors combined. The rise in the height of the histogram blocks at high currents indicates that the

operators hold the tong gripped tightly shut much of the time. This is also indicated in Table 9, where it can be seen that the tong motor remained continuously above 60% of peak current for an average of 27.7 s for each task.

Table 9. Average and maximum continuous time above 60% current (in seconds)

| Motor | Average time over 60% current per task | Maximum time over 60% (overall) |
|---|---|---|
| Upper shoulder | 0.03 | 5.9 |
| Lower shoulder | 0.4 | 13.8 |
| Elbow pitch | 0.3 | 9.7 |
| Elbow roll | 0.3 | 10.1 |
| Left wrist | 0.8 | 11.8 |
| Right wrist | 1.0 | 12.6 |
| Tong | 27.7 | 273.1 |

## 3.4 JOINT VELOCITIES

Figures 24 through 29 present the use of the DOF velocities in histogram form. Each DOF is scaled individually to its design range. The design ranges were given in Table 2.

A rise in the percentage time at high velocities (>90%) compared to the percentage of time in the 70 to 90% range is an indication that a higher maximum velocity is desirable. When a DOF is moving at close to its maximum velocity, there is very little force feedback in that DOF. Note that high-velocity spikes can occur due to collisions with the surroundings. This is the case with the shoulder pitch. It is clear that the velocities indicated in the 98 to 100% block were caused by such collisions rather than continuous input from the operator because there were very few (<.001%) velocities above the 52% block.

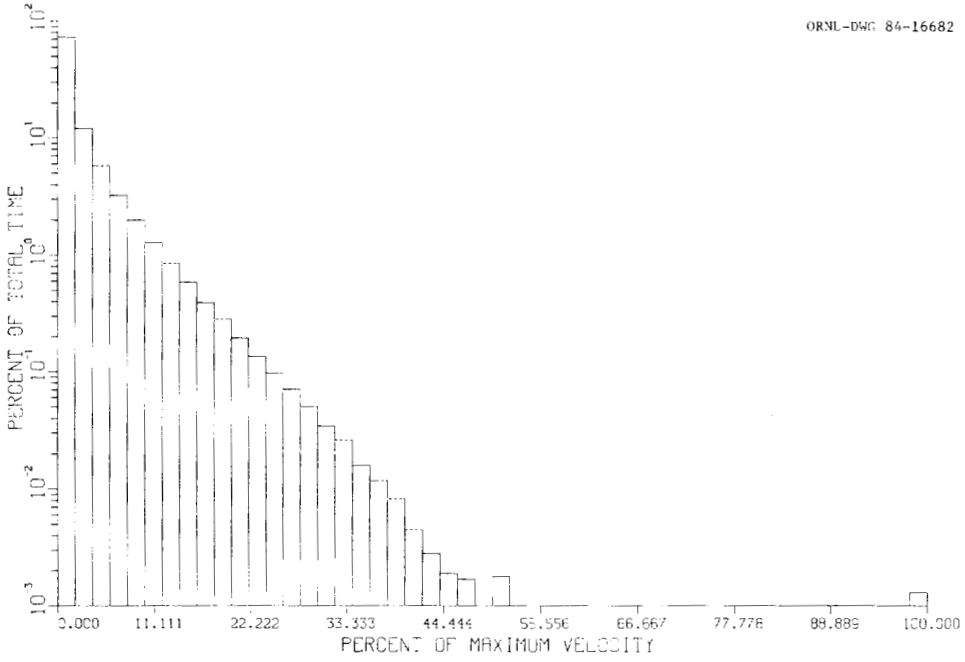


Fig. 24. Velocity histogram for shoulder pitch.

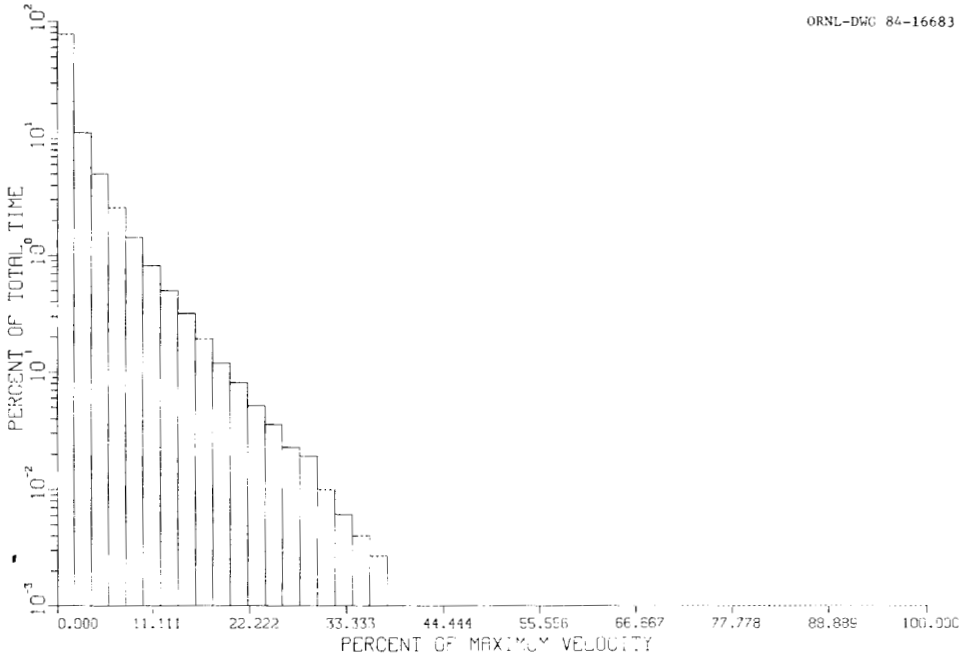


Fig. 25. Velocity histogram for shoulder roll.

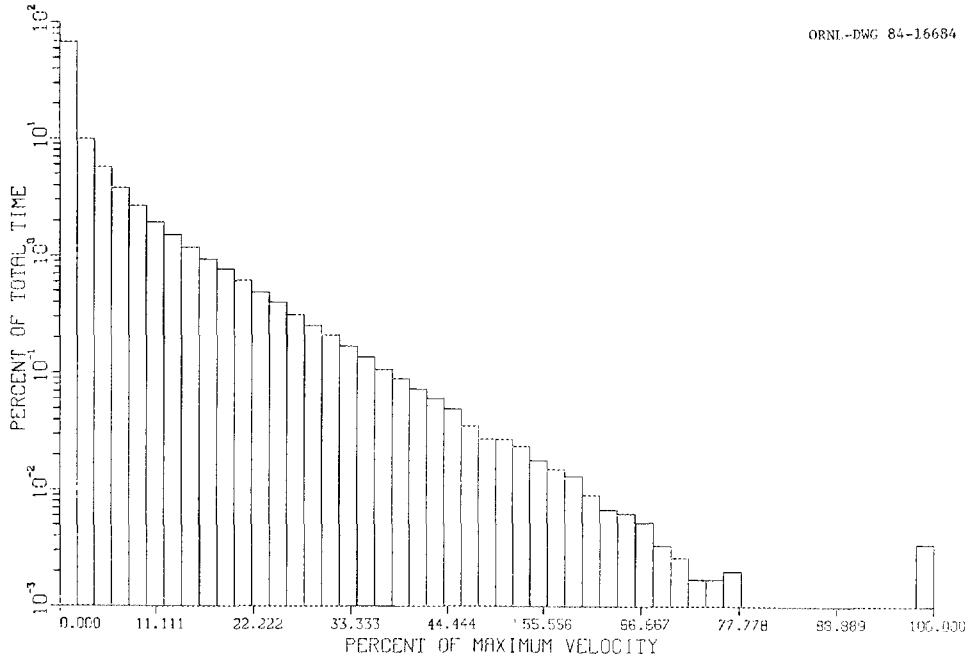


Fig. 26. Velocity histogram for elbow pitch.

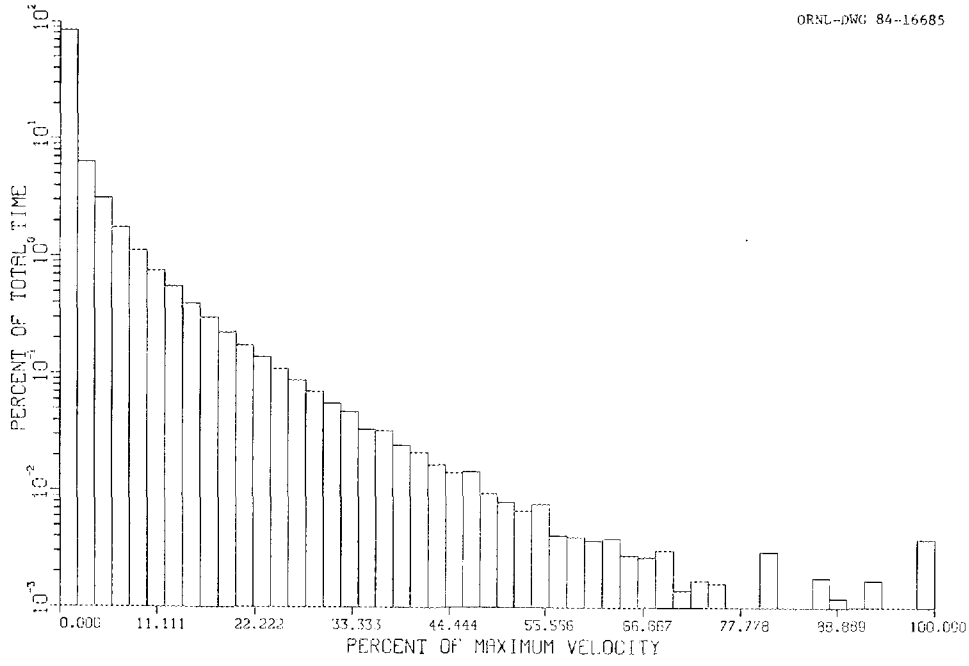


Fig. 27. Velocity histogram for elbow roll.

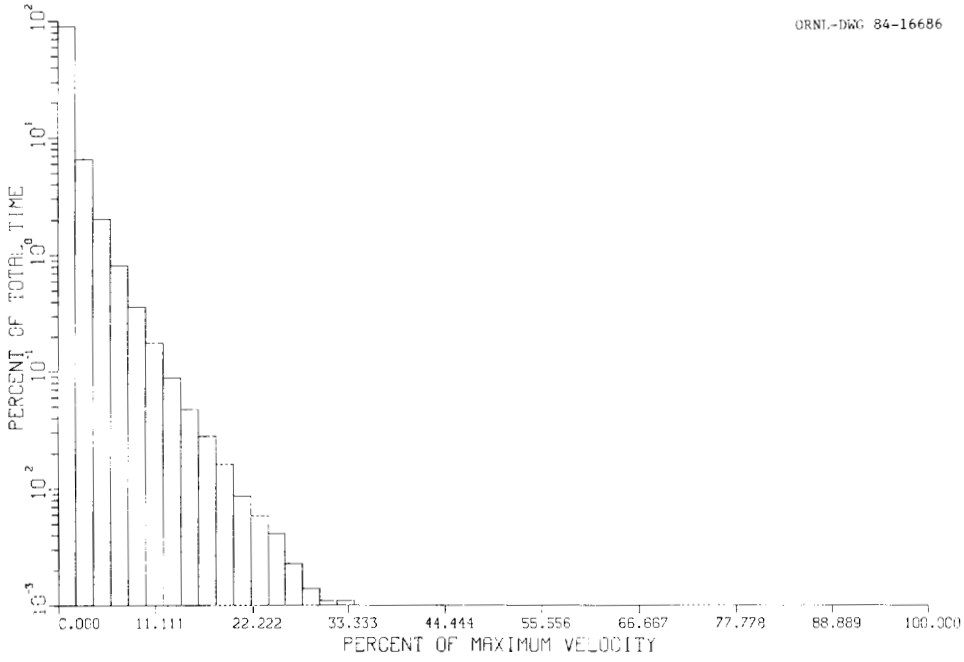


Fig. 28. Velocity histogram for wrist pitch.

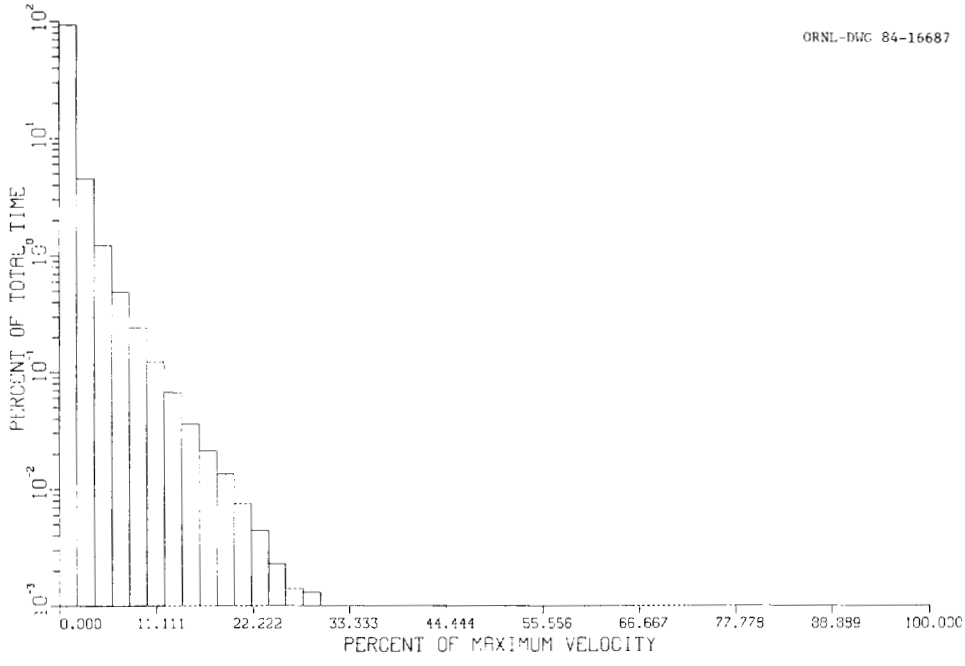


Fig. 29. Velocity histogram for wrist roll.

The elbow DOF histograms (Figs. 26 and 27) indicate that a higher maximum velocity may be desirable for these DOFs. The wrist DOF histograms (Figs. 28 and 29) indicate the opposite: their maximum velocities are well above the highest velocity ever used by the operators. The shoulder DOF histograms (Figs. 24 and 25) indicate design maximum velocities considerably above those applied by the operators, but again it must be emphasized that the control system did not allow full voltage to be applied to these motors.

Table 10 presents the average peak values of velocity and acceleration per task for each DOF.

Table 10. Average peak velocities and accelerations per task

| DOF | Average peak velocity (rad/s) (percentage of maximum) | Average peak acceleration (rad/s$^2$) |
|---|---|---|
| Shoulder pitch | 0.323 (25.4%) | 1.232 |
| Shoulder roll | 0.368 (18.7%) | 1.519 |
| Elbow pitch | 0.530 (43.7%) | 2.423 |
| Elbow roll | 2.244 (31.6%) | 15.74 |
| Wrist pitch | 1.733 (12.0%) | 13.59 |
| Wrist roll | 2.141 (9.3%) | 16.08 |

## 3.5 MECHANICAL POWER AND ENERGY

The motor current and joint velocity data will now be combined as mechanical power data. The data will be expressed in the joint coordinate system, and thus the normalized shoulder and wrist pitch torques are the sum of the two motor currents divided by twice the maximum current per motor, and the shoulder and wrist roll torques are the difference of the two motor currents divided by twice the maximum current per motor.

The mechanical power for each DOF is presented as 3-D histograms in Figs. 30 through 36. The independent variables are the normalized

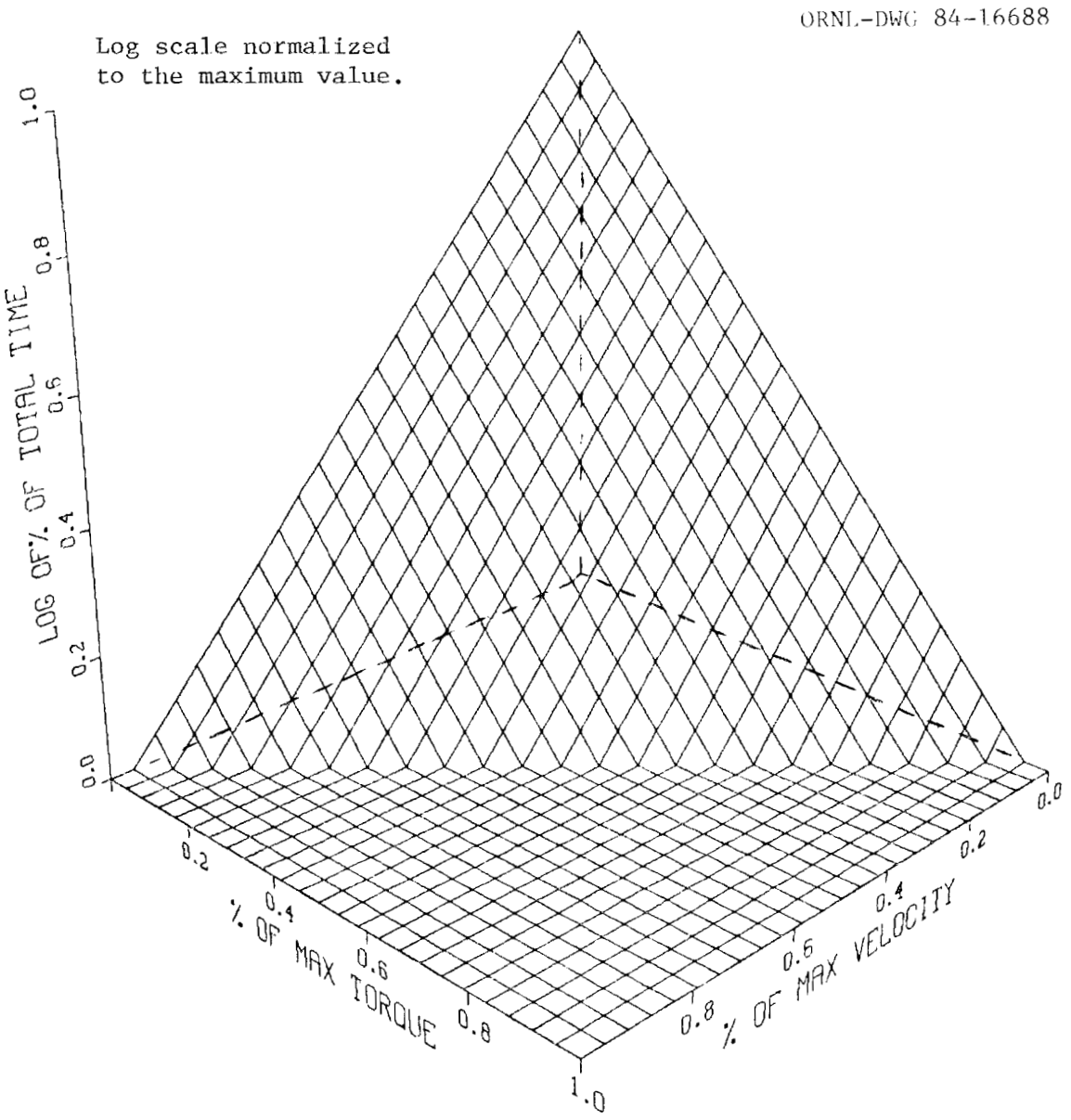


Fig. 30. Ideal mechanical power grid.

ORNL-DWG 84-16689

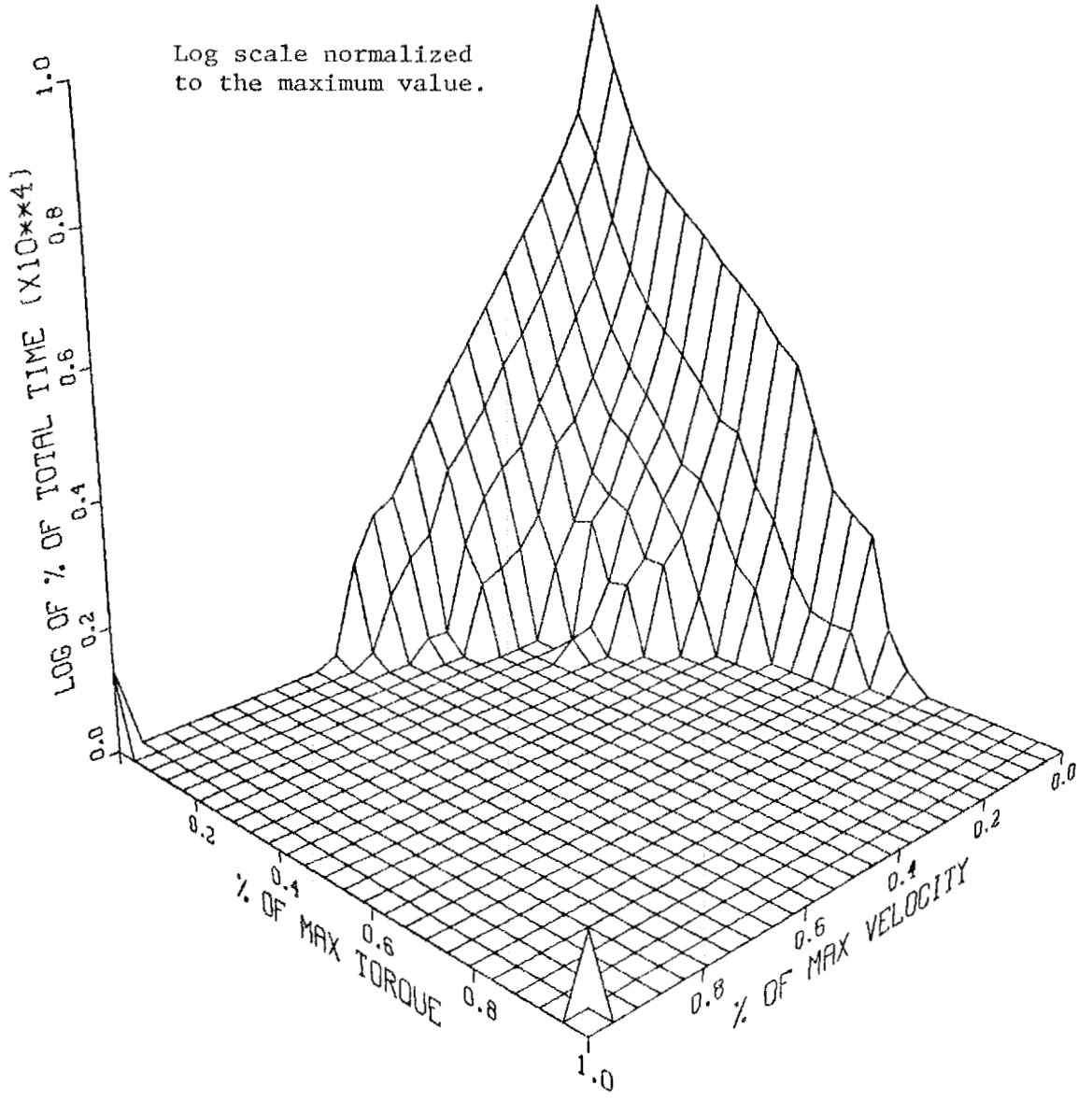


Fig. 31. Mechanical power grid for shoulder pitch.

ORNL-DWG 84-16690

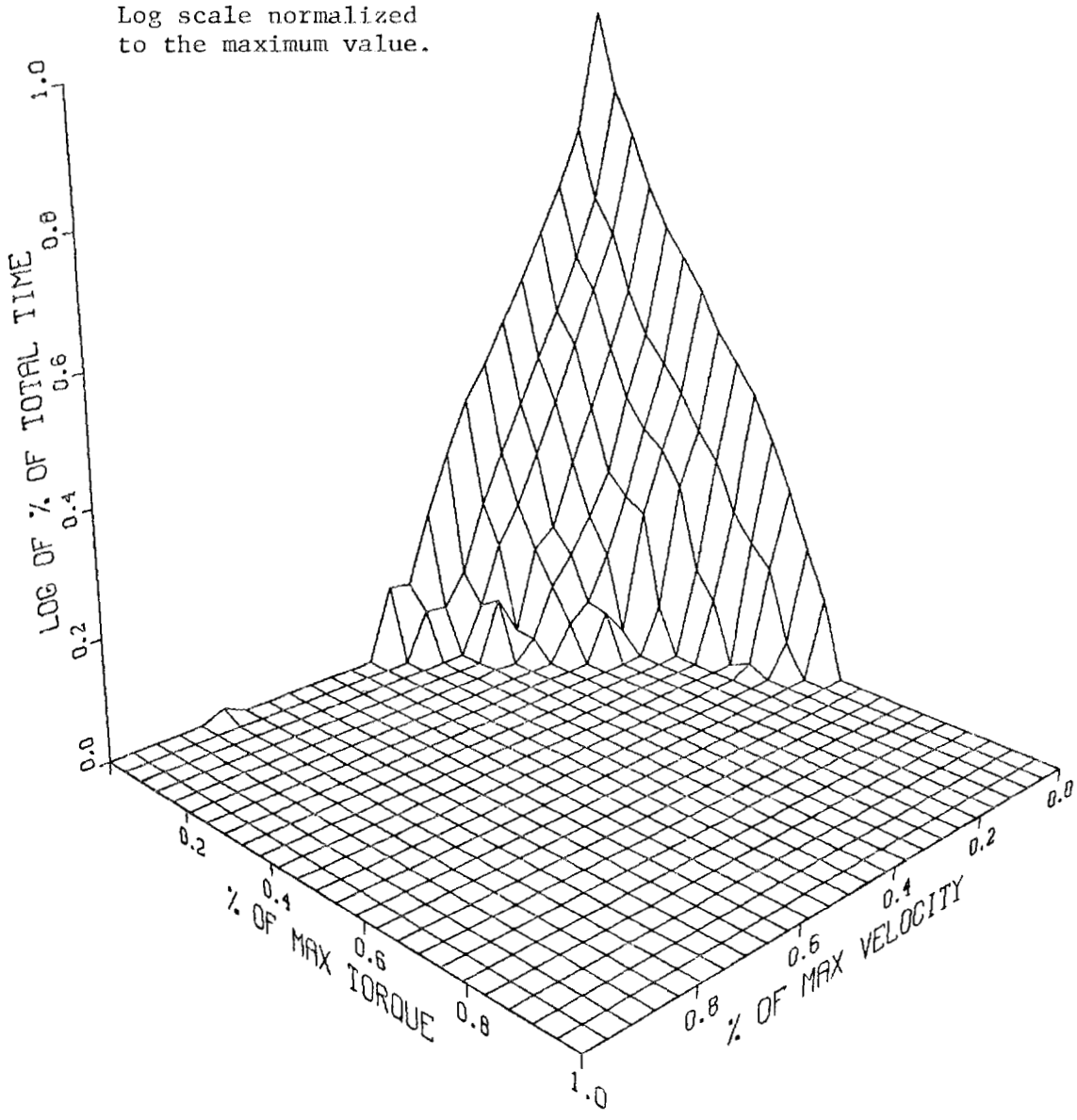


Fig. 32. Mechanical power grid for shoulder roll.

ORNL-DWG 84-16691

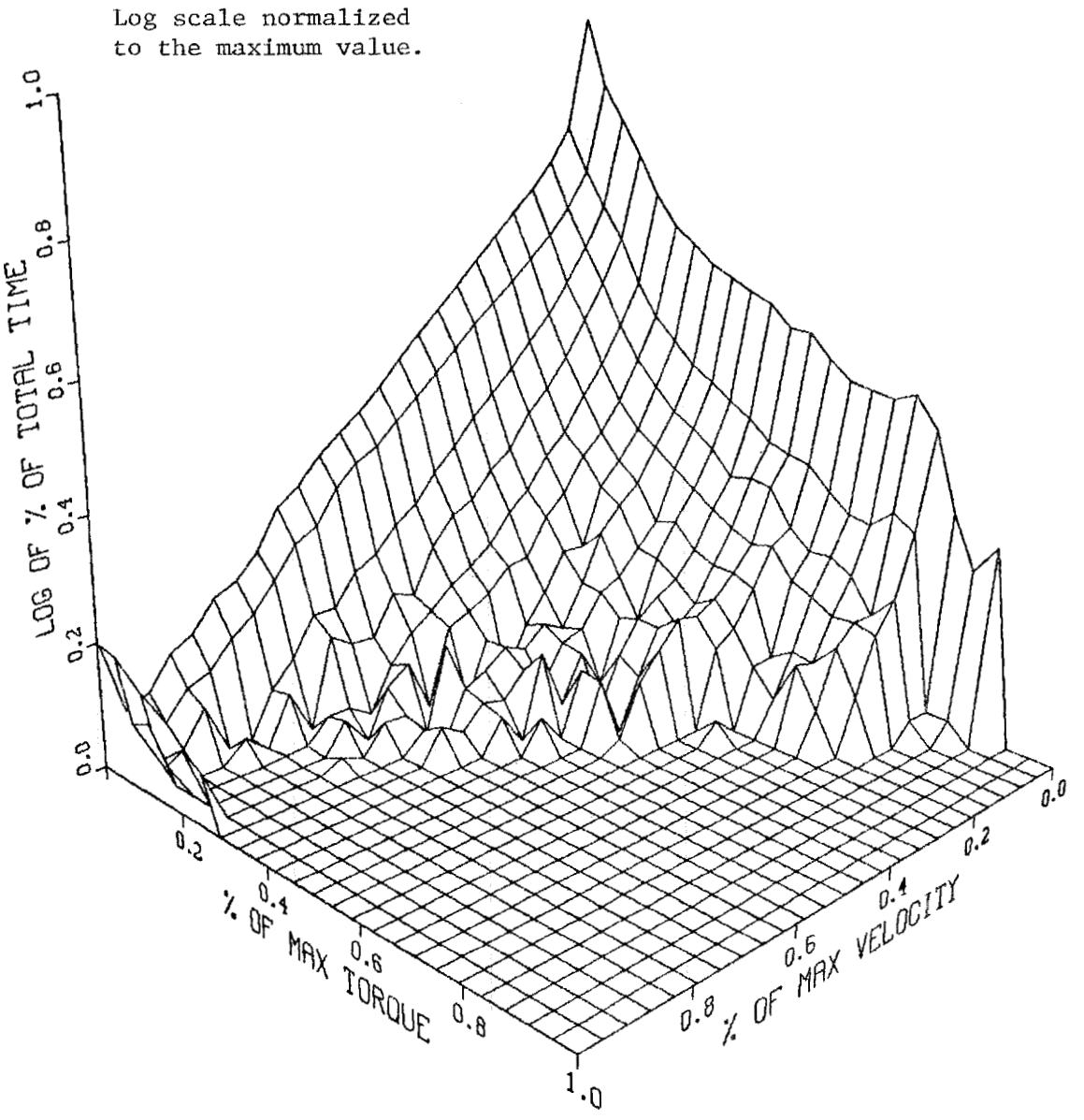


Fig. 33. Mechanical power grid for elbow pitch.

ORNL-DWG 84-16692

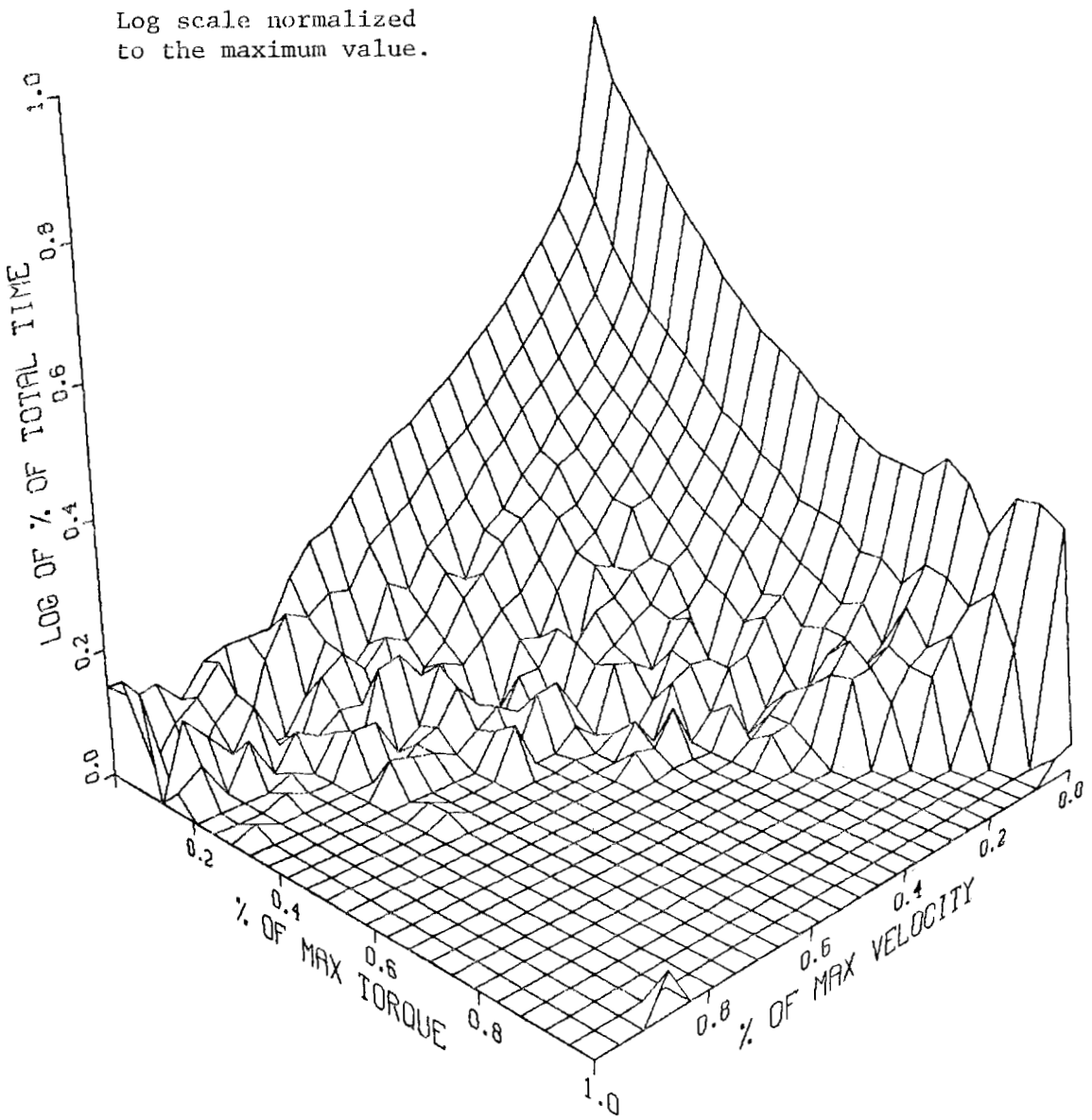


Fig. 34. Mechanical power grid for elbow roll.

ORNL-DWG 84-16693

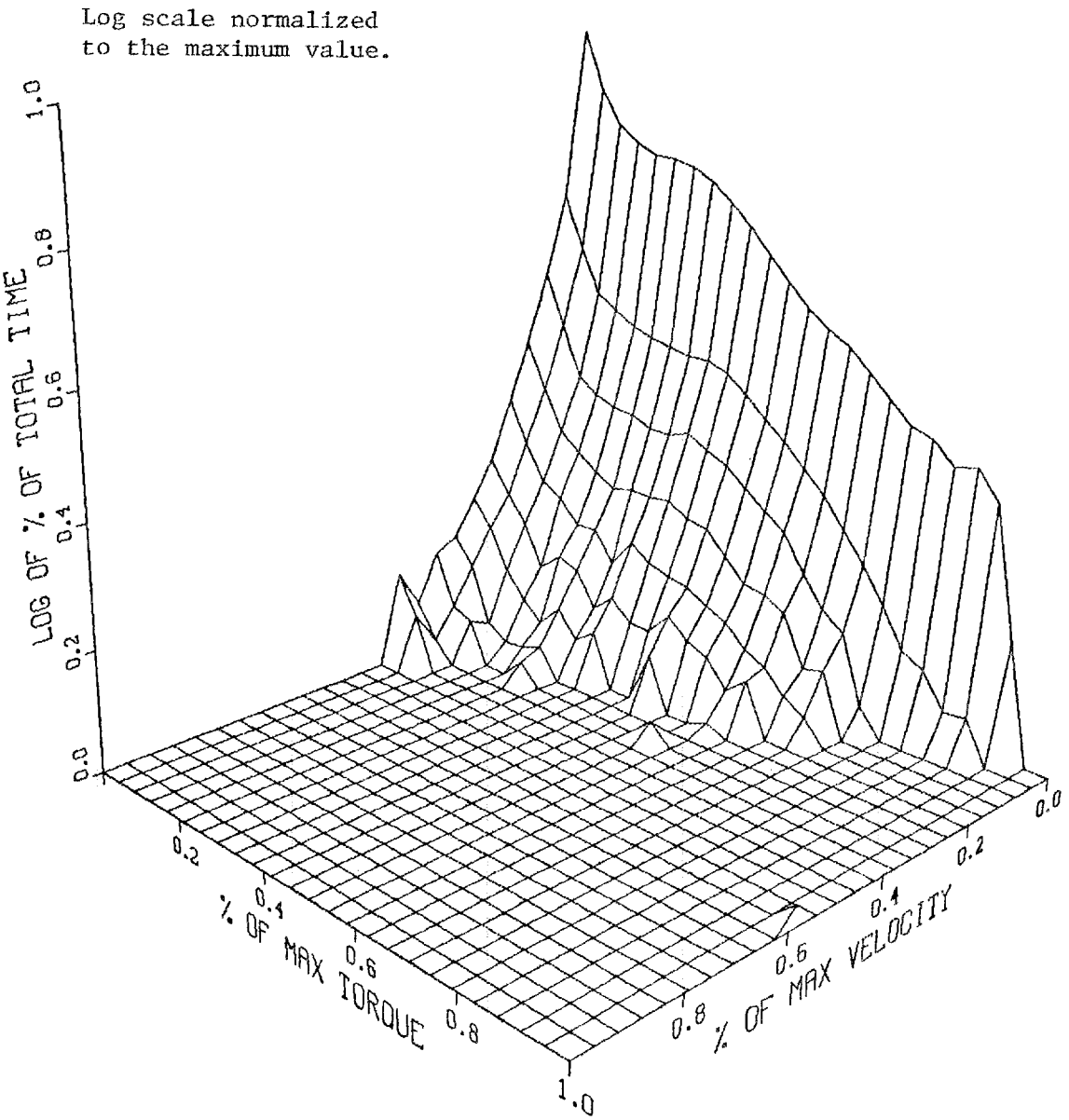


Fig. 35. Mechanical power grid for wrist pitch.

ORNL-DWG 84-16694

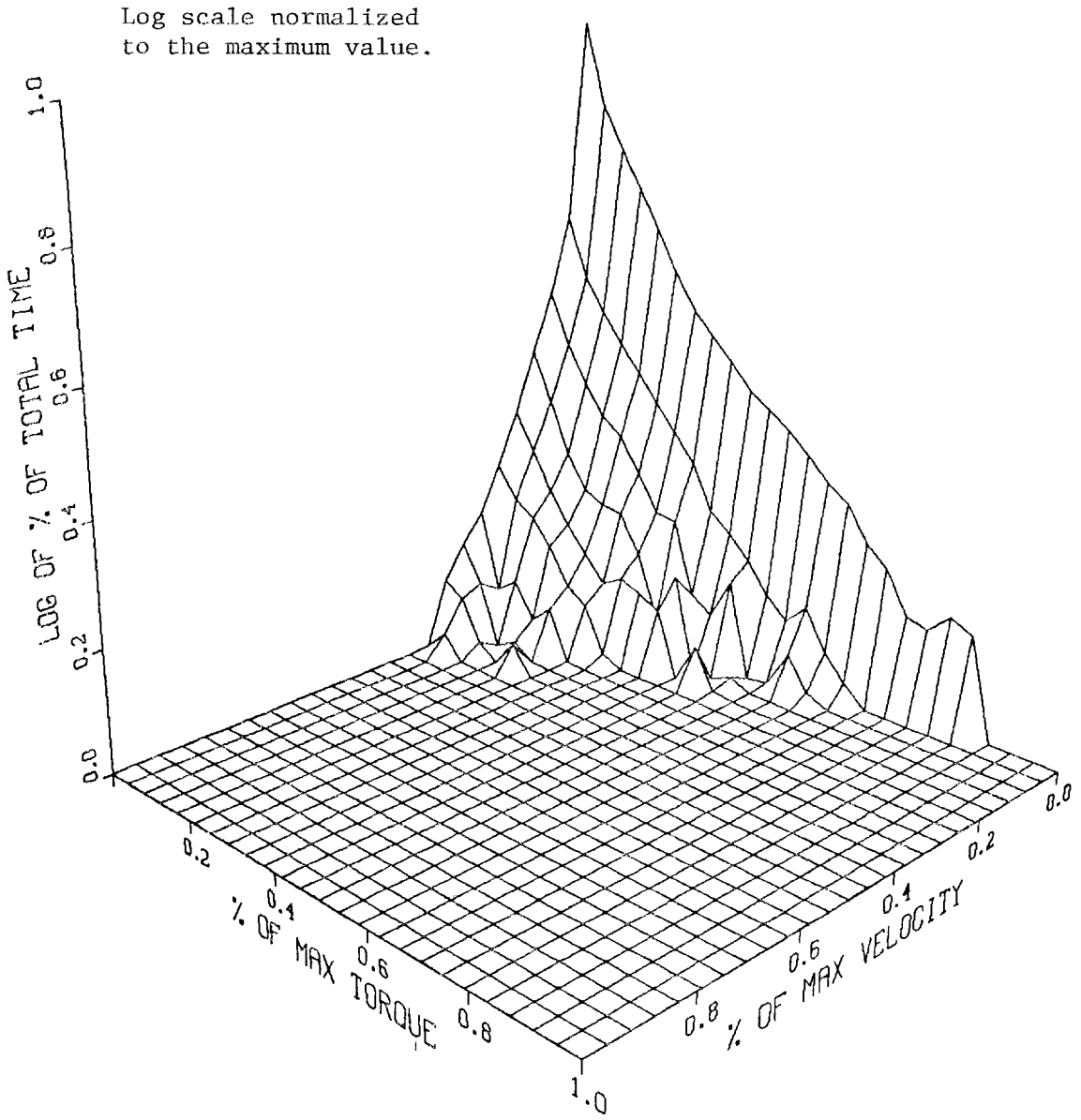


Fig. 36. Mechanical power grid for wrist roll.

velocity and torque, and the dependent variable is the log of the percentage of total operation time. The log scale was again used to emphasize the relatively short times that the DOF is used along the diagonal which ranges from peak torque through peak power (at 50% torque and 50% velocity) to peak velocity. For ease of presentation the dependent variable at each grid point was further normalized to the highest grid block, which for every DOF was the 0 to 4% torque and 0 to 4% velocity block.

Note that on some of the grids, "spikes" can be seen that indicate that time was spent at high torque and high velocity. Recall that the 2-axis scale is logarithmic, so these spikes represent very short periods of time and were most probably caused by collisions with the surroundings.

Figure 30 presents what this author feels is an "ideal" power grid. While the exact shape of this "ideal" grid is primarily a philosophical question, the points to be emphasized are that the grid is symmetric about the main diagonal (the velocity and torque potential are used equally) and is nonzero 96% of its potential in both velocity and torque. If the grid is not symmetrical about the main diagonal, then the gear reduction is such that the power of the motor is not being transferred to the joint as effectively as desired. If the grid extends to 100% of potential in either velocity or torque, particularly if it rises near 100%, then a greater potential may be needed. This can be achieved by changing the gear reduction (if the grid was not symmetric) or by using a larger motor or changing the drive method (i.e., direct drive or differential drive).

The shoulder pitch and roll grids (Figs. 31 and 32) at first glance indicate that the motors are larger than needed. The reader is again reminded, however, that full power could not be attained with these motors. In addition, the mean operating configuration of the manipulator was such that a gravity load resulted in simultaneous pitch and roll torques. The maximum torque and velocity of the shoulder pitch are based on there being no load on the shoulder roll (recall the differential drive), and the actual shoulder pitch (roll)

capacity being reduced when there is a load on the shoulder roll (pitch). Thus, the true capacity for pitch and roll torques varies from the indicated (maximum) value down to half of this value, depending on the loading. The grids are relatively symmetrical, indicating that the gear reduction is appropriate. The grids extend a little farther along the torque axis than the velocity axis so that the gear reduction should be reduced slightly.

The elbow pitch grid (Fig. 33) has a noticeable rise at 100% of velocity, indicating that this maximum velocity should be increased. The grid is relatively symmetrical, indicating that the gear reduction is appropriate. Thus, to increase the maximum velocity, a larger motor must be used. Along the torque axis, the grid drops slowly. This is primarily due to the significant friction in this DOF.

The elbow roll grid (Fig. 34) has a slight rise at peak velocity, but it is not as noticeable as it was on the elbow pitch. Significant time is spent at high torque. The grid is relatively symmetrical about the diagonal. The slight rises at peak velocity and peak torque indicate a possible need for a larger motor.

The wrist grids (Figs. 35 and 36) show that the gear reduction is inappropriate. The grids "hug" the torque axis, extending to almost 100%, but do not exceed about 40% of peak velocity. The gear reductions could easily be doubled for these DOFs.

The mechanical energy generated in each joint was calculated for each task by integrating the absolute value of torque times angular velocity. This gave the total flow of energy per joint, <u>not</u> the net energy applied by the manipulator. Note that this energy includes both that lost to friction and that used to accelerate and decelerate masses. These results are given as an average value per task in Table 11 along with an average value of the peak power per task.

## 3.6 POSITION-TORQUE RELATIONSHIPS

It is of interest to know the position of the joints at the time they experience high torques. This has applications in analyzing the wear and stress in the various components. These data are presented

in Figs. 37 through 42. The format is much the same as for the mechanical power grids, although the perspective has been changed to more clearly view the torque distribution along a given position line.

The shoulder pitch grid (Fig. 37) shows that moderate torques (<40%) are distributed in an approximate Gaussian time distribution about the mean operating position (-9.8°). Peak torques are at about -8° and about -40°. The shoulder pitch is at about -40° when the wrench holder is accessed.

Table 11. Average mechanical energy and peak power per task

| DOF | Energy in $lb_f$ (Percentage of shoulder pitch) | Average peak power in $lb_f/s$ (Percentage of maximum) |
|---|---|---|
| Shoulder pitch | 407 (100%) | 57 (12%) |
| Shoulder roll | 298 (73%) | 26 (5%) |
| Elbow pitch | 406 (100%) | 43 (19%) |
| Elbow roll | 292 (72%) | 54 (19%) |
| Wrist pitch | 369 (91%) | 48 (11%) |
| Wrist roll | 175 (43%) | 24 (4%) |

The shoulder roll (Fig. 38) experiences highest torques when rolled in toward the operator close to its limit. This is where gravity loading produces the highest torque on this DOF. Note that the torque dips down very low at 0°, where gravity loading produces no torque on this DOF.

The elbow pitch (Fig. 39) experiences high torques at around -10°. Note that gravity loading produces very little torque in this position (unless the shoulder is pitched considerably) so that this torque is primarily due to forward pushing and pulling loads. High torque also occurs at the back end of the range (-45°). This could be due to pushing against the limit if the master stop was slightly behind the slave stop. High torque occurs again at around +60°, probably due to gravity loading.

The elbow roll torque (Fig. 40) is fairly evenly distributed about the mean position (-42°) except for significant times at high

ORNL-DWG 84-16695

Log scale normalized
to the maximum value.

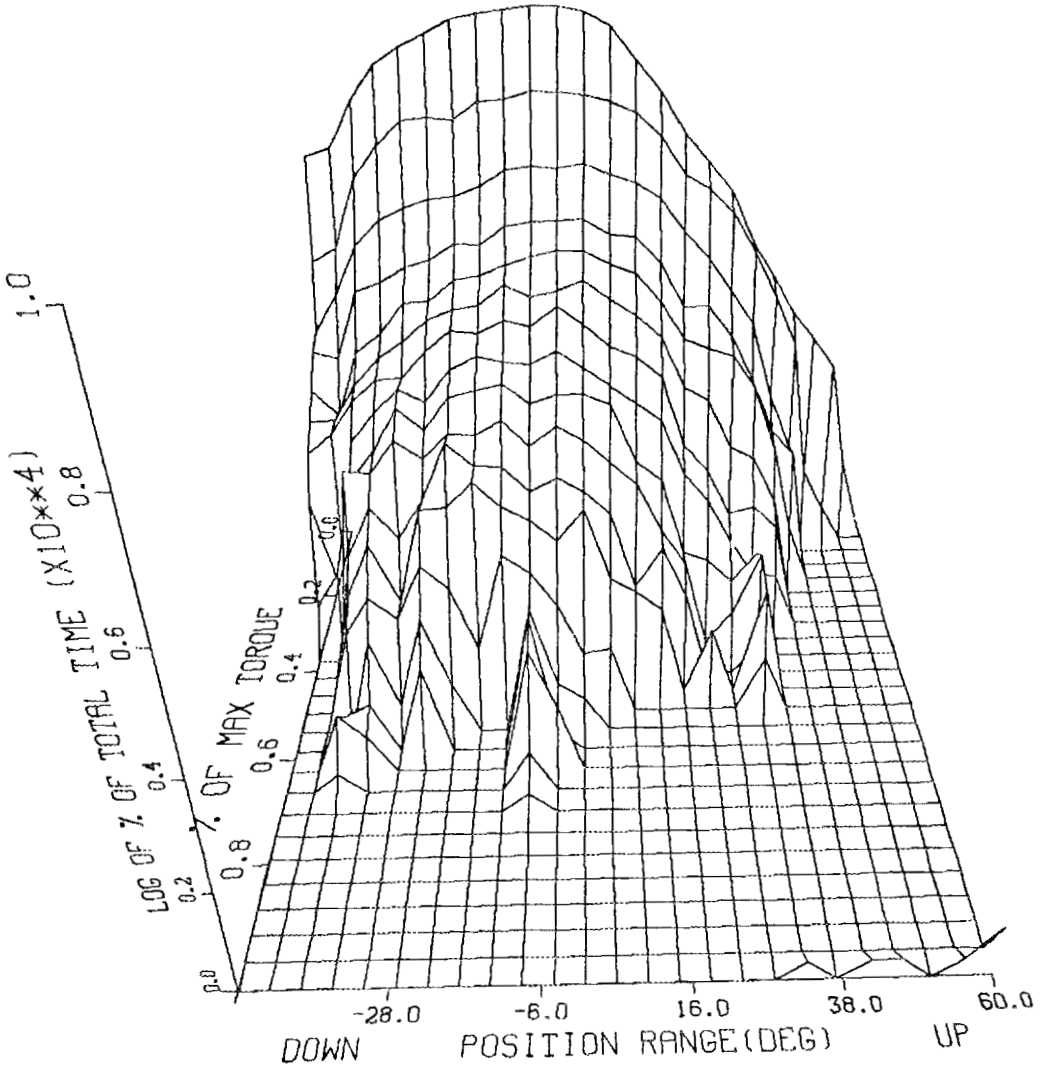


Fig. 37. Position-torque grid for shoulder pitch.

ORNL-DWG 84-16696

Log scale normalized
to the maximum value.

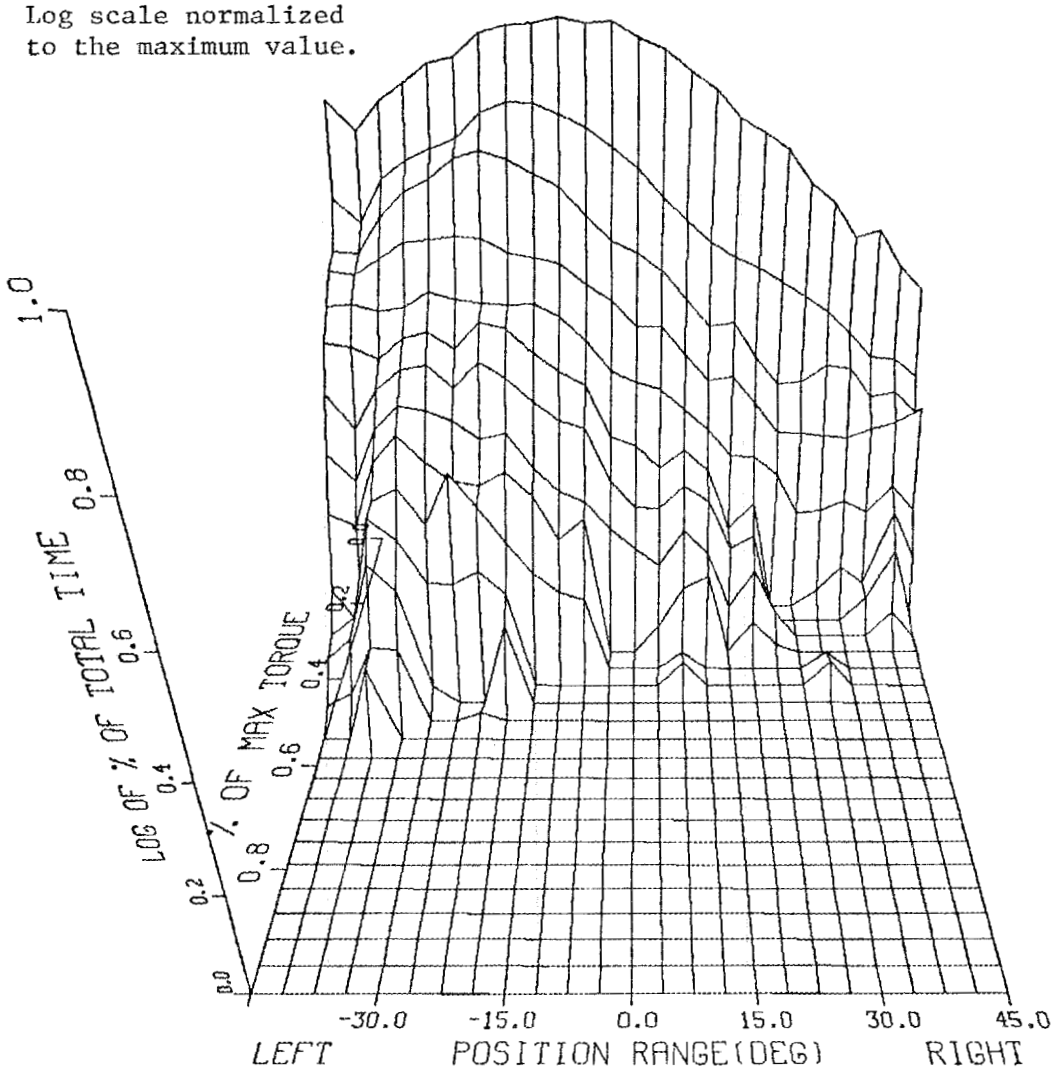


Fig. 38. Position-torque grid for shoulder roll.

ORNL-DWG 84-16697

Log scale normalized
to the maximum value.

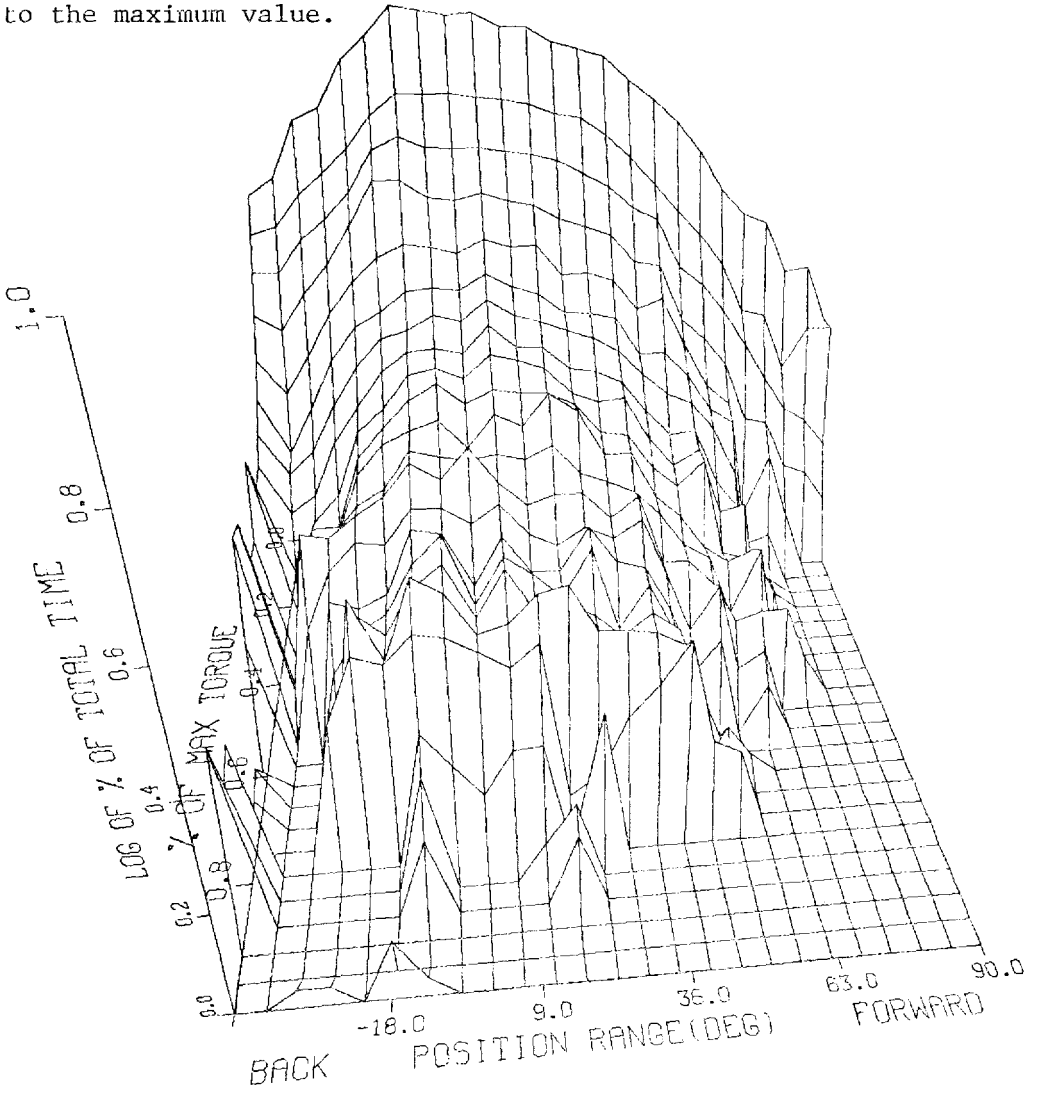


Fig. 39. Position-torque grid for elbow pitch.

ORNL-DWG 84-16698

Log scale normalized
to the maximum value.

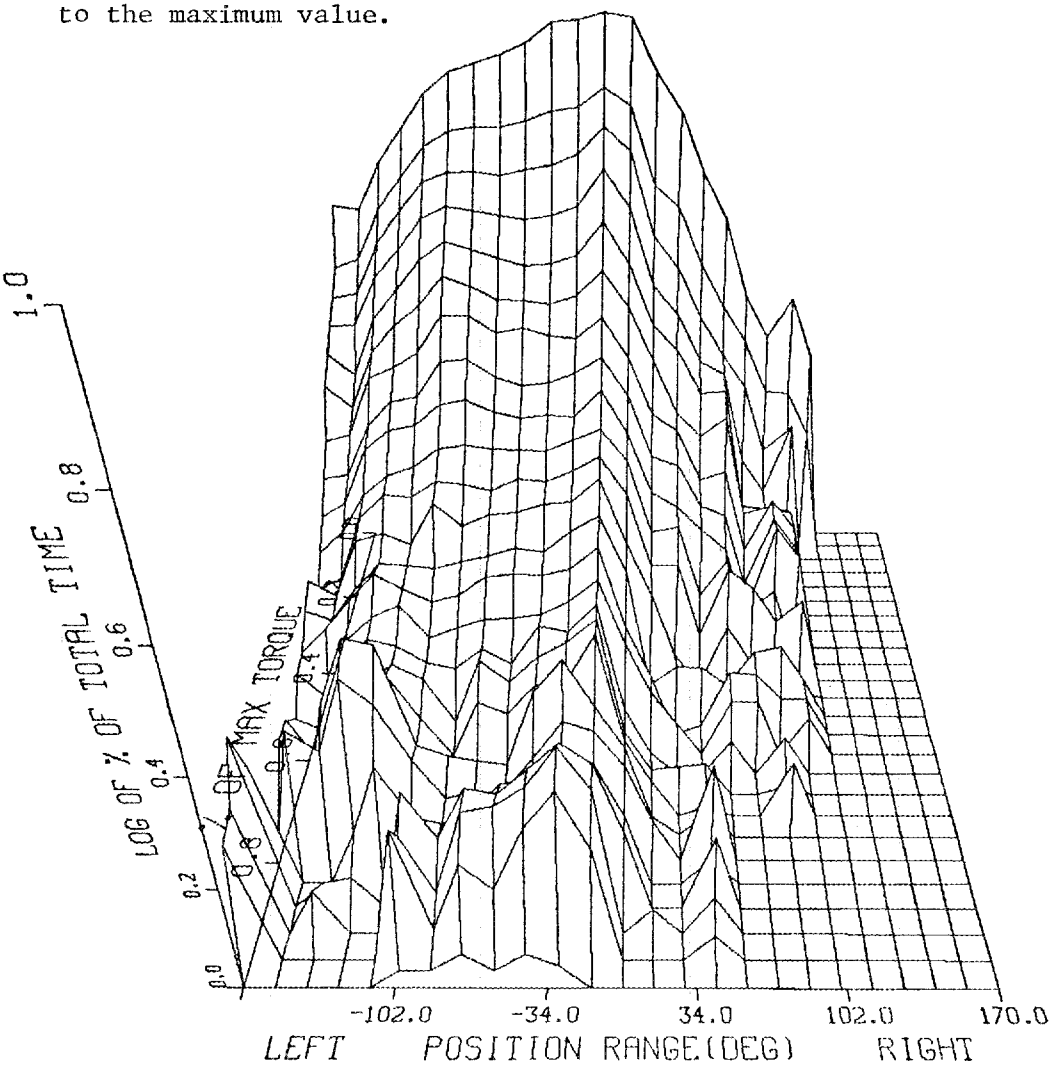


Fig. 40. Position-torque grid for elbow roll.

ORNL-DWG 84-16699

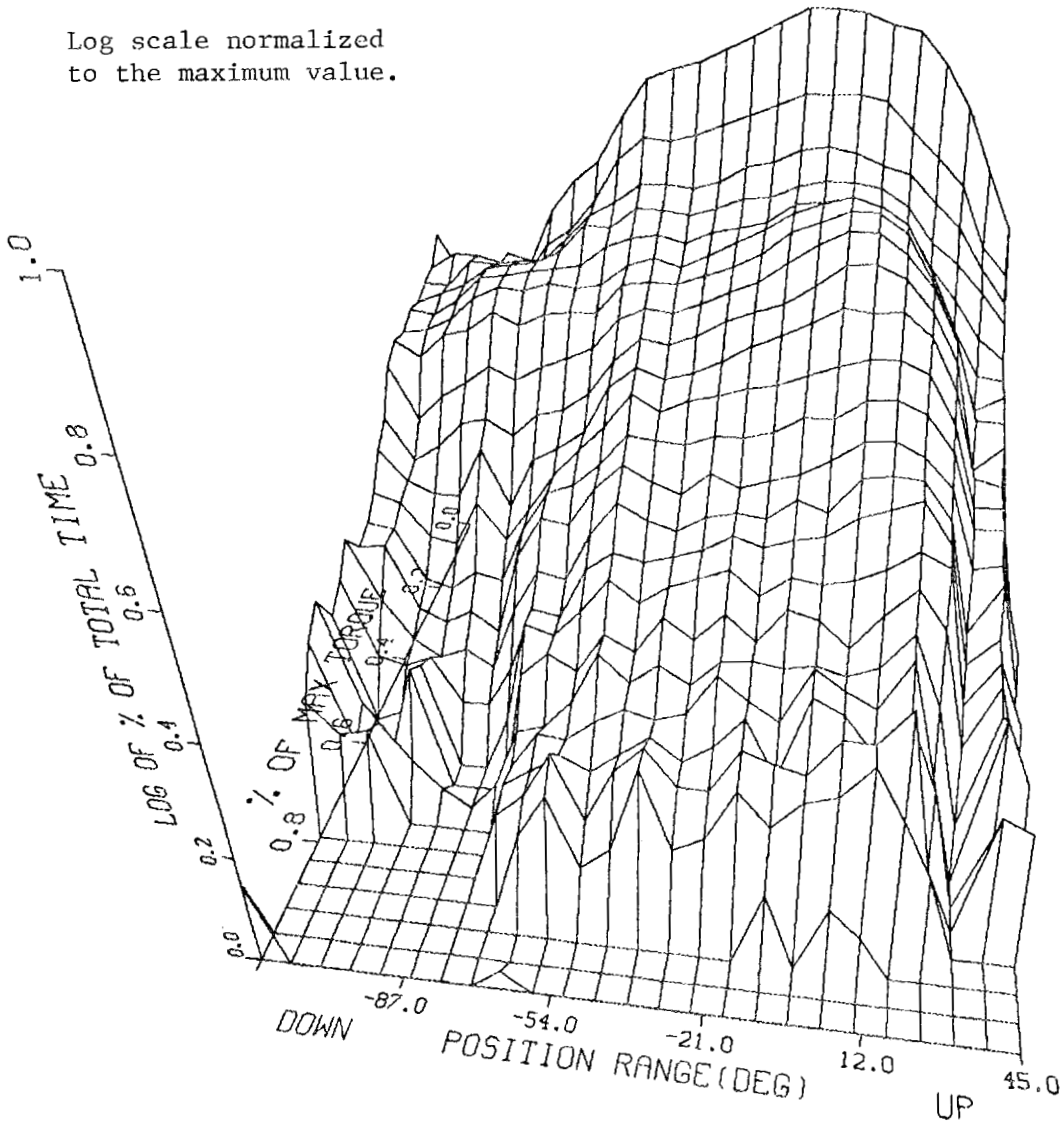


Fig. 41. Position-torque grid for wrist pitch.

ORNL-DWG 84-16700

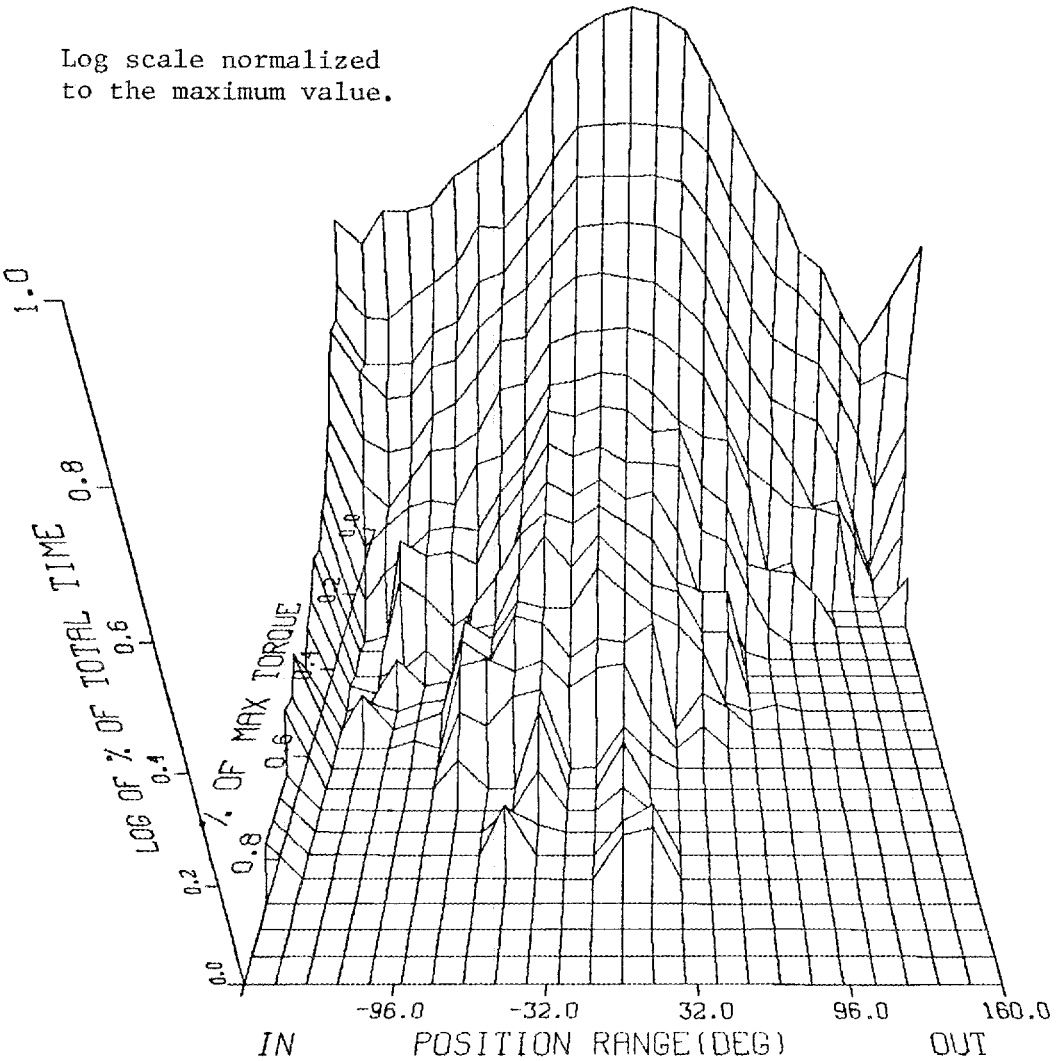


Fig. 42. Position-torque grid for wrist roll.

torque at the leftmost limit. This could be due again to slight difference in the positions of the master and slave stops, or due to pushing against the holder when removing or replacing the impact wrench.

The wrist pitch torque (Fig. 41) is evenly distributed, with peak torque occurring around 0°, where the gravity load is generally the highest. The wrist roll torque (Fig. 42) peaks at the center and at the innermost limit.

# 4. APPLICATIONS TO MANIPULATOR DESIGN

This study has many valuable applications to the design of servo-manipulators. The optimization will be accomplished with respect to the measured duty cycle data. Much effort was put into making these data as generic as possible so that the results can be generalized. The optimal kinematic range for each of the DOFs will be presented based on the position histograms in Figs. 7 through 12. Optimal gear reductions will be presented based on velocity and current data, and on how the mechanical power grids of Figs. 31 through 36 are made symmetrical as discussed earlier. The distribution of joint torques for nominal loads on the tong in the mean configuration of the manipulator will be presented. Relative actuator sizings will be discussed based on scaling the power grids (after including improved gear reductions) up or down so that they reach zero just below 100% on the torque and velocity axes. These sizings will be compared to the sizings needed to equalize the relative loads on each motor for nominal loads in the mean and worst-case configurations.

The effectiveness of the differential drive configurations of the shoulder and wrist will be discussed, and changes in mounting configurations that could improve this effectiveness will be presented. Finally, stress problems and possible ways of eliminating them will be discussed.

## 4.1 MOTION RANGES

The data presented in Table 6 provide an excellent basis for selecting improved DOF motion ranges. Note that if the data suggest that a range should be extended, there is no way to determine exactly how much it should be extended. The author will suggest a good "seat of the pants" estimate of what the range should be. The reader is cautioned that there are no data available to substantiate the magnitude of an increase in range, only that an increase is indeed appropriate.

The lower end of the shoulder pitch range should be increased as it has an end ratio of greater than unity and significant time-at-end. While the data suggest that a slight reduction could be made in the upper end range, this is not advised because this range can become critical for floor-based manipulators. An increase of 10 to 15° in the lower end of the shoulder pitch range seems appropriate.

The outer shoulder roll limit is scaled to near perfection. The range is used all the way to the end but has an end ratio of less than one, indicating that the operators do not hold the arm against this limit. The shoulder roll range is symmetric about its reference position, but this is not the mean use position of the DOF. The operators prefer to roll the shoulder inward so that the wrists are closer together. Because of this, the inner range is inadequate, and the operators hold the manipulator against the inner limit nearly 2% of the time. The inner limit should be increased by about 15°.

The elbow pitch has a large outer range that was never used. The manipulator becomes very difficult to work with when the elbow is pitched so that the arm is nearly straight. The elbow is free to travel an additional 45° past this point, but this range was never used. This author believes it has little use, and could be eliminated without shedding a tear. The elbow pitch can travel only 45° back toward the body. This limit had a greater than unity end ratio and significant time-at-end and therefore should be increased by about 5 to 10°.

The elbow roll (yaw) has a range which is symmetric about its reference position. This is inappropriate and does not reflect the control motions of the human operator. It is much easier to yaw the wrist in than out. Consider also that the operator (unlike the manipulator) can yaw his or her shoulder as well as the wrist to apply an inward elbow roll motion to the master quite easily, but this motion is difficult and cramped when applying an outward elbow roll motion (the operator's elbow jams against the ribs). This is reflected in the position-use graph of the elbow roll. Note that the elbow roll is just in from 0° much of the time, but when it is moved, it is nearly always taken inward. A slight increase in the inward range of

approximately 10° is needed while the outward range could be reduced by up to 45°, although a lesser reduction of 30° is suggested to accommodate novel tasks.

The upper wrist pitch range is well scaled and should not be changed. The lower range has a greater than unity end ratio and should be increased by about 5 to 10°.

The wrist roll could use a slightly increased clockwise range (from behind) of approximately 10°. An even larger increase may be appropriate for future applications such as robotic assembly of threaded parts. These results are summarized in Table 12.

Table 12. Improved motion ranges

| DOF | Direction | Motion range[a] (degrees) | Suggested change |
|---|---|---|---|
| Shoulder pitch | up | 60 | none |
| Shoulder pitch | down | 50 | increase 10-15° |
| Shoulder roll | in (left) | 45 | increase 15° |
| Shoulder roll | out (right) | 45 | none |
| Elbow pitch | forward | 135 | decrease 45° |
| Elbow pitch | backward | 45 | increase 5-10° |
| Elbow roll | in (left) | 170 | increase 10° |
| Elbow roll | out (right) | 170 | decrease 30° |
| Wrist pitch | up | 45 | none |
| Wrist pitch | down | 120 | increase 5-10° |
| Wrist roll | CW | 160 | none |
| Wrist roll | CCW | 160 | increase 10° |

[a]From reference position.

## 4.2 GEAR REDUCTIONS

Improvements in the gear reductions can be determined from the mechanical power grids (Figs. 31 through 36), the idea being to make them symmetrical about the main diagonal so that the motor is being used equally for speed and torque. Unfortunately, this can be difficult if the data extend all the way to 100% along one of the axes.

This makes it impossible to tell what "scale factor" will shift the grid so that it is symmetrical about its diagonal. For this reason, another technique is also used that is based on equalizing the normalized average peak currents per task (Table 8) and average peak velocities per task (Table 10). For example, the average peak current in the shoulder motors was 24.7% and 35.1%. This is slightly greater that the average peak shoulder pitch velocity of 25.4%. The average peak current of the two motors was 29.9%. Increasing the gear reduction by 8.5% would match the peak velocity and peak current (average of two values) at 27.56%. Examining the shoulder pitch power grid confirms this value. The grid goes to zero at about 76% along the torque axis and at about 60% along the velocity axis, implying a needed increase of about 8% in the gear reduction.

Using the average of the two peak currents as the peak shoulder pitch torque assumes that the peak current in each motor occurred simultaneously in the same direction. This is not a dangerous assumption as the pitch will support considerably more torque than the roll in most configurations, and if there is a discrepancy, it will be toward an increased torque capability. Making a similar assumption about the roll torques does not seem appropriate, however. Fortunately, the power grids for the shoulder and wrist rolls do not extend to 100% along either axis, and they will be used to determine the improved gear reductions for these DOFs.

The shoulder roll power grid drops to zero at 52% along the velocity axis and at 60% along the torque axis. The suggested change in the gear reduction is an increase of 4% to match the zero crossings of the grid at 56%.

The average per-task peak elbow pitch velocity was 43.7% of maximum, while the peak current was 36.9%. These can be matched at 40.2% with a decrease of 9% in the gear reduction.

Analyzing the wrist pitch gear reduction by the two different techniques yields very different results. Matching the average peak values suggests an increase of 117%, while making the grid cross zero at the same distance along each axis suggests an increase of 45%. Recalling that the wrist torque was insufficient for some tasks (such

as reinstalling the 6-in. flange) suggests that actual generic uses of the manipulator would require torques greater than 100% of present capacity. This would indicate that the higher value is more appropriate. Using the full increase of 117% would cause the wrist grid to reach zero at about 100% along the velocity axis. For this reason, a gear reduction that causes the grid to reach zero at 90% on the velocity axis was chosen as the improved reduction for this DOF. Note that this increased torque capacity will result in higher stresses in the drive tapes and gears.

The elbow roll gear reduction was selected by matching the average peak values, while the wrist roll gear reduction was selected by matching the zero points of the power grid along each axis.

The improved gear reductions are summarized in Table 13. Note that the average peak velocity and current scaled to the improved gear reductions give an indication of the ideal relative motor sizings.

Table 13. Improved gear reductions

| DOF | Actual gear reduction (approximation)[a] | Suggested change (%) | Improved gear reduction | Average peak velocity and torque per task (%)[b] |
|---|---|---|---|---|
| Shoulder pitch | 39.93 | +8.5 | 43.32 | 27.5 |
| Shoulder roll | 29.4 | +4 | 30.58 | 19.5 |
| Elbow pitch | 43.47 | -8.8 | 39.64 | 40.2 |
| Elbow roll | 8.065 | +10.7 | 8.928 | 35.0 |
| Wrist pitch | 3.912 | +96 | 7.682 | 26.0 |
| Wrist roll | 3.267 | +54 | 5.038 | 14.3 |

[a]See Table 3.
[b]Using the improved gear reductions.

The tong gear reduction was not discussed. The main problem with the tong is that large amounts of energy are consumed when the motor is simply holding a static torque. This can be disturbing if the manipulator is used with a battery-powered system. It should be noted

that one alternative would be to use an increased gear reduction with a smaller motor.

## 4.3 ACTUATOR SIZINGS

Traditionally, actuators and gear reductions have been selected on the basis of providing a certain maximum speed and sufficient torque to handle worst-case loading in each DOF. This technique will not be abandoned, but extensive use will be made of the power grids of Figs. 31 through 36.

The distribution of joint torques for nominal vertical, forward, and transverse loads centered 1 in. in front of the tong tip with the manipulator in the mean configuration (see Table 7) were determined using a technique described in Appendix D and are presented in Table 14.

Table 14. Joint torque distribution in the mean configuration

| DOF | Load[a] | | |
|---|---|---|---|
| | Gravity | Forward | Transverse |
| Shoulder pitch | 28.13 | 28.35 | 1.18 |
| Shoulder roll | -11.56 | 0.97 | -26.76 |
| Elbow pitch | 6.34 | 24.34 | 1.09 |
| Elbow roll | 1.79 | -5.51 | 6.07 |
| Wrist pitch | 7.14 | -1.59 | 1.47 |
| Wrist roll | 0 | 0 | 0 |

[a]Torques are in in./$lb_f$; nominal load is one $lb_f$.

Examining the shoulder pitch grid (Fig. 31), it would appear that smaller motors could produce the velocity and torque capability required in this DOF. Using the improved gear reduction, the grid would reach zero at about 70% along the torque and velocity axes. Thus, motors 25% smaller (in torque <u>and</u> velocity) could handle this

load. Similar reasoning on the shoulder roll grid would indicate that motors 45% smaller would be sufficient.

The reader is warned that the differential drive configuration reaches full capacity (both motors at peak torque) only in pure pitch or pure roll. If a combination pitch and roll torque is applied, the effectiveness decreases, and at a certain ratio of pitch-to-roll torque (that ratio being the ratio of pitch-to-roll gear reduction) the effectiveness is reduced to a minimum where all the torque is put on one of the motors. Due to the configuration in which the manipulator is used, gravity loading produces this combination pitch and roll torque (see Table 14), and this motor size reduction cannot be incorporated unless the configuration is changed (this will be discussed in the next section).

If direct drive were to be used on the shoulder pitch and roll, the velocity capability would be the same but the torque capacity would be cut in half. Thus, the gear reduction on the shoulder pitch would have to be increased by 60% over the reduction presently used (again to make the shoulder pitch grid symmetrical). The grid would then reach zero at about 94% on each axis, implying that the presently used motor would be the proper size. For direct drive of the shoulder roll, an increase of 53% in the gear reduction over the value presently used would cause the grid to reach zero at the value presently used and would cause the grid (Fig. 32) to reach zero at about 76% on each axis, implying that a motor 20% smaller would be sufficient.

In summary, the shoulder motors can be reduced in size (velocity and torque capacity) by up to 25% if differential drive is used and if the configuration is changed such that pitch and roll torques do not occur simultaneously. Alternatively, the motor size presently used would be used on the pitch with a 20% smaller motor on the roll (along with very different improved gear reductions) if direct drive is used.

The elbow pitch and roll grids (Figs. 33 and 34) indicate undersized motors. One might be tempted to use a differential drive on these joints, but again this may lead to problems with simultaneous pitch and roll torques. In addition, the pitch and roll gear

reductions at the elbow differ by a factor of about four to five, which would make the design of the differential difficult.

Using the improved gear reduction on the elbow pitch (-8.8%), the grid can be extrapolated to reach zero at about 100%. This may be considered ideal, but due to the considerable time spent at high torque, this author suggests an increase of 5 to 10% in the elbow pitch motor.

The elbow roll grid is difficult to extrapolate due to the height of the grid at 100% along each axis. This author suggests a 10% increase in the size of this motor.

The wrist pitch grid (Fig. 35) is skewed so much toward the torque axis that accurate extrapolation is difficult. Using the improved gear reduction, the grid would drop to zero at about 90% on the velocity axis. While it would appear to drop to zero at considerably less than 100% along the torque axis, the reader is reminded that some tasks, such as replacing the 6-in. flange, were not possible due to the excessive wrist pitch torque. No change is recommended in the size of the wrist motors.

No power grid was done for the tong motor, as this motor was used primarily for holding a static torque. Note that this is the only motor that works against itself. For battery-powered manipulator systems, an alternative must be found that will reduce the energy consumed in tong actuation. The improved actuator sizings are summarized in Table 15.

## 4.4 DIFFERENTIAL DRIVE LOAD SHARING

The idea behind the use of a differential drive in joint actuation is that if the torque is applied as a pure pitch or pure roll torque but not as a combination pitch and roll torque, two motors can share the load and thus double the capacity. Just the opposite is

Table 15. Improved actuator sizes

| Motor | Change[a] (%) |
|---|---|
| Upper shoulder[b] | -25 |
| Lower shoulder[b] | -25 |
| Shoulder pitch[c] | no change |
| Shoulder roll[c] | -20 |
| Elbow pitch | +10 |
| Elbow roll | +10 |
| Wrist (both) | no change |

[a]The change refers to an increase or decrease in both velocity and torque capacity.

[b]For differential drive, the configuration must be changed to eliminate simultaneous pitch and roll torque.

[c]For direct drive.

true of direct drive: the motors share the load when simultaneous pitch and roll torques are applied, but only one motor supports the load of pure pitch or roll torque.

Note that when expressing the pitch and roll capacities of a joint, a differentially driven joint has twice the capacity of a directly driven joint with the same gear reduction. This can be deceiving if one does not bear in mind that the capacity of the differentially driven joint drops to one-half that capacity when the load is a simultaneous pitch and roll (i.e., there's no such thing as a free lunch).

The wrist joint is perhaps the ideal location for a differential drive. When holding a gravity load, the torque is entirely along the pitch axis. When applying a roll torque (such as when removing or engaging connections), there is usually no load on the pitch.

In the reference position, the shoulder also appears to be well suited to a differential. Forward and gravity loads are supported entirely by the pitch, while the roll supports transverse loads.

However, as human operators prefer to roll the shoulder inwards from the reference position so that the wrists are in a better working position, gravity loading (the most common load) provides simultaneous pitch and roll torques, which destroys the effectiveness of the differential.

In order to remove the roll torque from the shoulder in the mean operating position, the mounting of the manipulator must be such that the shoulder roll angle is zero when the wrist is where the operators want it to be. This can be accomplished by mounting the manipulator arms closer together or by mounting the arms such that they point inward about 20° rather than directly forward (i.e., the shoulder yawed inward 20°), or by some combination of these two. This change in the mounting configuration is the simplest design improvement suggested here. It is also directly applicable to all elbows-up servo-manipulators with differentially driven shoulders and will result in improved performance.

## 4.5 ADDITIONAL APPLICATIONS

It was mentioned earlier that the wrist torque capacity should be increased considerably. This will, of course, increase the stresses in the wrist drive tapes and therefore reduce reliability. These tapes therefore should be increased in size or replaced with an alternative drive method. One alternative--chains--is advantageous in that one chain can provide both forward and reverse drive and thereby replace two tapes. The chains can therefore be more than twice as wide as the tapes, which will increase capacity and reliability.

The wrist tapes travel over the elbow and down the lower arm tube, and therefore they twist with the elbow roll (yaw) motion. This twist is zero when the elbow roll is in the reference position. This twist causes increased stresses in the tapes, but the tape stresses can be reduced by making the twist zero when the elbow is rolled inward somewhat, say to the mean position of 42.5°.

# 5. CONCLUSIONS

This report has presented the first known detailed study of servomanipulator duty cycles. These duty cycles have been clearly defined to serve as a baseline for future studies in this area.

Kinematic relationships were derived and expressed (Appendix D) which make the coordinate frame relationships understandable. These relationships also prove useful in applying the results of the duty cycle analysis, particularly in analyzing the joint torque distributions for nominal tong loads in various configurations.

The experimental system was representative of the work environments of servomanipulators, and the data were recorded for remote tasks that were specially selected to be generic and representative of servomanipulator tasks.

This study has furthered our understanding of the operation and uses of servomanipulators. The applications to future designs are many and include nearly every component of the system.

The use of only four operators in the testing provided a statistical limitation to the results. While the quantitative results can be expected to change somewhat when a larger number of operators are considered, the qualitative results are expected to remain valid.

## LIST OF REFERENCES


1. J. Takahashi, "Advanced Two-Arm Servomanipulator Having New Multi-Joints and Ingenious Wrist," Proc. Am. Nucl. Soc. Top. Meet. Robotics and Remote Handling in Hostile Environ. (April 1984).

2. Ray Goertz, "Some Work on Manipulator Systems at ANL; Past, Present, and a Look at the Future," Proc. Semin. Remotely Oper. Spec. Equip., USAEC Report CONF-641120 (May 1964).

3. Ray Goertz, "Manipulator Systems Development at ANL," Proc. Conf. Remote Syst. Technol., Am. Nucl. Soc. (Nov. 1964).

4. W. R. Hamel and H. L. Martin, "Robotics-Related Technology in the Nuclear Industry," Proc. SPIE, Vol. 442, Robotics and Robot Sensing Sys. (August 25, 1983).

5. J. N. Herndon et al., "The State-of-the-Art Model M-2 Maintenance System," Proc. Am. Nucl. Soc. Top. Meet. Robotics and Remote Handling in Hostile Environ. (April 1984).

6. J. Vertut et al., "Protection, Transfer and Maintenance of the MA-23 Bilateral Servomanipulator," Proc. Conf. Remote Syst. Technol. Am. Nucl. Soc. (Nov 1978).

7. J. Vertut et al., "Advances in a Computer Aided Bilateral Servomanipulator System," Proc. Am. Nucl. Soc. Top. Meet. Robotics and Remote Handling in Hostile Environ. (April 1984).

8. J. V. Draper and M. C. Clarke, personal communication, Oct. 1983.

9. Operation and Maintenance Manual, Model SM-229, TeleOperator Systems Corp., Bohemia, N.Y.

10. J. N. Herndon, personal communication, June 1983.

11. ORNL Acceptance Testing Procedures, May 1982.

12. Digital Equipment Corporation, Vendor Documentation RSX-11M, Version 3.2, Vol. 5A, Sect. 14.

# APPENDIX A

# UNCERTAINTY ANALYSIS

## UNCERTAINTY ANALYSIS

The shoulder DOF positions were measured directly against the gravity vector and, as such, had an uncertainty due only to the direct measurement.

$$W_{SP} = W_{SR} = \pm 0.75° \quad .$$

It was assumed that the differential drive increased the measurement uncertainty by $\sqrt{2}$, as two angles had to be measured. Thus

$$W_{SP} = W_{SR} = 1.06° \ .$$

Note that the uncertainty in the slope is much lower

$$\text{slope} = \frac{\Delta s \pm W_{\Delta s}}{\Delta(\text{counts}) \pm W_{\Delta \text{counts}}} \quad .$$

So,

$$\left[\left(\frac{W_{\text{slope}}}{\text{slope}} = \frac{W_{\Delta s}}{\Delta s}\right)^2 + \left(\frac{W_{\Delta \text{counts}}}{\Delta \text{counts}}\right)^2\right]^{1/2}$$

$$= \left[\left(\frac{1}{100}\right)^2 + \left(\frac{4}{3400}\right)^2\right]^{1/2}$$

$$= \simeq 0.01 = 1\%$$

for the shoulder pitch.

The elbow pitch is relative to the shoulder pitch position, so its uncertainty is increased by a factor of $\sqrt{2}$ over the shoulder pitch uncertainty.

$$W_{EP} = \sqrt{2}\ (\pm 0.75°) = \pm 1.06°.$$

In the configuration used to calibrate the elbow roll, the shoulder pitch and elbow pitch uncertainty contributed only very weakly to the elbow roll measurement uncertainty. Thus, the elbow roll measurement uncertainty is increased $\sqrt{2}$ over the shoulder roll measurement uncertainty.

$$W_{ER} = \sqrt{2}\ (\pm 0.75°) = 1.06° \ .$$

The wrist pitch calibration depended on the shoulder and elbow pitch calibrations, and the wrist roll calibration depended on the shoulder roll calibration. Additionally, the wrist position measurements were more difficult to make than those of the upper DOFs. The small size of the tong made some measurement positions cramped, and the drive tapes would stretch slightly when the weight of the plate and protractor was placed on the wrist. For this reason, measurement uncertainty for the wrist DOFs was assumed to be about ±1.5° for both pitch and roll. Again, the differential drive configuration was assumed to increase the final uncertainty of each by $\sqrt{2}$.
Thus,

$$W_{WP} = \sqrt{2}\ \left[W_{SP}^{\ 2} + W_{EP}^{\ 2} + (1.5)^2\right]^{1/2}$$

$$W_{WP} = \pm 2.8°,$$

and

$$W_{WR} = \sqrt{2}\ \left[W_{SR}^{\ 2} + (1.5)^2\right]^{1/2}$$

$$W_{WR} = \pm 2.4° \ .$$

Note, however, that the uncertainties in the slopes are not increased, as the brake on the upper DOFs assured that they did not move during the calibration, and thus any error they introduced was subtracted out. Uncertainties in the slopes were assumed to be 1% for the shoulder and elbow DOFs and 2.5% for the wrist DOFs.

Backlash in the gearing produced an additional uncertainty in the position signals. Its effect on the slopes was eliminated by making all measurements with the gears pushed into contact in the same direction.

The backlash on each DOF was measured by locking the brakes and measuring the angle the DOFs could still travel. These angles are given in Table A.1.

Table A.1. Approximate DOF gearing backlash

| DOF | Backlash (approximate degree)[a] |
|---|---|
| SP | 0.75 |
| SR | 0.75 |
| EP | 0 |
| ER | 0.25 |
| WP | 1.0 |
| WR | 0.75 |

[a]angles measured at the DOF.

This backlash contributes to the uncertainty in the position signals. The probable (3 σ) position uncertainty is given by

$$W_{pos} = \left[ \left( W_{calib} \right)^2 + \left( \frac{\text{backlash}}{2} \right)^2 \right]^{1/2} .$$

The probable position uncertainties are given in Table A.2.

The calibration data for all DOFs were very nearly linear. Calibration parameters were determined by a least-squares straight line fit to the data.

Voltage dividers were added to each position signal just before input to the PDP 11/34 to reduce the signals to ±10 V. These dividers consisted of nominal 10-KΩ and 5-KΩ resistors in series. The signals

Table A.2. Probable position uncertainties

| DOF | Uncertainty (± degrees) |
|---|---|
| SP | 1.30 |
| SR | 1.30 |
| EP | 1.06 |
| ER | 1.09 |
| WP | 2.84 |
| WR | 2.40 |

were put across both resistors with the PDP 11/34 reading the voltage across the 10-KΩ resistor. A precision digital ohmmeter* was used to find the exact ratio of the resistors used on each signal, which was then included in the position signal slopes. A digital voltmeter* was used to measure the signal voltage with and without the dividers. This was to ensure that the dividers did not alter the signal, which they did not. The resistance values were read with an accuracy of about ±2 Ω, and thus did not contribute significantly to the position uncertainty.

Velocities. The velocity algorithm used (see Appendix C) was

$$f_i = \frac{-f_{i+2} + 8f_{i+1} - 8f_{i-1} + f_{i-2}}{12\Delta t} .$$

This can be rewritten

*Tektronics Model *DM501 Digital Multimeter IC043154.

$$f_i = \frac{(f_{i-2} - f_{i+2}) + 8(f_{i+1} - f_{i-1})}{12\Delta t} ,$$

which clearly shows that the position signal uncertainty to be used is the uncertainty in a position change.

In determining this uncertainty, the effects of backlash in the gearing were ignored. It should be noted that the calculated velocities are then actually proportional to the gear train velocities at the potentiometer location. This will differ from the actual joint velocity only when the joint acceleration changes direction and the joint travels through the backlash region.

The position change uncertainty is then due only to calibration slope (not intercept) uncertainty, A/D conversion error, and signal noise. Signal noise was tested using a test program which read the position signals and current signals approximately four times per second. The program was executed with the arms energized but not in motion.

The average change per sample on each channel was calculated after 1000 samples. No detectable noise was seen on the position signals--a tribute to the 11-Hz low-pass filters. The program was run for a variety of arm configurations to include any possible position-correlated noise. Note that velocity-correlated noise, if present, was not included in these results. The program was run several times over a period of two weeks. The results changed insignificantly.

The uncertainty due to the slope calibration (~1%) and A/D conversion (±1/2 count) and signal noise was estimated as ±3 counts for the shoulder and elbow DOFs and ±5 counts for the wrist DOFs. Since the shoulder and wrist DOFs have differential drives, their uncertainties are multiplied by $\sqrt{2}$ for uncertainties of 4.24 and 7.07 counts respectively. The timestep uncertainty is negligible (see Appendix B), so the velocity uncertainty is given by:

$$W_{f_i} = \frac{1}{12\Delta t} \left[9\ W_{\Delta f}\right]$$

$$= 7.5 \text{ W} \quad s^{-1}$$
$$\Delta f$$

Incorporating the position-signal slopes, the velocity uncertainties are presented in Table A.3. Recall that the expected truncation error is about 7%. Note that as the results have been composited over many hours of manipulator operation, most errors due to truncation should average out.

Motor Currents. Some noise was present in the motor current signals. The primary source of current signal error, however, was found to be the difference between master and slave ground. This

Table A.3. Probable velocity uncertainties

| DOF | Uncertainty (±rad/s) | Percentage of maximum |
|---|---|---|
| SP | .0161 | 1.26 |
| SR | .0239 | 1.22 |
| EP | .0206 | 1.70 |
| ER | .0392 | 0.55 |
| WP | .0589 | 0.41 |
| WR | .0695 | 0.30 |

difference was observed daily for about one month. The difference would remain relatively constant on a given day but would fluctuate from day to day. This difference was actually measured by switching the slave-to-computer drive, zeroing the drive signals, and looking at the "voltage" across the slave shunt (0.1-Ω) resistors (i.e., the motor-current signals). Since no current was given to the motors, the variable end of the signals represented slave ground, while the ground reference was tied to master ground. As expected, all seven signals were within one count of one another. The average ground difference was ±16 counts = 10 mV (2000 counts = 1.25 V), with a maximum observed difference of 26 counts. This corresponds to a current uncertainty of ±0.1 A or 2% of maximum. The shunt resistors are accurate to ±1% (manufacturer's specifications).

Joint Torques. The uncertainty in applied joint torques is difficult to measure. The applied torque is given by

$$T_j = T_m(GR)\ \eta_g - T_f$$

where

$T_m$ = motor torque (sum or difference for differential joints),
GR = gear ratio,
$\eta$ = efficiency of the gearing,
$T_f$ = additional drive train friction involving nearly all, nonlinear friction effects.

Fortunately, these difficult-to-measure parameters apply almost equally whether one is applying full torque or some percentage of full torque to the joint. Thus, the percentage of maximum torque varies only weakly with these parameters, and at the highest percentage of maximum torque (the data of most interest), the errors are minimal. Thus, the histogram torque data uncertainty was estimated at about 50% greater than the current uncertainty, or about 3%. Note that this is independent of the torque calibration.

The absolute applied torque uncertainty was estimated as follows. Referring to Eq. (1),

$$\frac{W_k}{k} = \left[\left(\frac{W_F}{F}\right)^2 + \left(\frac{W_L}{L}\right)^2 + \left(\frac{W_I}{I}\right)^2 + \left(\frac{W_{\cos\theta}}{\cos\theta}\right)^2\right]^{1/2} .$$

The current signal uncertainty was about 16 counts. Again, the average measured current was used to determine the percentage of uncertainty in the current measurement. The uncertainty parameters are presented in Table A.4.

Table A.4. Torque calibration uncertainty parameters

| DOF | $F_{mean}$ ($lb_f$) | X (in.) | $I_{mean}$ (counts) | $\frac{W_F}{F}$ | $\frac{W_x}{X}$ | $\frac{W_I}{I}$ | $\frac{W_{\cos\theta}}{\cos}$ | $\frac{W_K}{K}$ |
|---|---|---|---|---|---|---|---|---|
| SP | 23.6 | 19 | 452[a] | 0.042 | 0.013 | 0.071 | 0.0024 | 0.083 |
| SR | 8.8 | 24.25 | 301[b] | 0.114 | 0.010 | 0.020 | 0.0024 | 0.116 |
| EP | 10.5 | 24.25 | 249 | 0.095 | 0.010 | 0.064 | 0.0024 | 0.115 |
| ER | 12.0 | 6.25 | 349 | 0.083 | 0.040 | 0.045 | 0.0024 | 0.103 |
| WP | 12.4 | 5.25 | 763[a] | 0.081 | 0.049 | 0.042 | 0.0024 | 0.103 |
| WR | 7.5 | 5.0 | 480[b] | 0.133 | 0.050 | 0.013 | 0.0024 | 0.143 |

[a]Average sum of two drive motors.
[b]Average difference of two drive motors.

Note that the current signal uncertainty is due primarily to a difference in ground reference between the master and slave. Thus, the shoulder and wrist pitch torques have current measurement uncertainties of about 32 counts as they are the sum of two signals, while the shoulder and wrist roll torques have very low current measurement uncertainties--about 6 counts--as they are the difference of two signals.

Electrical Energy. The electrical energy was determined by

$$E_e = \sum_i I_i^2 \, R \, \Delta t$$

where

$I_i$ = the motor current (A) at data sample i

R = motor resistance, 5.5 Ω, nominal

$\Delta t$ = timestep between samples, 0.1 s.

Since $\frac{W_I}{I} = 0.02$, $\frac{W_{I^2}}{I^2} = 0.04$, so

$$\left[\frac{W_{E_e}}{E_e} = \left(\frac{W_R}{R}\right)^2 + \left(\frac{W_{\Delta t}}{\Delta t}\right)^2 + \left(\frac{W_{\sum I_i^2}}{\sum I_i^2}\right)^2\right]^{1/2} .$$

If the current signal uncertainty is assumed to be caused by uncorrelated zero mean noise, the uncertainty in $\Sigma I_i^2$ would reduce to near zero due to the large number of points sampled. To be conservative, this will not be assumed; rather, it will be assumed that

$$\frac{W_{\sum I_i^2}}{\sum I_i^2} = \frac{W_I^2}{I_i^2} = 0.04 .$$

Recall that the energy per motor presented was based on the nominal value of the resistance, 5.5 Ω. The actual resistances differed from this, but to generalize the results, the presented values are based only on $\int I^2 dt$.

Thus,

$$\frac{W_{E_e}}{E_e} = 4.0\% .$$

<u>Mechanical Energy</u>. The mechanical energy generated per DOF was determined by

$$E_m = \sum_i T_i \omega_i \Delta t$$

where

$T_i$ = the applied torque on the joint at sample i, ft-lb

$\omega_i$ = the joint angular velocity at sample i, rad/s.

The applied torque calibration uncertainty was about 11%. Note that the calculated mechanical energy includes the energy lost to friction. The percentage of uncertainty in the angular velocity,

neglecting the truncation error, depends on the choice of a nominal velocity. Fortunately, histogram velocity usage data are available. The nominal velocity for each DOF was estimated by finding the mean value of the histogram plots, assuming each histogram block to be a discrete point located at the center of the block. (For example, if 6% of the time was spent at 10 to 12% of maximum velocity, it is assumed that 6% of the time was spent at 11% of maximum velocity). Also, it was assumed that each DOF was moving about one third of the time, and therefore 67% was subtracted from the 0 to 2% block. This resulted in the mean velocities given in Table A.5. The mechanical energy uncertainty was then conservatively estimated as

$$\frac{W_{E_n}}{E_m} = \left[ \left( \frac{W_{T_i}}{T_i} \right)^2 + \left( \frac{W_{\omega_i}}{\omega_i} \right)^2 \right]^{1/2} ,$$

The results are listed in Table A.5.

Table A.5. Mechanical energy uncertainties

| DOF | $(W_{T_i}/T_i)$ | $\omega_{i_{ave}}$ (rad/s) | $W_{\omega_i}/\omega_i$ | $W_{E_m}/E_m$ (%) |
|---|---|---|---|---|
| SP | .083 | .0673 | .239 | 25.3 |
| SR | .116 | .0783 | .305 | 32.6 |
| EP | .115 | .1079 | .191 | 22.3 |
| ER | .103 | .2889 | .136 | 17.0 |
| WP | .103 | .2920 | .202 | 22.6 |
| WR | .143 | .3872 | .180 | 23.0 |

Maximum time over 60% current. These data have no uncertainty if they are considered to be the maximum time over a random value between 58 and 62% (i.e., ± the current signal uncertainty).

# APPENDIX B

# CALIBRATIONS AND TESTS

## CALIBRATIONS AND TESTS

### Slave Arm Position Calibration

Procedure. Angles were measured with respect to the gravity vector using a bubble balance protractor.

$$\text{Accuracy} = \pm 0.75°.$$

The computer program written to aid this calibration would flip the slave brakes on or off and print the values of the analog inputs to the PDP 11/34 on the screen as requested. A computer terminal was brought into the cell and the program was initiated. Calibration data for the slave arm shoulder, elbow, and wrist are given in Tables B.1, B.2, and B.3.

Shoulder pitch calibration. After the slave was put into the reference position (shoulder and elbow DOFs only) and the brakes energized, shoulder DOF position potentiometer data were recorded. The brakes were released and the shoulder was repositioned to a new pitch angle (holding the roll angle at zero). The brakes were then reenergized, and the new data were recorded. This was repeated for eight different shoulder-pitch angles from +50° to -50°.

The shoulder-pitch angle was measured on a flat surface at the pitch axis which rotated with the pitch but not the roll. The roll angle was measured on a flat surface just above the elbow joint which rotated with both the shoulder pitch and roll.

Shoulder roll. Shoulder pitch calibration was repeated holding the shoulder pitch angle at 0° and varying the shoulder roll. Six data points were recorded from +40° to -40°.

Elbow pitch. The shoulder DOFs were put into the reference position, the brakes were energized, and the elbow pitch brake was manually loosened so that the DOF could be moved but sufficient friction remained to hold the arm in a set position. Data were

Table B.1. Slave arm shoulder position calibration data (January 5, 1984)

| Measured angles | AINDAT # | Value | Calculated angles | Remarks |
|---|---|---|---|---|
| SP = 0° | 9 | -651 | SP = 0.1° | SP : + = toward left |
| SR = 0° | 11 | -587 | SR = -0.5° | SR : + = facing forward |
| SP = -10° | 9 | -404 | SP = -9.8° | EP : + = left |
| SR = 0° | 11 | -323 | SR = 0.0 | ER : + = down |
| | | | | WP = + = left |
| SP = -20° | 9 | -136 | SP = -20.2° | WR : + = forward |
| SR = 0° | 11 | -43 | SR = 0.4° | |
| SP = -40° | 9 | 370 | SP = -39.6° | |
| SR = 0° | 11 | 476 | SR = 1.0° | |
| SP = -50° | 9 | 635 | SP = -50.0° | |
| SR = 0° | 11 | 754 | SR = 1.4° | |
| SP = 20° | 9 | -1147 | SP = 18.9° | |
| SR = 0 | 11 | -1085 | SR = -0.7° | |
| SP = +40° | 9 | -1708 | SP = 40.2° | |
| SR = 0 | 11 | -1652 | SR = -1.0° | |
| SP = +50° | 9 | -1986 | SP = 50.6° | |
| SR = 0 | 11 | -1922 | SR = -0.8° | |
| SP = 0 | 9 | -639 | SP = -0.6° | |
| SR = 0 | 11 | -571 | SR = 0.0° | |
| SP = 0 | 9 | -308 | SP = -0.3° | |
| SR = -20° | 11 | -925 | SR = -20.0° | |
| SP = 0 | 9 | 40 | SP = -0.6° | |
| SR = -40° | 11 | -1265 | SR = -39.8° | |
| SP = 0 | 9 | 377 | SP = -0.2° | |
| SR = -60° | 11 | -1633 | SR = -60.0° | |
| SP = 0 | 9 | -1009 | SP = 0.2° | |
| SR = +20° | 11 | -238 | SR = 19.8° | |
| SP = 0 | 9 | -1380 | SP = 0.8° | |
| SR = +40° | 11 | 111 | SR = 40.4° | |

Table B.2. Slave arm position calibration (January 5, 1984)

| Measured angle (deg) | AINDAT | Calculated angle (deg) |
|---|---|---|
| Elbow Pitch: SP = SR = 0° | | |
| 0 | 1138[a] | -0.1 |
| -20 | 545[a] | -20.2 |
| -40 | -37[a] | -40.0 |
| -60 | -620[a] | -59.8 |
| +20 | 1736[a] | 20.2 |
| Elbow roll: EP = -90° SP = SR = 0° | | |
| 0 | -42[b] | -0.4 |
| 20 | -351[b] | 20.0 |
| 40 | -657[b] | 40.2 |
| 60 | -952[b] | 59.7 |
| 90 | -1411[b] | 90.0 |
| -30 | 399[b] | -29.6 |
| -60 | 845[b] | -59.0 |
| -90 | 1320[b] | -90.4 |
| -120 | 1774[b] | -120.4 |

[a]AINDAT (10).
[b]AINDAT (14).

Table B.3. Slave arm wrist calibration data
(January 5, 1984)

| Measured angles | | | | Calculated angles | |
|---|---|---|---|---|---|
| WP (deg) | WR (deg) | AINDAT (12) | AINDAT (13) | WP (deg) | WR (deg) |
| Wrist Pitch and Roll: EP = 0° SP = SR = 0° | | | | | |
| 0 | 0 | -394 | -664 | 0.5 | -0.1 |
| 25 | 0 | -115 | -371 | 24.6 | -0.7 |
| 50 | 0 | 204 | -96 | 49.5 | 1.6 |
| 90 | -0 | 667 | 414 | 90.4 | -0.5 |
| -10 | 0 | -511 | -795 | -9.8 | 0.5 |
| 0 | 40 | -54 | -1097 | -3.2 | 38.1° |
| 0 | 120 | 701 | -1912 | -5.6 | 115.9 |
| 0 | -40 | -873 | -304 | -4.5 | -41.7 |
| 0 | -145 | -1916 | 791 | -2.6 | -147.6 |

recorded for five elbow pitch angles from +20° to -60°. The angle was measured on a flat surface just below the elbow which moved with the shoulder pitch and roll and with the elbow pitch.

Elbow roll. The elbow pitch brake was tightened and the brakes were released. After the elbow pitch was moved -90° so that the lower arm was horizontal and parallel with the upper arm, the brakes were reset and the elbow roll brake was manually released as before. Nine different data points were recorded from +90° to -120°. The angle was measured on a flat surface just above the wrist which moved with the shoulder and elbow DOFs only.

Wrist calibration. The brakes were released the elbow pitch and roll were returned to the reference position, and the brakes were again locked. The wrist brakes were loosened as before. A flat plate was bolted onto the tong, and angles were measured on the plate. Four pitch angles were recorded from -10° to 90°, and five roll angles were recorded from +120° to -145°.

After including the voltage divider factors, the least-squares fit resulted in:

$$SP = -0.0005061[AIN(9) + 0.9854AIN(11)] - 0.412$$

$$SR = 0.000753[1.015\ AIN(11) - AIN(9)] - 0.0382$$

$$EP = 0.000914AIN(10) - 0.6766$$

$$ER = -0.001742AIN(14) - 0.056$$

$$WP = 0.001111[AIN(12) + 0.9981AIN(13)] + 0.7845$$

$$WR = 0.001311[AIN(12) - 0.996AIN(13)] - 0.232$$

Torque calibration

The slave right arm was switched to computer drive and the brakes disabled. A computer terminal was brought into the cell to change the analog outputs that drive the slave and to read the motor current signals. Joint torques are given in Table B.4.

Table B.4. Joint torque calibration

| DOF | Torque (lb) | Uncertainty (%) |
|---|---|---|
| SP | 160 (US + LS)[a] | 8.3 |
| SR | 116.3 (US - LS) | 11.6 |
| EP | 157.3 (EL) | 11.5 |
| ER | 38.0 (YAW) | 10.3 |
| WP | 12.89 (LW + RW) | 10.3 |
| WR | 12.78 (RW - LW) | 14.3 |

[a]The torque is proportional to the motor currents. For example, the SP torque = 160 (US + LS) where US, LS are shoulder motor currents in amperes.

An equal drive signal was sent to the two shoulder motors. This resulted in approximately equal currents in each shoulder motor. A

spring-force scale was used to hold the arm in static equilibrium. The spring scale was attached to the arm at the upper arm elbow opening. The spring scale was shaken repeatedly and allowed to settle before a reading was taken to reduce friction errors. This was done three times for each measurement taken with repeatability within 0.5 $lb_f$. The spring-scale axis was held as close to orthogonal to the torque-arm plane as could be judged by eye. This uncertainty was estimated at ±4°. The force measurement uncertainty was estimated at ±1 $lb_f$. Five different measurements were taken. The moment arm was measured with a ruler with estimated uncertainty ±1/4 in.

The procedure was repeated for the remaining DOFs with signals sent to the appropriate motors. The forces were measured at the forearm wrist opening for the shoulder-roll and elbow-pitch torques, and on the tong thumb connection for the lower DOF torques. The elbow pitch torque calibration was performed with the shoulder brakes locked and in the reference position. The elbow-roll torque calibration was performed with the shoulder and elbow pitch brakes locked and in the reference position. The wrist torque calibrations were done with all shoulder and elbow DOF brakes locked. Calibration data are given in Table B.5.

The calibration parameters were determined by a least-squares straight-line fit to the data. The calibration uncertainties were estimated using the mean force measured to estimate the percentage of uncertainty in the force measurement. Let

$$K = \frac{\text{Torque}}{I} = \frac{LF\cos\theta}{I} \tag{1}$$

where

$F$ = measured force, $lb_f$,

$L$ = measured moment arm,

$I$ = motor current (measured in counts),

$\theta$ = angle between the measured force vector and the torque-arm plane.

Table B.5. Applied torque calibration data

Shoulder pitch (+ = left)

| IADC(17)[a] | IADC(19) | Force (lb)[b] | Torque (lb) |
|---|---|---|---|
| - 90 | -100 | 9 | 171 |
| -160 | -173 | 16 | 304 |
| -210 | -240 | 23.5 | 447 |
| -217 | -308 | 32.5 | 618 |
| -342 | -367 | 37.0 | 703 |

Shoulder roll (+ = forward)

| IADC(17) | IADC(19) | Force (lb)[c] | Torque |
|---|---|---|---|
| - 90 | 80 | 5 | 126 |
| -150 | 145 | 8 | 202 |
| -218 | 220 | 13.5 | 341 |

Elbow pitch (+ = left)

| IADC(18) | Force[c] | Torque |
|---|---|---|
| 235 | 10 | 253 |
| 393 | 16 | 404 limit |
| 119 | 5.5 | 139 |

Yaw (+ = down)

| IADC(22) | Force (lb)[d] | Torque |
|---|---|---|
| 208 | 6.5 | 41 |
| 349 | 12 | 75 |
| 491 | 17.5 | 109 |

Wrist pitch (+ = left)

| IADC(20) | IADC(21) | Force[e] | Torque |
|---|---|---|---|
| 143 | 170 | 5.5 | 28 |
| 338 | 355 | 11.5 | 59 |
| 510 | 569 | 17.0 | 87 |
| 481 | 485 | 15.5 | 79 |

Wrist roll (+ = forward)

| IADC(20) | IADC(21) | Force (lb)[f] | Torque |
|---|---|---|---|
| 158 | -184 | 5.5 | 28 |
| 288 | -331 | 9.5 | 48 |

[a]Current = IADC( ) $\left(.00625 \frac{v}{count}\right)\left(10 \frac{amps}{V}\right)$ .

[b]Measured at upper arm elbow opening. L = 19 in.

[c]Measured at the wrist opening. L = 24 1/4 in.

[d]Measured on the tong at L = 6 1/4 in. thumb connection.

[e]Same place, but L = 5 1/8 in.

[f]L = 2  2 1/2 in. = 5 in.

Right Slave Motor Resistances

The arm was switched to computer drive and all analog outputs were zeroed. One at a time, drive signals were sent to the slave motors. The voltage was read with a digital voltmeter.* The current was read as the voltage across the shunt resistors by the PDP 11/34. The measured resistance parameters are summarized in Table B.6.

Timestep Variation Test

The data logger was timed to record a data sample every 0.1 s. The timer used was an internal software clock. The data logger issued a mark time directive instructing the system to declare a significant event and set an event flag when the time (0.1 s) expired. The logger then immediately prompted the A/D converter to scan the data. The data logger was given the highest priority of any operating task to

Table B.6. Motor resistance measurement parameters

| Motor | $R_{avg}$ ($\Omega$) | $\sigma$ | Number of measurements |
|---|---|---|---|
| US | 6.20 | 0.22 | 4 |
| EL | 6.61 | - | 2 |
| LS | 6.39 | 0.31 | 4 |
| RW | 7.61 | 0.12 | 5 |
| LW | 6.59 | 0.42 | 4 |
| YHW | 6.85 | 0.39 | 4 |
| TG | 6.54 | - | 2 |

*Tektronics Model DM501 IC #043154.

ensure that it had immediate access to the CPU when the timer expired. Naturally, it was of interest to determine the variation in the actual time between samples.

To determine the timestep variation, a waveform generator *was connected to one of the analog input ports and set to output a sinusoidal signal of frequency 0.5 Hz. The signal was given a few minutes to ensure that no transient signal was present, and then the data logger was initiated. These data were recorded for 5 min.

A separate task was written to open this data file. The task then synchronized the input data with a separate "timer" being increased by $\pi/10$ each iteration and subtracting $\pi$ when the value exceeded $\pi$. The task then took the inverse sine of the input data (which should increase by $\pi/10$ each sample). The difference between the two was the timestep error for the particular iteration. The absolute value of the error signal was summed and divided by the total number of data samples.

The results were a pleasant surprise. The timestep variation was zero to eight significant digits. It is possible that both signals could have varied simultaneously due to variations in power frequency from TVA, but it is clear that no other random timestep variations occurred.

---

*Wavetek Model 175 US-DOE-X #130191.

# APPENDIX C

# SELECTION OF VELOCITY ALGORITHM

## SELECTION OF VELOCITY ALGORITHM

First develop a general 5-point velocity algorithm:

$$f_{i-1} = f_i + f_i' \Delta t + f_i'' \frac{\Delta t^2}{2} + f''' \frac{\Delta t^3}{6} + \ldots$$

$$x \quad -f_{i-1} = -f_i + f_i' \Delta t - f_i'' \frac{\Delta t^2}{2} + f_i''' \frac{\Delta t^3}{6} \pm \ldots$$

$$x \quad f_{i+2} = f_i + f_i' \, 2\Delta t + f_i'' \, 2\Delta t^2 + f_i''' \frac{4}{3} \Delta t^3 + \ldots$$

$$-f_{i-2} = -f_i + f_i' \, 2\Delta t - f_i'' \, 2\Delta t - f_i''' \, 2\Delta t^2 + f_i \quad \frac{4}{3} \Delta t^3 \pm \ldots$$

The sum of the above equations yields:

$$f_{i+2} + xf_{i+1} - xf_{i-1} - f_{i-2} = f_i' \, (\Delta t)(4 + 2x) + f_i'''(\Delta t^3)(\frac{8+x}{3})$$

$$f_i' = \frac{f_{i+2} + xf_{i+1} - xf_{i-1} - f_{i-2}}{(4 + 2x) \, \Delta t} \quad \frac{(8 + x)}{3(4 + 2x)} \quad \Delta t^2 f_i'''$$

The timestep uncertainty is negligible (see Appendix B). Neglect the truncation error for now, and optimize the velocity uncertainty with regard to position-signal uncertainty:

$$W_{f_i} = \left[ \sum_i \frac{\partial f_i}{\partial \Delta f_i}^2 \right]^{1/2}$$

$$= \left[ \frac{1 + x^2}{(4+2x)^2 \Delta t^2} \right]^{1/2} W_{f_i}$$

$$= \left( \frac{1}{2} \quad W_{f_i} \right) \left( \frac{1}{\Delta t} \right) \left[ \frac{(1 + x2)}{(x + 2)}^{1/2} \right] .$$

$$\frac{dW_{f_i}}{dx} = \left(\frac{1}{2}\frac{W_{f_i}}{\Delta t}\right) \frac{d}{dx} \left[\frac{(x^2 + 1)^{1/2}}{(x + 2)}\right]$$

$$= \frac{1}{2}\frac{W_{f_i}}{\Delta t}\left[\frac{1}{(x + 2)(x^2 + 1)^{1/2}}\right] \times \left[-\frac{x^2 + 1}{x + 2}\right] .$$

setting this to zero results in

$$x = 1/2$$

for which

$$W_{f_i'} = 0.1581 \frac{W_{f_i}}{\Delta t}$$

and

$$E_t = 0.5667\ \Delta t^2\ f_i \quad .$$

The truncation error is given by

$$E_x = \frac{8 + x}{3(4 + 2x)}\ \Delta t\ f_i'' \quad .$$

Optimizing $f_i'$ with regard to truncation error results in

$$x = -8$$

and

$$f_i' = \frac{-f_{i+2} + 8f_{i+1} - 8f_{i-1} + f_{i-2}}{2\Delta t} + O(\Delta t^4) \quad .$$

for which

$$W_{f_i} = 0.475 \quad \frac{W_{f_i}}{\Delta t} \quad .$$

Comparison:

For a sinsusoidal input of $\omega = 2\pi \ \frac{\text{rad}}{\text{s}}$ (1 Hz)

$$f_i = A\omega \cos \omega t$$

$$f_i = A\omega^3 \cos \omega t$$

so,

$$\frac{E_x}{f_i} = \omega^2 \frac{(8 + x)}{3(4 + 2x)} \Delta t^2$$

for $W_{f_i}$ = 3 counts ≅0.003 rad, the uncertainty and truncation error bound are presented in Table C.1. Note that $W_{f_i}$ is actually the uncertainty in a position <u>change</u> measurement. The absolute position cannot be measured this accurately, but it is believed that changes in position can be if the backlash in the gearing is neglected.

As computational capabilities necessitated the use of the 0.1-s timestep, the algorithm minimizing the truncation error was selected. Note that this is a relatively high estimate of the truncation error. The expected contribution to the uncertainty will be lower, because the expected (mean) frequency component of the real signal will be below 1 Hz. Assuming that a mean frequency of 0.67 Hz yields an expected truncation error of about 7%.

For the 5-point central difference formula, $E_x \alpha$ 5th-order derivative in the Taylor expansion

$$E_x = \frac{16(\Delta t^5/120) + 2(\frac{4\Delta t^5}{15}) \quad f_i \ \bar{v}}{-12\Delta t} \quad ,$$

$$= \frac{2}{3} \Delta t^4 f_i \ddot{\underline{v}} \quad ,$$

and

$$\frac{E_x}{f_i} = \frac{2}{3} \Delta t^4 \omega^4 \quad ,$$

for

$$\omega = 2\pi \text{ rad/s} \quad ,$$

and

$$\Delta t = 0.1 \text{ s} \quad ,$$

$$\frac{E_x}{f_i} \times 100 = 10.4\% \quad .$$

Table C.1. Velocity uncertainty and truncation error

| X | $\Delta t$(s) | $W_{f_i}$ (rad/s) | $W_{f_i}/x \times 100\%$ |
|---|---|---|---|
| 1/2 | 1/30 | 0.021 | 2.48% |
| 1/2 | 1/15 | 0.0104 | 9.9% |
| 1/2 | 1/10 | 0.0069 | 22.37% |
| -8 | 1/30 | 0.0621 | ~0 |
| -8 | 1/15 | 0.031 | 2.05% |
| -8 | 1/10 | 0.0189 | 10.4% |

# APPENDIX D

# KINEMATICS

# KINEMATICS

This appendix covers kinematic relationships for Model SM-229 manipulator arms. This includes relationships between joint positions and base frame positions and orientations, differential changes in joint positions, differential changes in base frame and end effector positions and orientations, and static joint torque distributions for general tong loads.

All of the relationships presented in this appendix are specific applications of general techniques/relationships.*

## Kinematic Modeling

Each motion of the arm is represented by an "A" transform. This transform, a 4 × 4 matrix, represents one independent motion. It may also represent physical characteristics of the system, such as the length of one of the linkages, and/or mathematical manipulations that simplify the model, such as a shifting of the reference axes. The coordinate frames and modeling parameters are shown schematically in Fig. 2.

The following describes the calculations required to determine the A transforms describing the position and orientation of the Model SM-229 manipulator.

Transform $A_n$ represents the following process:

1. Rotation about the $Z_{n-1}$ axis an angle $\theta_n$
2. Translation along the $Z_{n-1}$ axis a distance $d_n$
3. Transform $A_3$ and $A_4$: Translate along the $Y_{n-1}$ axis a distance $d_3$, $d_4$
4. Rotation of the reference axes an angle $\alpha_n$ about the x axis <u>or</u> an angle $\beta_n$ about the y axis.

Parameters for the A transforms are given in Table D.1.

The A transforms are determined as follows:

$$A_3 = \mathrm{Rot}(z,\theta_3)\ \mathrm{Trans}(0,-d_3,0)\ \mathrm{Rot}(y,\pi/2)$$

---

*R. P. Paul, <u>Robot Manipulators</u>, MIT Press, 1981.

The term Rot(y, $\pi/2$) represents the angle $\beta$ given in Table D.1. An angle $\alpha$ would correspond to Rot(x,$\alpha$). These terms are included only for consistency, so that all variable rotations are about the z axis (helpful when modeling system dynamics).

For each matrix, the first three elements of the first column represent the x,y,z components of the new x axis. Similarly, the first three elements of the second and third columns represent the x, y, and z components of the new y and z axes. The fourth column's first three elements represent the x, y, and z distances of the new origin from the base origin in the directions of the base origin.

Table D.1. Transformation parameters

| Transform | Variable | $\alpha$ | $\beta$ | d | Motion |
|---|---|---|---|---|---|
| 1 | $\Theta_1$ | $\pi/2$ | 0 | 0 | Shoulder pitch |
| 2 | $\Theta_2$ | $-\pi/2$ | 0 | $d_2$ | Shoulder roll |
| 3 | $\Theta_3$ | 0 | $\pi/2$ | $-d_3$ | Elbow pitch |
| 4 | $\Theta_4$ | 0 | $-\pi/2$ | $d_4, -d_4'$ | Elbow roll* |
| 5 | $\Theta_5$ | $\pi/2$ | 0 | 0 | Wrist pitch |
| 6 | $\Theta_6$ | $-\pi/2$ | 0 | $d_6$ | Wrist roll |

*$d_4$ is in the y direction.

$$A_3 = \begin{bmatrix} C_3 & -S_3 & 0 & 0 \\ S_3 & C_3 & 0 & 0 \\ 0 & 0 & 1 & 0 \\ 0 & 0 & 0 & 1 \end{bmatrix} \times \begin{bmatrix} 1 & 0 & 0 & 0 \\ 0 & 1 & 0 & -d_3 \\ 0 & 0 & 1 & 0 \\ 0 & 0 & 0 & 1 \end{bmatrix} \times \begin{bmatrix} 0 & 0 & 1 & 0 \\ 0 & 1 & 0 & 0 \\ -1 & 0 & 0 & 0 \\ 0 & 0 & 0 & 1 \end{bmatrix}$$

$$A_3 = \begin{bmatrix} 0 & -S_3 & C_3 & d_3S_3 \\ 0 & C_3 & S_3 & -d_3C_3 \\ 1 & 0 & 0 & 0 \\ 0 & 0 & 0 & 1 \end{bmatrix} \qquad (1)$$

The rest of the A matrices are as follows:

$$A_1=\begin{bmatrix} C_1 & 0 & S_1 & 0 \\ S_1 & 0 & -C_1 & 0 \\ 0 & 1 & 0 & 0 \\ 0 & 0 & 0 & 1 \end{bmatrix} \tag{2}$$

$$A_2=\begin{matrix} C_2 & 0 & -S_2 & 0 \\ S_2 & 0 & C_2 & 0 \\ 0 & -1 & 0 & d_2 \\ 0 & 0 & 0 & 1 \end{matrix} \tag{3}$$

$$A_4=\begin{bmatrix} 0 & -S_4 & -C_4 & S_4 d_4 \\ 0 & C_4 & -S_4 & -C_4 d_4 \\ 1 & 0 & 0 & d_4 \\ 0 & 0 & 0 & 1 \end{bmatrix} \tag{4}$$

$$A_5=\begin{bmatrix} C_5 & 0 & S_5 & 0 \\ S_5 & 0 & -C_5 & 0 \\ 0 & 1 & 0 & 0 \\ 0 & 0 & 0 & 1 \end{bmatrix} \tag{5}$$

$$A_6=\begin{bmatrix} C_6 & 0 & -S_6 & 0 \\ S_6 & 0 & C_6 & 0 \\ 0 & -1 & 0 & d_6 \\ 0 & 0 & 0 & 1 \end{bmatrix} \tag{6}$$

Forward Kinematics

The positions and orientations of each joint with respect to the fixed frame or each other are easily found by multiplying the appropriate A transforms.

Elbow matrix = $T_2 = A_2\ A_2=$

$$T_2=\begin{bmatrix} C_1C_2 & -S_1 & -C_1S_2 & d_2S_1 \\ S_1C_2 & C_1 & -S_1S_2 & -d_2C_1 \\ S_2 & 0 & C_2 & 0 \\ 0 & 0 & 0 & 1 \end{bmatrix} \tag{7}$$

Wrist matrix = $T_4= A_1A_2A_3A_4$

$$T_4 = \begin{bmatrix} W_{11} & W_{12} & W_{13} & W_{14} \\ W_{21} & W_{22} & W_{23} & W_{24} \\ W_{31} & W_{32} & W_{33} & W_{34} \\ 0 & 0 & 0 & 1 \end{bmatrix} \tag{8}$$

where

$$\begin{aligned}
W_{11} &= C_1C_2C_3 - S_1S_3 \\
W_{21} &= S_1C_2C_3 + C_1S_3 \\
W_{31} &= S_2C_3 \\
W_{12} &= -C_1C_2S_3C_4 - S_1C_3C_4 - C_1S_2S_4 \\
W_{22} &= -S_1C_2S_3C_4 + C_1C_3C_4 - S_1S_2S_4 \\
W_{32} &= -S_2S_3C_4 + C_2S_4 \\
W_{13} &= C_1C_2S_3S_4 + S_1C_3S_4 - C_1S_2C_4 \\
W_{23} &= S_1C_2S_3S_4 - C_1C_3S_4 - S_1S_2C_4 \\
W_{33} &= S_2S_3S_4 + C_2C_4 \\
W_{14} &= C_1C_2(C_3d_4 + S_3d_3 + S_3C_4d_4') \\
&\quad - S_1(S_3d_4 - C_3d_3 - C_3C_4d_4') \\
&\quad + S_1d_2 + C_1S_2S_4d_4' \\
W_{24} &= S_1C_2(C_3d_4 + S_3d_3 + S_3C_4d_4') \\
&\quad + C_1(S_3d_4 - C_3d_3 - C_3C_4d_4) \\
&\quad - C_1d_2 + S_1S_2S_4d_4' \\
W_{34} &= S_2(C_3d_4 + d_3S_3 + S_3C_4d_4') \\
&\quad - C_2C_4d_4'
\end{aligned}$$

$W_{14,24,34}$ = x,y,z position of the wrist.

Tong gripper matrix = $T_6 = A_1A_2A_3A_4A_5A_6$

$$T_6 = \begin{bmatrix} T_{11} & T_{12} & T_{13} & T_{14} \\ T_{21} & T_{22} & T_{23} & T_{24} \\ T_{31} & T_{32} & T_{33} & T_{34} \\ 0 & 0 & 0 & 1 \end{bmatrix} \tag{9}$$

where

$$\begin{aligned}
T_{11} &= W_{11}C_5C_6 + W_{12}S_5C_6 + W_{13}S_6 \\
T_{21} &= W_{21}C_5C_6 + W_{22}S_5C_6 + W_{23}S_6 \\
T_{31} &= W_{31}C_5C_6 + W_{32}S_5C_6 + W_{33}S_6
\end{aligned}$$

$$
\begin{aligned}
T_{12} &= W_{12}C_5 - W_{11}S_5 \\
T_{22} &= W_{22}C_5 - W_{21}S_5 \\
T_{32} &= W_{32}C_5 - W_{31}S_5 \\
T_{13} &= W_{11}C_5S_6 - W_{12}S_5S_6 + W_{13}C_6 \\
T_{23} &= -W_{21}C_5S_6 - W_{22}S_5S_6 + W_{23}C_6 \\
T_{33} &= -W_{31}C_5S_6 - W_{32}S_5S_6 + W_{33}C_6 \\
T_{14} &= W_{11}S_5d_6 - W_{12}C_5S_6 + W_{14} \\
T_{24} &= W_{21}S_5d_6 - W_{22}C_5d_6 + W_{24} \\
T_{34} &= W_{31}S_5d_6 - W_{32}C_5d_6 + W_{34} \; .
\end{aligned}
$$

The final matrix, $T_6$, contains the tong (or wrist) position and orientation. The wrist position is given if the final transfer distance, $d_6$ (from wrist pivot to tip of tong), is zero. The orientation of the tong x axis is given by the first three elements of the first column of $T_6$ ($T_{11}^6$, $T_{21}^6$, $T_{31}^6$). The superscript denotes the reference matrix or frame (in this case, $T_6$) while the subscript denotes the element of the matrix. (The superscript may be omitted if the reference matrix is obvious.) The component in the base frame x direction is $T_{11}^6$, in the y direction $T_{21}^6$, and in the z direction $T_{31}^6$.

Similarly, the tong y-axis orientation is given by $T_{12}^6$, $T_{22}^6$, and $T_{32}^6$, and the tong z-axis orientation is given by $T_{13}^6$, $T_{23}^6$, and $T_{33}^6$. The tong (or wrist) position is given by $T_{14}$ (x position), $T_{24}$ (y position), and $T_{34}$ (z position), again relative to and in the direction of the <u>base</u> frame.

## Reverse Kinematics

In the reverse kinematic problem, the tong orientations and position are given (thus, numeric values for $T_6$ are known) and the joint coordinates must be determined.

The joint coordinate solutions are obtained by equating transform expressions. For each transform equation, 12 nontrivial equations are obtained. These equations can be manipulated by noting that as

$$T_6 = A_1\ A_2\ A_3\ A_4\ A_5\ A_6,$$
$$A_1^{-1}\ T_6 = A_2\ A_3\ A_4\ A_5\ A_6, \quad \text{and}$$
$$A_2^{-1}\ A_1^{-1}\ T_6 = A_3\ A_4\ A_5\ A_6 \quad \text{and so on.}$$

A few more relevent matrices are first presented. The leading superscript denotes the reference frame in which the matrix is expressed. The leading zero superscript is often omitted for matrices expressed in the base frame.

$$^5T_6 = A_6 = \begin{bmatrix} C_6 & 0 & -S_6 & 0 \\ S_6 & 0 & C_6 & 0 \\ 0 & -1 & 0 & d_6 \\ 0 & 0 & 0 & 1 \end{bmatrix}$$

$$^4T_6 = A_5A_6 = \begin{bmatrix} C_5C_6 & -S_5 & -C_5S_6 & d_6S_5 \\ S_5C_6 & C_5 & -S_5S_6 & -d_6C_5 \\ S_6 & 0 & C_6 & 0 \\ 0 & 0 & 0 & 1 \end{bmatrix} \tag{10}$$

$$^3T_6 = A_4A_5A_6 = \begin{bmatrix} 0 & -S_4 & -C_4 & 0 \\ 0 & C_4 & -S_4 & 0 \\ 1 & 0 & 0 & d_4 \\ 0 & 0 & 0 & 1 \end{bmatrix} \qquad ^4T_6$$

$$^3T_6 = \begin{bmatrix} -S_4S_5C_6-C_4S_6 & -S_4C_5 & S_4S_5S_6-C_4C_6 & S_4C_5d_6 \\ C_4S_5C_6-S_4S_6 & C_4C_5 & -C_4S_5S_6-S_4C_6 & -C_4C_5d_6 \\ C_5C_6 & -S_5 & -C_5S_6 & S_5d_6 + d_4 \\ 0 & 0 & 0 & 1 \end{bmatrix} \tag{11}$$

$$^2T_6 = A_3A_4A_5A_6 = \begin{bmatrix} 0 & -S_3 & C_3 & d_3S_3 \\ 0 & C_3 & S_3 & -d_3C_3 \\ -1 & 0 & 0 & 0 \\ 0 & 0 & 0 & 1 \end{bmatrix} \qquad ^3T_6$$

$$
{}^{2}T_6 = \begin{bmatrix}
S_3S_4C_6 - S_3C_4S_5C_6 + C_3C_5C_6 & -S_3C_4C_5 - C_3S_5 & S_3(C_4S_5S_6 + S_4C_6) - C_3C_5S_6 & S_3C_4C_5d_6 + C_3(S_5d_6 + d_4) + S_3d_3 \\
C_3C_4S_5C_6 - C_3S_4S_6 + S_3C_5C_6 & C_3C_4C_5 - S_3S_5 & -C_3(C_4S_5S_6 + S_4C_6) - S_3C_5S_6 & -C_3C_4C_5d_6 + S_3(S_5D_6 + d_4) - C_3d_3 \\
S_4S_5C_6 + C_4S_6 & S_4C_5 & -S_4S_5S_6 + C_4C_6 & -S_4C_5d_6 \\
0 & 0 & 0 & 1
\end{bmatrix} \qquad (12)
$$

$$
{}^{1}T_6 = A_2A_3A_4A_5A_6 = A_2\ {}^{2}T_6
$$

For conciseness in the following equations, the following subscript is raised to a superscript, and the subscript denotes the specific element of the matrix that is

$$
{}^{1}T^{6}_{ij} = \sum_{k=1}^{4} A^{2}_{ik}\ {}^{2}T^{6}_{kj}
$$

so,

$$
{}^{1}T^{6} = \begin{bmatrix}
C_2\ {}^{2}T^{6}_{11} - S_2\ {}^{2}T^{6}_{31} & C_2\ {}^{2}T^{6}_{12} - S_2\ {}^{2}T^{6}_{32} & C_2\ {}^{2}T^{6}_{13} - S_2\ {}^{2}T^{6}_{33} & C_2\ {}^{2}T^{6}_{14} - S_2\ {}^{2}T^{6}_{34} \\
S_2\ {}^{2}T^{6}_{11} + C_2\ {}^{2}T^{6}_{31} & S_2\ {}^{2}T^{6}_{12} + C_2\ {}^{2}T^{6}_{32} & S_2\ {}^{2}T^{6}_{13} + C_2\ {}^{2}T^{6}_{33} & S_2\ {}^{2}T^{6}_{14} + C_2\ {}^{2}T^{6}_{34} \\
-{}^{2}T^{6}_{21} & -{}^{2}T^{6}_{22} & -{}^{2}T^{6}_{23} & -{}^{2}T^{6}_{24} + d_2 \\
0 & 0 & 0 & 1
\end{bmatrix} \qquad (13)
$$

Note: To solve the inverse kinematic problem, it is necessary to specify $d_6 = 0$, so that the "position" angles, $\theta_1$ to $\theta_3$, can be separated from the "orientation" angles, $\theta_4$ to $\theta_6$. No information is lost in this way. For simplicity, the wrist pivot offset (~1 in.) was neglected. If this is not done, the elbow roll motion affects the wrist position, and no convenient separation between wrist-positioning angles and orienting angles would exist. Thus, the known matrix, $T_6$, should be entered as the desired tong orientation and the desired position vector of the intersection point of the wrist pitch and elbow roll axes relative to the shoulder pivot.

Inverse A transforms

$$A_1^{-1} = \begin{bmatrix} C_1 & S_1 & 0 & 0 \\ 0 & 0 & 1 & 0 \\ S_1 & -C_1 & 0 & 0 \\ 0 & 0 & 0 & 1 \end{bmatrix} \tag{14}$$

$$\begin{aligned} A_2^{-1} &= (\mathrm{Rot}\ (z,\ \theta_2)\ \mathrm{Trans}\ (z,\ d_2)\ \mathrm{Rot}\ (x,\ -\pi/2))^{-1} \\ &= \mathrm{Rot}\ (x,\ +\pi/2)\ \mathrm{Rot}\ (z,\ -\theta_2)\ \mathrm{Trans}\ (z,\ d_2) \end{aligned}$$

$$= \begin{bmatrix} 1 & 0 & 0 & 0 \\ 0 & 0 & -1 & 0 \\ 0 & 1 & 0 & 0 \\ 0 & 0 & 0 & 1 \end{bmatrix} \times \begin{bmatrix} C_2 & S_2 & 0 & 0 \\ -S_2 & C_2 & 0 & 0 \\ 0 & 0 & 1 & 0 \\ 0 & 0 & 0 & 1 \end{bmatrix} \times \begin{bmatrix} 1 & & 0 & 0 \\ 0 & 1 & 0 & 0 \\ 0 & 0 & 1 & -d_2 \\ 0 & 0 & 0 & 1 \end{bmatrix}$$

$$A_2^{-1} = \begin{bmatrix} C_2 & S_2 & 0 & 0 \\ 0 & 0 & -1 & d_2 \\ -S_2 & C_2 & 0 & 0 \\ 0 & 0 & 0 & 1 \end{bmatrix} \tag{15}$$

$$A_3^{-1} = \begin{bmatrix} 0 & 0 & -1 & 0 \\ -S_3 & C_3 & 0 & -d_3 \\ C_3 & S_3 & 0 & 0 \\ 0 & 0 & 0 & 1 \end{bmatrix} \tag{16}$$

$$A_4^{-1} = \begin{bmatrix} 0 & 0 & 1 & -d_4 \\ -S_4 & C_4 & 0 & 0 \\ -C_4 & -S_4 & 0 & 0 \\ 0 & 0 & 0 & 1 \end{bmatrix} \tag{17}$$

$$A_5^{-1} = \begin{bmatrix} C_5 & S_5 & 0 & 0 \\ 0 & 0 & 1 & 0 \\ S_5 & -C_5 & 0 & 0 \\ 0 & 0 & 0 & 1 \end{bmatrix} \tag{18}$$

$$A_2^{-1}A_1^{-1} = \begin{bmatrix} C_1C_2 & S_1C_2 & S_2 & 0 \\ -S_1 & C_1 & 0 & d_2 \\ -C_1S_2 & -S_1S_2 & C_2 & 0 \\ 0 & 0 & 0 & 1 \end{bmatrix} \tag{19}$$

$$A_3^{-1}A_2^{-1}A_1^{-1} = \begin{bmatrix} C_1S_2 & S_1S_2 & -C_2 & 0 \\ -C_1C_2S_3-S_1C_3 & -S_1C_2S_3 + C_1C_3 & -S_2S_3 & C_3d_2 + d_3 \\ C_1C_2C_3-S_1S_3 & S_1C_2C_3 + C_1S_3 & S_2C_3 & S_3d_2 \\ 0 & 0 & 0 & 1 \end{bmatrix} \tag{20}$$

$$A_4^{-1}A_3^{-1}A_2^{-1}A_1^{-1} = \begin{bmatrix} C_1C_2C_3-S_1S_3 & S_1C_2C_3 + C_1S_3 & S_2C_3C & S_3d_2 - d_4 \\ -C_1C_2S_3C_4 - S_1C_3C_4 - C_1S_2S_4 & -S_1C_2S_3C_4 + C_1C_3C_4 - S_1S_2S_4 & -S_2C_3C_4 + C_2S_4 & C_3C_4d_2 + C_4d_3 \\ C_1C_2S_3S_4 + S_1C_3S_4 - C_1S_2C_4 & S_1C_2S_3S_4 - C_1C_3S_4 - S_1S_2C_4 & S_2S_3S_4 + C_2C_4 & -C_3S_4d_2 - S_4d_3 \\ 0 & 0 & 0 & 1 \end{bmatrix} \tag{21}$$

$$A_1^{-1}T_6 = A_2A_3A_4A_5A_6 = {}^1T_6$$

$$A_1^{-1}T_6 = \begin{bmatrix} C_1 & S_1 & 0 & 0 \\ 0 & 0 & 1 & 0 \\ S_1 & -C_1 & 0 & 0 \\ 0 & 0 & 0 & 1 \end{bmatrix} \times \begin{matrix} n_x & o_x & a_x & p_x \\ n_y & o_y & a_y & p_y \\ n_z & o_z & a_z & p_z \\ 0 & 0 & 0 & 1 \end{matrix}$$

n, o, a, p = the known $T_6$ vectors

$$= \begin{bmatrix} f_{11}(n) & f_{11}(o) & f_{11}(a) & f_{11}(p) \\ f_{12}(n) & f_{12}(o) & f_{12}(a) & f_{12}(p) \\ f_{13}(n) & f_{13}(o) & f_{13}(a) & f_{13}(p) \\ 0 & 0 & 0 & 1 \end{bmatrix} \tag{22}$$

where

$$f_{11} = C_1\ x + S_1\ y$$
$$f_{12} = z$$
$$f_{13} = S_1\ x - C_1\ y$$

The 14, 24, and 34 elements yield three equations which must be solved simultaneously:

$$C_1 p_x + S_1\ p_y = C_2(C_3 d_4 + S_3 d_3) \tag{23}$$

$$p_z = S_2(C_3 d_4 + S_3 d_3) \tag{24}$$

$$S_1 p_x - C_1\ p_y = C_3 d_3 - S_3 d_4 + d_2 \tag{25}$$

The following solution was obtained from Dr. J. A. Euler:

let

$$d^2 = p_x^2 + p_y^2 + p_z^2 \tag{26}$$

$$(23) \quad C_1 p_x + S_1 p_y = C_2(C_3 d_4 + S_3 d_3) \equiv A \tag{27}$$

$$(25) \quad S_1 p_x - C_1 p_y = C_3 d_3 - S_3 d_4 + d_2 \equiv B \tag{28}$$

$$(27)\ \frac{p_y}{p_x} + (28) \text{ yields}$$

$$S_1 \frac{p_y^2}{p_x} + S_1\ p_x = \frac{p_y A}{p_x} + B$$

$$S_1 = \frac{\frac{p_y}{p_x} A + B}{\frac{p_y^2}{p_x} + p_x}$$

$$S_1 = \frac{p_y A + p_x B}{p_y^2 + p_x^2} \tag{29}$$

$(27) p_x - (28)\ p_y$:

$$C_1\ p_x^2 + C_1\ p_y^2 = p_x A - p_y B$$

$$C_1 = \frac{p_x A - p_y B}{p_x^2 + p_y^2} \tag{30}$$

$(29)^2 + (30)^2$ yields

$$S_1^2 + C_1^2 = 1 \quad \frac{(p_y A + p_x B)^2 + (p_x A - p_y B)^2}{(p_x^2 + p_y^2)^2}$$

$$(p_x^2 + p_y^2)^2 = A^2 (p_x^2 + p_y^2) + B^2 (p_x^2 + p_y^2)$$

$$p_x^2 + p_y^2 = A^2 + B^2$$

Substituting Eqs. (27) and (28) yields

$$p_x^2 + p_y^2 = C_2^2 (C_3 d_4 + S_3 d_3)^2 + (C_3 d_3 - S_3 d_4 + d_2)^2$$

add Eq. $(24)^2$:

$$d^2 = p_x^2 + p_y^2 + p_z^2 = C_2^2 (C_3 d_4 + S_3 d_3)^2 + (C_3 d_3 - S_3 d_4 + d_2)^2$$

$$+ S_2^2 (C_3 d_4 + S_3 d_3)$$

$$= (C_3 d_4 + S_3 d_3)^2 + (C_3 d_3 - S_3 d_4 + d_2)^2$$

$$d^2 = d_2^2 + d_3^2 + d_4^2 + 2C_3 d_2 d_3 - 2S_3 d_2 d_4$$

$$d_3 C_3 - d_4 S_3 = \frac{d^2 - d_2^2 - d_3^2 - d_4^2}{2\, d_2} = \text{RHS} \qquad (31)$$

define: $d_3 = r \sin \phi$

$d_4 = r \cos \phi$

where

$$r = +\sqrt{d_3^2 + d_4^2}$$

$$\phi = \tan^{-1} \frac{d_3}{d_4}$$

then,

$$rS_\phi C_3 - rC_\phi S_3 = RHS$$

$$S_\phi C_3 - C_\phi S_3 = RHS/r$$

$$\sin(\phi - \theta_3) = RHS/r$$

$$\phi - \theta_3 = \sin^{-1}(RHS/r)$$

so,

$$\theta_3 = \tan^{-1} \frac{d_3}{d_4} - \sin^{-1}\left[\frac{p_x^2 + p_y^2 + p_z^2 - d_2^2 - d_3^2 - d_4^2}{2\, d_2\, (d_3^2 + d_4^2)^{1/2}}\right]$$

with

$\tan^{-1}(d_3/d_4) = (+)$

Now rewrite Eq. (25),

$$S_1 p_x - C_1 p_y = C_3 d_3 - S_3 d_4 + d_2 ,$$

let

$$p_y = r \sin \phi ,$$
$$p_x = r \cos \phi ,$$

then

$$r = +\sqrt{p_x^2 + p_y^2} \quad , \qquad \phi = \tan^{-1} (p_y/p_x)$$

and,

$$rS_1C_\phi - r\,C_1S_\phi = C_3d_3 - S_3d_4 + d_2$$

$$\sin(\theta_1 - \phi) = \frac{C_3d_3 - S_3d_4 + d_2}{r}$$

$$\sin(\theta_1 - \phi) = \frac{C_3d_3 - S_3d_4 + d_2}{r}$$

$$\theta_1 = \sin^{-1} \frac{C_3d_3 - S_3d_4 + d_2}{p_x^2 + p_y^2 \quad {}^{1/2}} + \tan^{-1} (p_y/p_x) \tag{33}$$

$$\frac{\text{Eq. (24)}}{\text{Eq. (23)}} = \frac{S_2}{C_2} = \frac{p_z}{C_1p_x + S_1p_y}$$

$$\theta_2 = \tan^{-1} \frac{p_z}{C_1\ p_x + S_1\ p_y} \tag{34}$$

Here the inverse tangent is completely defined as the signs of both the numerator and denominator are known

$$A_3^{-1}A_2^{-1}A_1^{-1}T_6 = {}^3T_6$$

$$A_3^{-1}A_2^{-1}A_1^{-1}T_6 = \begin{bmatrix} f_{31}(n) & f_{31}(o) & f_{31}(a) & f_{31}(p) \\ f_{32}(n) & f_{32}(o) & f_{32}(a) & f_{32}(p) + C_3d_2 + d_3 \\ f_{33}(n) & f_{33}(o) & f_{33}(a) & f_{33}(p) + C_3d_2 \\ 0 & 0 & 0 & 1 \end{bmatrix} \tag{35}$$

where

$$f_{31} = (C_1S_2)x + (S_1S_2y) - (C_2z)$$
$$f_{32} = (-C_1C_2S_3 - S_1C_3)x + (-S_1C_2S_3 + C_1C_3)y + (-S_2S_3)z$$
$$f_{33} = (C_1C_2C_3 - S_1S_3)x + (S_1C_2C_3 + C_1S_3)y + (S_2C_3)z$$

look at elements 1,2 and 2,2

$$\frac{S_4C_5}{C_4C_5} = \frac{-C_1S_2o_x - S_1S_2o_y + C_2o_z}{(-C_1C_2S_3 - S_1C_3)o_x + (-S_1C_2S_3 + C_1C_3)o_y - S_2S_3o_z} \tag{36}$$

so

$$\theta_4 = \tan^{-1} \frac{-C_1S_2o_x - S_1S_2o_y + C_2o_z}{(-C_1C_2S_3 - S_1C_3)o_x + (-S_1C_2S_3 + C_1C_3)o_y - S_2S_3o_z} \tag{37}$$

Again, the signs of the numerator and denominator determine the quadrant, and

$$\theta_4 = \theta_4 \pm 180° \text{ if } \pi/2 < \theta_5$$

Degeneracy occurs for $\theta_5 = \pi/2$

If $\theta_5 = \pi/2$, assign the current value to $\theta_4$.

$$A_4^{-1}A_3^{-1}A_2^{-1}A_1^{-1}T_6 = {}^4T_6$$

$$A_4^{-1}A_3^{-1}A_2^{-1}A_1^{-1}T_6 = \begin{bmatrix} f_{41}(n) & f_{41}(o) & f_{41}(a) & f_{41}(p) + S_3d_z - d_4 \\ f_{42}(n) & f_{42}(o) & f_{42}(a) & f_{42}(p) + C_3C_4d_2 + C_4d_3 \\ f_{43}(n) & f_{43}(o) & f_{43}(a) & f_{43}(p) - C_3S_4d_2 - S_4d_3 \\ 0 & 0 & 0 & 1 \end{bmatrix} \tag{38}$$

where

$$f_{41} = (C_1C_2C_3 - S_1S_3)x + (S_1C_2C_3 + C_1S_3)y + (S_2C_3)z$$

$$f_{42} = (-C_1C_2S_3C_4 - S_1C_3C_4 - C_1S_2S_4)x + (-S_1C_2S_3C_4 + C_1C_3C_4 - S_1S_2S_4)y + (-S_2C_3C_4 + C_2S_4)z$$

$$f_{43} = (C_1C_2S_3S_4 + S_1C_3S_4 - C_1S_2C_4)x + (S_1C_2S_3S_4 - C_1C_3S_4 - S_1S_2C_4)y + (S_2S_3S_4 + C_2C_4)z$$

Examine the 1,2 and 2,2 elements

$$\frac{-S_5}{C_5} = \frac{(C_1C_2S_3C_4 + S_1C_3C_4 + C_1S_2S_4)\ o_x + (S_1C_2S_3S_4 - C_1C_3C_4 + S_1S_2S_4)\ o_y + (S_2C_3C_4 - C_2S_4)\ o_z}{(S_1S_3 - C_1C_2C_3)\ o_x - (S_1C_2C_3 + C_1S_3)\ o_y - S_2C_3o_z} \tag{39}$$

$\theta_5 = -\tan^{-1}$ [num/denom]

The first three elements of the first two rows of $A_5^{-1}A_4^{-1}A_3^{-1}A_2^{-1}A_1^{-1}$ are needed to find $\theta_6$:

$$A_5^{-1}A_4^{-1}A_3^{-1}A_2^{-1}A_1^{-1} = \begin{matrix} (C_1C_2C_3 - S_1S_3)C_5 - (C_1C_2S_3C_4 + S_1C_3C_4 + C_1S_2S_4)S_5 \\ C_1C_2S_3S_4 + S_1C_3S_4 - C_1S_2C_4 \\ ? \\ 0 \end{matrix}$$

(2nd col)

$$\begin{matrix} (S_1C_2C_3 + C_1S_3)\ C_5 - (S_1C_2S_3C_4 - C_1C_3C_4 + S_1S_2S_4)\ S_5 \\ S_1C_{234} - C_1C_3S \quad S_1S_2C_4 \\ ? \\ 0 \end{matrix}$$

(3rd col)

$$\begin{matrix} S_2C_3C_5 + (C_2S_4 - S_2C_3C_4)\ S_5 \\ S_2S_3S_4 + C_2C_4 \\ ? \\ 0 \end{matrix}$$

(4th col)

$$\begin{matrix} ? \\ ? \\ ? \\ 1 \end{matrix} \tag{40}$$

Examining the 1,3 and 2,3 elements of Eq. (40) results in

$$\begin{aligned} S_6 = {} & [(S_1S_3 - C_1C_2C_3)\ C_5 + (C_1C_2S_3C_4 + S_1C_3C_4 + C_1S_2S_4)\ S_5]a_x \\ & + [(-S_1C_2C_3 - C_1S_3)C_5 + (S_1C_2S_3C_4 - C_1C_3C_4 + S_1S_2S_4)S_5]a_y \\ & + \ [-S_2C_3C_5 + (S_2C_3C_4 - C_2S_4)S_5]a_z \\ C_6 = {} & (C_1C_2S_3S_4 + S_1C_3S_4 - C_1S_2C_4)a_x \\ & + (S_1C_2S_3S_4 - C_1C_3S_4 - S_1S_2C_4)a_y + (S_2S_3S_4 + C_2C_4)a_z \end{aligned} \tag{41}$$

and,

$$\theta_6 = \tan^{-1} \frac{S_6}{C_6}$$

Again, since the signs of the sines and cosines of $\theta_5$ and $\theta_6$ are known, the angles are completely determined.

Note that some calculations may have to be repeated because the sign of $C_5$ must be assumed to determine $\theta_4$. After the equation for $\theta_5$ is solved, the assumption must be checked. If it is inconsistent, $\theta_4$ and $\theta_5$ must be redetermined.

The possibility of degeneracy occurs in these calculations. Physically, this means that two or more DOFs have lined up so as to produce the same motion (for example, when the wrist pitch is such that the tong and forearm axes are aligned, the effect of the elbow and wrist roll motions are indistinguishable. Recall that the wrist offset has been neglected.) When this occurs, the first degenerate

DOF is arbitrarily assigned its current value. The remaining degenerate DOF can then be determined.

Solution of the reverse kinematic problem is of primary importance in operating the manipulator as a robot. In many pick-and-place tasks, the desired tong orientation and position are known. The corresponding joint coordinates are needed to determine the control trajectory. Teach/playback robotic operation is possible without using the inverse kinematics but would be cumbersome because every task would have to be taught. Given a flange of known size and orientation with, say, 30 bolts, the operator can teach the robot how to remove one bolt. The inverse kinematics can then be used to transfer this task to the remaining 29 bolts, with all of these bolts removed robotically. The inverse kinematics will also indicate when the desired bolt cannot be reached from the current manipulator position.

The equations developed here will also have applications in solving the reverse Jacobian problem.

## The Manipulator $T_6$ Jacobian

The manipulator $T_6$ Jacobian, transferring differential changes in joint coordinates to differential translations and rotations in the $T_6$ frame, will now be derived.

Introduction. All DOFs of Model SM-229 are revolute, so differential changes in joint coordinates refer to a six-element column vector of differential joint rotations. Recall that the A transforms were set up so that all variable rotations were about the z axis. A rotation about the z axis of an angle $\theta$ is expressed as:

$$\text{Rot}\ (z,\theta) = \begin{bmatrix} \cos\theta & -\sin\theta & 0 & 0 \\ \sin\theta & \cos\theta & 0 & 0 \\ 0 & 0 & 0 & 0 \\ 0 & 0 & 0 & 1 \end{bmatrix}$$

As $\theta \to 0$, $\sin\theta \to \theta$ and $\cos\theta \to 1$.

Thus, a <u>differential</u> rotation about the z axis is given by

$$\text{Rot}\ (z,\ d\theta) = \begin{bmatrix} 1 & -d\theta & 0 & 0 \\ d\theta & 1 & 0 & 0 \\ 0 & 0 & 1 & 0 \\ 0 & 0 & 0 & 1 \end{bmatrix}$$

and the <u>differential change matrix</u> given by

$$\Delta = \text{Rot}\ (z,\ d\theta) - I = \begin{bmatrix} 0 & -d\theta & 0 & 0 \\ d\theta & 0 & 0 & 0 \\ 0 & 0 & 0 & 0 \\ 0 & 0 & 0 & 0 \end{bmatrix}$$

Thus, given a matrix T,

$dT = \Delta T$ if the differential rotation is given in the base frame, and

$dT = T\ \Delta$ if the differential change is given in the T frame. Similarly, the differential change matrix due to a differential rotation about the x and y axes are given by

$$\Delta = \begin{bmatrix} 0 & 0 & d\theta & 0 \\ 0 & 0 & 0 & 0 \\ -d & 0 & 0 & 0 \\ 0 & 0 & 0 & 0 \end{bmatrix} \quad \text{and } \Delta = \begin{bmatrix} 0 & 0 & 0 & 0 \\ 0 & 0 & -d\theta & 0 \\ 0 & d\theta & 0 & 0 \\ 0 & 0 & 0 & 0 \end{bmatrix}$$

respectively.

It is interesting to note that in multiplying any combination of differential rotation (not change!) matrices, higher order differentials can be neglected, so that <u>the result is independent of the order</u>.

Given a coordinate frame, T,

$$T = \begin{bmatrix} n_x & o_x & a_x & p_x \\ n_y & o_y & a_y & p_y \\ n_z & o_z & a_z & p_z \\ 0 & 0 & 0 & 1 \end{bmatrix}$$

relative to, say, the base frame, the differential translations and rotations of the T frame due to a differential rotation about the z axis of the base frame are given by:

$$T_{d_x} = n \cdot (k \times p)$$

$$T_{d_y} = o \cdot (k \times p) \qquad (42)$$

$$T_{d_z} = a \cdot (k \times p) \ ,$$

where k is the unit vector in the (base) z direction, and

$$T_\delta = n_z \ i + o_z \ j + a_z \ k \ . \qquad (43)$$

These two (differential translation and rotation) vectors contain all of the differential changes in the T frame due to a differential rotation about the base frame z axis. In matrix form, it would be written as

$$\frac{\partial T}{\partial q_1} = T \begin{bmatrix} 0 & -a_z & o_z & n \cdot (k \times p) \\ a_z & 0 & -n_z & o \cdot (k \times p) \\ -o_z & n_z & 0 & a \cdot (k \times p) \\ 0 & 0 & 0 & 0 \end{bmatrix}$$

It is convenient to extract the six independent elements of the differential change matrix and form a column vector. Thus,

$$\frac{"\partial T"}{\partial q_1} = \left[ {}^T d_x \;\; {}^T d_y \;\; {}^T d_z \;\; {}^T \delta_x \;\; {}^T \delta_y \;\; {}^T \delta_z \right]^T \tag{44}$$

where the quotes are used because the true partial is the 4 × 4 matrix.

Derivation of the Manipulator Jacobian. Define:

${}^T 6d_i$ = The differential position change vector in the $T_6$ frame due to a differential rotation of joint i, and

${}^T 6\delta_i$ = The differential orientation change vector in the $T_6$ frame due to a differential rotation of joint i.

Since all variable rotations are about the z axis, equations (42) and (43) yield

$${}^T 6d_i = (-n_x p_y + n_y p_x)\, i + (-o_x p_y + o_y p_x)\, j + (-a_x p_y + a_y p_x)\, k \tag{45}$$

$${}^T 6\delta_i = n_z i + o_z j + a_z k$$

where n, o, a and p are the vectors of ${}^{i-1}T_6$.

So,

$${}^T 6d_{1_x} = -\,({}^0T_{11}^6)\,({}^0T_{24}^6) + ({}^0T_{21}^6)\,({}^0T_{14}^6) \tag{46}$$

$${}^T 6d_{1_y} = -\,({}^0T_{12}^6)\,({}^0T_{24}^6) + ({}^0T_{22}^6)\,({}^0T_{14}^6)$$

$${}^T 6d_{1_z} = -\,({}^0T_{13}^6)\,({}^0T_{24}^6) + ({}^0T_{23}^6)\,({}^0T_{14}^6)$$

Again, no information is lost by specifying $d_6 = 0$, and the above equations simplify to

$$
\begin{aligned}
{}^{T}6d_{1_x} = {} & C_2[(C_4S_5C_6 - S_4S_6)(d_4 - S_3d_2) + C_5C_6(C_3d_2 + C_4d_4)] \\
& + S_2[(S_4S_5C_6 + C_4S_6)(S_3d_4 - C_3d_3 - d_2) + (S_3S_4C_5C_6 - C_3S_6)]d_4
\end{aligned}
\tag{47}
$$

$$
\begin{aligned}
{}^{T}6d_{1_y} = {} & C_2[C_4C_5(d_4 - S_3d_2) - S_5(d_3 + C_3d_2 + C_4d_4)] + \\
& + S_2\{S_4[C_5(S_3d_4 - C_3d_3 - d_2) - S_3S_5d_4]\}
\end{aligned}
\tag{48}
$$

and

$$
\begin{aligned}
{}^{T}6d_{1_z} = {} & C_2\{S_6[C_4(S_5(A) - C_5d_4 - C_5(d_3 + C_3d_2)] + C_6S_4(A)\} + \\
& + S_2\{S_6[S_4(S_5(B) - C_5S_3d_4)] + C_6[-C_4(B) - C_3d_4]\}
\end{aligned}
\tag{49}
$$

where

$$A = S_3d_2 - d_4$$

$$B = C_3d_3 - S_3d_4 + d_2$$

$${}^{T}6\delta_{1_x} = {}^{0}T_{3}^{6}{}_{1}$$

$$
\begin{aligned}
{}^{T}6\delta_{1_x} = {} & C_2(S_4S_5C_6 + C_4S_6) + \\
& S_2(C_3C_5C_6 - S_3C_4S_5C_6 + S_3S_4S_6
\end{aligned}
\tag{50}
$$

$$^{T}6\delta_{1_y} = {}^{0}T_{3\,2}^{\,6}$$

$$^{T}6\delta_{1_z} = C_2(S_4C_5) - S_2(S_3C_4C_5 + C_3C_5) \tag{51}$$

$$^{T}6\delta_{1_z} = {}^{0}T_{3\,3}^{\,6}$$

$$^{T}6\delta_{1_z} = C_2(-S_4S_5S_6 + C_4C_6) + S_2(-C_3C_5S_6 + S_3C_4S_5S_6 + S_3S_4C_6) \tag{52}$$

$$^{T}6d_{2_x} = (-{}^{1}T_{1\,1}^{\,6})({}^{1}T_{2\,4}^{\,6}) + ({}^{1}T_{2\,1}^{\,6})({}^{1}T_{1\,4}^{\,6})$$

$$^{T}6d_{2_y} = (-{}^{1}T_{1\,2}^{\,6})({}^{1}T_{2\,4}^{\,6}) + ({}^{1}T_{2\,2}^{\,6})({}^{1}T_{1\,4}^{\,6})$$

$$^{T}6d_{2_z} = (-{}^{1}T_{1\,3}^{\,6})({}^{1}T_{2\,4}^{\,6}) + ({}^{1}T_{2\,3}^{\,6})({}^{1}T_{1\,4}^{\,6})$$

$$^{T}6d_{2_x} = C_3[(D)d_4 + S_4C_5C_6d_4] + S_3[(D)d_3 + S_6d_4] \tag{53}$$

where

$$(D) = C_4S_6 + S_4S_5C_6$$

$$^{T}6d_{2_y} = S_4C_5[C_3(d_4 - d_4) + S_3d_3] \tag{54}$$

$$^{T}6d_{2_z} = \{C_3[-S_4C_5S_6d_4 + (C_4C_6 - S_4S_5S_6)d_4] + S_3[C_6d_4 + (C_4C_6 - S_4S_5S_6)d_3]\} \tag{55}$$

$^{T}6\delta_{2_x} = {}^{1}T_{3\,1}^{\,6}$, $^{T}6\delta_{2_y} = {}^{1}T_{3\,2}^{\,6}$, $^{T}6\delta_{2_z} = {}^{1}T_{3\,3}^{\,6}$, so

$$^{T}6\delta_{2_x} = [-C_3(C_4S_5C_6 - S_4S_6) - S_3C_5C_6] \tag{56}$$

$$^{T}6\delta_{2_y} = (S_3S_5 - C_3C_4C_5) \tag{57}$$

$$^{T}6\delta_{2_z} = [C_3(C_4S_5S_6 + S_4C_6) + S_3C_5S_6] \tag{58}$$

$$^{T}6d_{3_x} = (-{}^{2}T_{1\,1}^{\,6})({}^{2}T_{2\,4}^{\,6}) + ({}^{2}T_{2\,1}^{\,6})({}^{2}T_{1\,4}^{\,6})$$

$$^{T}6d_{3_y} = (-{}^{2}T_{1\,2}^{\,6})({}^{2}T_{2\,4}^{\,6}) + ({}^{2}T_{2\,2}^{\,6})({}^{2}T_{1\,4}^{\,6})$$

$$^{T}6d_{3_z} = (-{}^{2}T_{1\,3}^{\,6})({}^{2}T_{2\,4}^{\,6}) + ({}^{2}T_{2\,3}^{\,6})({}^{2}T_{1\,4}^{\,6})$$

So,

$$^{T}6d_{3_x} = C_5C_6(d_3 + C_4d_4) + d_4(C_4S_5C_6 - S_4S_6) \tag{59}$$

$$^{T}6d_{3_y} = -S_5(d_3 + C_4d_4) + d_4(C_4C_5) \tag{60}$$

$$^{T}6d_{3_z} = -C_5C_6(d_3 + C_4d_4) - d_4(C_4S_5S_6 + S_4C_6) \tag{61}$$

$^{T}6\delta_3 = {}^{2}T_{3\,1}^{\,6}$, $^{T}6\delta_3 = {}^{2}T_{3\,2}^{\,6}$, $^{T}6\delta_3 = {}^{2}T_{3\,3}^{\,6}$, so

$$^{T}6\delta_{3_x} = C_4S_6 + S_4S_5C_6 \tag{62}$$

$$^{T}6\delta_{3_y} = S_4C_5 \tag{63}$$

$$^{T}6\delta_{3_z} = C_4C_6 - S_4S_5S_6 \tag{64}$$

$$^{T}6d_{4_x} = (-{}^{3}T_{1}{}^{6}_{1})({}^{3}T_{2}{}^{6}_{4}) + ({}^{3}T_{2}{}^{6}_{1})({}^{3}T_{1}{}^{6}_{4})$$

$$^{T}6d_{4_y} = (-{}^{3}T_{1}{}^{6}_{2})({}^{3}T_{2}{}^{6}_{4}) + ({}^{3}T_{2}{}^{6}_{2})({}^{2}T_{1}{}^{6}_{4})$$

$$^{T}6d_{4_z} = (-{}^{3}T_{1}{}^{6}_{3})({}^{3}T_{2}{}^{6}_{4}) + ({}^{3}T_{2}{}^{6}_{3})({}^{3}T_{1}{}^{6}_{4})$$

$$^{T}6d_{4_x} = -S_6d_4 \tag{65}$$

$$^{T}6d_{4_y} = 0 \tag{66}$$

$$^{T}6d_{4_z} = -C_6d_4 \tag{67}$$

$$^{T}6\delta_{4_x} = C_5C_6 \tag{68}$$

$$^{T}6\delta_{4_y} = -S_5 \tag{69}$$

$$^{T}6\delta_{4_z} = -C_5S_6 \tag{70}$$

As

$$^{4}T_{1}{}^{6}_{4} = {}^{4}T_{2}{}^{6}_{4} = 0,$$

$$^{T}6d_{5_x} = {}^{T}6d_{5_y} = {}^{T}6d_{5_z} = 0 \tag{71}$$

And,

$$^{T}6\delta_{5_x} = S_6 \tag{72}$$

$$^{T}6\delta_{5_y} = 0 \tag{73}$$

$$^{T}6\delta_{5_z} = C_6 \tag{74}$$

As

$$^{5}T_{1}{}^{6}_{4} = {}^{5}T_{2}{}^{6}_{4} = 0,$$

$$^{T}6d_{6_x} = {}^{T}6d_{6_y} = {}^{T}6d_{6_z} = 0 \tag{75}$$

and,

$$^{T}6\delta_{6_x} = 0 \tag{76}$$

$$^{T}6\delta_{6_y} = -1 \tag{77}$$

$$^{T}6\delta_{6_z} = 0 \tag{78}$$

Thus the total $T_6$ Jacobian is given by Eqs. (47) through (78),

$$J = \begin{bmatrix} T_{6d_1x} & T_{6d_2x} & T_{6d_3x} & T_{6d_4x} & T_{6d_5x} & T_{6d_6x} \\ T_{6d_1y} & T_{6d_2y} & T_{6d_3y} & T_{6d_4y} & T_{6d_5y} & T_{6d_6y} \\ T_{6d_1z} & T_{6d_2z} & T_{6d_3z} & T_{6d_4z} & T_{6d_5z} & T_{6d_6z} \\ T_{6\delta_1x} & T_{6\delta_2x} & T_{6\delta_3x} & T_{6\delta_4x} & T_{6\delta_5x} & T_{6\delta_6x} \\ T_{6\delta_1y} & T_{6\delta_2y} & T_{6\delta_3y} & T_{6\delta_4y} & T_{6\delta_5y} & T_{6\delta_6y} \\ T_{6\delta_1z} & T_{6\delta_2z} & T_{6\delta_3z} & T_{6\delta_4z} & T_{6\delta_5z} & T_{6\delta_6z} \end{bmatrix} \tag{79}$$

$$= \begin{bmatrix} C_2[C_4S_5C_6-S_4S_6)(d_4-S_3d_2) + C_5C_6(C_3d_2 + d_3 + C_4d_4)] + S_2[(S_4S_5C_6 \\ \quad + C_4S_6)(S_3d_4 - C_3d_3 - d_2) + (S_3S_4C_5C_6 - C_3S_6)d_4 \\ C_2[C_4C_5(d_4 - S_3d_2) - S_5(d_3 + C_3d_2 + C_4d_4)] + S_2\{S_4[C_5(S_3d_4 - C_3d_3 \\ \quad - d_2) - S_3S_5d_4]\} \\ C_2\{S_6[C_4(S_5(A)^* - C_5d_4) - C_5(d_3 + C_3d_2)] + C_6S_4(A)^*\} \\ \quad + S_2\{S_6(S_5(B)^* - C_5S_3d_4)] - C_6[C_4(B)^* + C_3d_4]\} \\ \\ C_2(S_4S_5C_6 + C_4S_6) + S_2(C_3C_5C_6 - S_3C_4S_5C_6 + S_3S_4S_6) \\ C_2(S_4C_5) - S_2(S_3C_4C_5 + C_3S_5) \\ C_2(-S_4S_5S_6 + C_4C_6) + S_2(-C_3C_5S_6 + S_3C_4S_5S_6 + S_3S_4C_6) \end{bmatrix}$$

$*A = S_3d_2 - d_4$

$B = C_3d_3 - S_3d_4 + d_2$

(2nd column)

$$\{C_3[(C)^* d_4 + S_4C_5C_6d_4] + S_3\,[(C)^* d_3 + S_6d_4]\}$$

$$\{S_4C_5[C_3(d_4-d_4) + S_3d_3]\}$$

$$\{C_3[-S_4C_5S_6d_4 + (C_4C_6 - S_4S_5S_6)d_4] + S_3[C_6d_4 + (C_4C_6 - S_4S_5S_6)d_3]\}$$

$$[C_3(C_4S_5C_6 - S_4S_6) + S_3C_5C_6]$$

$$(S_3S_5 - C_3C_4C_5)$$

$$[C_3(C_4S_5S_6 + S_4C_6) + S_3C_5S_6]$$

(3rd column)

$$C_5C_6(d_3 + C_4d_4) + d_4(C_4S_5C_6 - S_4S_6)$$

$$-S_5(d_3 + C_4d_4) + d_4(C_4C_5)$$

$$-C_5C_6(d_3 + C_4d_4) - d_4(C_4S_5S_6 + S_4C_6)$$

$$C_4S_6 + S_4S_5C_6$$

$S_4C_5$

$C_4C_6 - S_4S_5S_6$

$$\begin{array}{ccc} \text{(4th column)} & \text{(5th column)} & \text{(6th column)} \end{array}$$
$$\begin{bmatrix} -S_6d_4' & 0 & 0 \\ 0 & 0 & 0 \\ -C_6d_4' & 0 & 0 \\ C_5C_6 & S_6 & 0 \\ -S_5 & 0 & -1 \\ -C_5S_6 & C_6 & 0 \end{bmatrix}$$

$(C)^* = C_4S_6 + S_4S_5C_6$

This Jacobian matrix transforms differential changes in joint coordinates to differential rotations and translations in the $T_6$ frame. It is also of interest to transform to the base frame. The procedure is again straightforward.

Earlier, the differential change, $dT_6$, was defined as

$$dT_6 = T_6 \, {}^{T}6\Delta_i \, dq_i = A_1A_2 \ldots A_{i-1} \, {}^{i-1}\Delta_i \, A_i \ldots A_6 \, dq_i$$

so that

$${}^{T}6\Delta = \left(A_i \, A_{i+1} \ldots A_6\right)^{-1} \, {}^{i-1}\Delta_i \left(A_i \, A_{i+1} \ldots A_6\right)$$

Thus, the vectors of ${}^{i-1}T_6$ were used to transfer between coordinate frames. To find the base frame Jacobian, define $dT_6$ as

$$dT_6 = {}^0\Delta_i \; T_6 \; dq_i = A_1 A_2 \; \ldots \; A_{i-1} \; {}^{i-1}\Delta_i A_i \; \ldots \; A_6 \; dq_i$$

Thus,

$$ {}^0\Delta_i = \left(A_1 \; A_2 \; \ldots \; A_{i-1}\right) \; {}^{i-1}\Delta_i \; \left(A_i \; \ldots A_6\right) \; T_6^{-1}$$

$$= \left(A_{i-1}^{-1} \ldots A_2^{-1} A_1^{-1}\right)^{-1} \; {}^{i-1}\Delta_i \; \left(A_{i-1}^{-1} \; A_2^{-1} \; A_1^{-1}\right) \qquad (80)$$

so that using the vectors of $\left({}^0T_{i-1}\right)^{-1}$ in place of the vectors of ${}^{i-1}T_6$ will yield relationships in the base frame.

Applications of the Jacobian. The Jacobian transformations have a wide range of applications in robotics and in advanced servo-manipulator control schemes.

In a vision feedback system, precise positioning can be obtained by calculating differential changes between the actual and desired position and orientation of the end effector as seen by a camera, and then transforming these changes to the $T_6$ frame.

Some advanced servomanipulator control concepts involve restricting the motions of the slave to a specified plane. To control this sort of motion, the discrete changes in joint coordinates of the master must be transformed to changes in base frame coordinates. The components that would drive the slave outside the plane are then filtered out of the drive signal. In addition, these same components are fed into the master drive so that the operator can feel that he is attempting to move outside the plane.

"Inverting" the Jacobian

Most applications of the Jacobian matrices give rise to a desire to have a solution to the inverse problem. That is, given the desired

changes in $T_6$ or base coordinates, what are the required changes in the joint coordinates?

For simpler manipulators, a direct symbolic inversion may be possible. Model SM-229, however, is complex enough to baffle this author. The approach followed here* is to differentiate the solutions to the reverse kinematic problem. This gives expressions for each differential change in joint coordinates as a function of differential changes in the elements of $dT_6$ and also of differential joint coordinates already obtained. If a calculated change is not possible due to the limit constraints, the change may be set to zero, resulting in a correct solution for the following joints. If the manipulator becomes degenerate, one solution will tend to blow up. If this occurs, the first degenerate differential change is set to zero. Recall Eq. (31):

$$d_3C_3 - d_4S_3 = \frac{p_x^2 + p_y^2 + p_z^2}{2d_2} - \frac{(d_2^2 + d_3^2 + d_4^2)}{2d_2}$$

Differentiating,

$$(-d_3S_3 - d_4C_3)d\theta_3 = \frac{p_x dp_x + p_y dp_y + p_z dp_z}{d_2}$$

and,

$$d\theta_3 = \frac{p_x dp_x + p_y dp_y + p_z dp_z}{d_2} \tag{81}$$

differentiating Eq. (25) results in

*R. P. Paul, Robot Manipulators, MIT Press, 1981.

$$(C_1p_x)d\theta_1 + S_1dp_x + (S_1p_y)d\theta_1 - C_1dp_y =$$

$$= (-S_3d_3)d\theta_3 - C_3d_4d\theta_3$$

or,

$$(C_1p_x + S_1p_y)d\theta_1 + S_1dp_x - C_1dp_y = -(S_3d_3 + C_3d_4)d\theta_3$$

$$d\theta_1 = \frac{C_1dp_y - S_1dp_x - (S_3d_3 + C_3d_4)d\theta_3}{C_1p_x + S_1p_y} \tag{82}$$

From Eq. (24),

$$dp_z = C_2d\theta_2(C_3d_4 + S_3d_3) + S_2(-S_3d_4 + C_3d_3)d\theta_3$$

$$d\theta_2 = \frac{dp_z + S_2(S_3d_4 - C_3d_3)d\theta_3}{C_2(C_3d_4 + S_3d_3)} \tag{83}$$

Note that this would yield inaccuracies when $\theta_2 \to \pm \pi/_2$, but joint limit restraints prevent this configuration. Inaccuracies also occur when $\tan \theta_3 \to -d_4/d_3$, or $\theta_3 \to -84.6°$. Physically, this corresponds to the wrist pivot point lining up with the upper arm (shoulder roll, $\theta_2$) axis, so that the shoulder roll has no effect on the wrist position. If this occurs, $d\theta_2$ can be set to zero.

From Eq. (36),

$$NS_4 = S_4C_5 = -C_1S_2o_x - S_1S_2o_y + C_2o_z$$

$$NC_4 = C_4C_5 = (-C_1C_2S_3 - S_1C_3)\ o_x + (-S_1C_2S_3 + C_1C_3)\ o_y - S_2S_3o_z$$

$$d\theta_4 = \frac{C_4d(NS_4) - S_4d(NC_4)}{N}\ ,\ N = C_5 \neq 0$$

$$d(NS_4) = (S_1S_2o_x)d\theta_1 - (C_1C_2o_x)d\theta_2 - (C_1S_2)do_x - (C_1S_2o_y)d\theta_1$$
$$-S_1S_2o_y)d\theta_2 - (S_1S_2)do_y - -(S_2o_z)d\theta_2 + C_2do_z$$

$$d(NS_4) = (S_1S_2o_x - C_1S_2o_y)d\theta_1 - (C_1C_2o_x + S_1C_2o_y + S_2o_z)d\theta_2$$
$$- C_1S_2do_x - S_1S_2do_y + C_2do_z$$

let $NC_4 - (D)o_x + (E)\ o_y + (F)o_z$

where

$$D = -C_1C_2S_3 - S_1C_3$$

$$dD = (S_1C_2S_3 - C_1C_3)d\theta_1 + (C_1S_2S_3)d\theta_2 + (S_1S_3 - C_1C_2C_3)d\theta_3$$

$$E = -S_1C_2S_3 + C_1C_3$$

$$dE = (-C_1C_2S_3 - S_1C_3)d\theta_1 + (S_1S_2S_3)d\theta_2 + (-S_1C_2C_3 - C_1S_3)d\theta_3$$

$$F = -S_2S_3$$

$$dF = -C_2S_3d\theta_2 - S_2C_3d\theta_3$$

thus,

$$d(NC_4) = (dD)o_x + (D)do_x + (dE)o_y + (E)do_y + (dF)o_z + (F)do_z$$

and

$$d\theta_4 = \frac{C_4 d(NS_4) - S_4 d(NC_4)}{C_5} \tag{84}$$

Note that $d\theta_4$ blows up when $\theta_5 \rightarrow \pm \pi/_2$. This represents the degeneracy of the manipulator in this configuration. $\theta = -\pi/_2$ is impossible, so if

$$\theta_5 \approx \pi/_2, \text{ set } d\theta_4 = 0$$

from Eq. (39),

$$S_5 = [C_4(D) + G]o_x + [C_4(E) + H]o_y + (I)o_z$$

$$d(S_5) = [-S_4(D)d\theta_4 + C_4(dD) + dG]o_x + [C_4(D) + G]do_x + [-S_4(E)d\theta_4 +$$

$$C_4[(dE) + dH]o_y + [C_4(E) + H]do_y + (dI)o_z + (I)do_z$$

where

$$G = -S_1C_2S_4$$

$$dG = (-C_1C_2S_4)d\theta_1 + (S_1S_2S_4)d\theta_2 + (-S_1C_2C_4)d\theta_4$$

$$H = -S_1S_2S_4$$

$$dH = (-C_1S_2S_4)d\theta_1 + (-S_1C_2S_4)d\theta_2 + (-S_1S_2C_4)d\theta_4$$

$$I = C_2S_4 - S_2C_3C_4$$

$$dI = (-S_2S_4 - C_2C_3C_4)d\theta_2 + (S_2S_3C_4)d\theta_3 + (C_2C_4 + S_2C_3C_4)d\theta_4$$

and

$$C_5 = (K)o_x + (L)o_y + (M)o_z$$

$$d(C_5) = (dK)o_x + Kdo_x + (dL)o_y + L(do_y) + (dM)o_z + Mdo_z$$

where

$$K = S_1S_3 - C_1C_2C_3$$

$$dK = (C_1S_3 + S_1C_2C_3)d\theta_1 + (C_1S_2C_3)d\theta_2 + (S_1C_3 + C_1C_2S_3)d\theta_3$$

$$L = -S_1C_2C_3 - C_1S_3$$

$$dL = (-C_1C_2C_3 + S_1S_3)d\theta_1 + (S_1S_2C_3)d\theta_2 + (S_1C_2S_3 - C_1C_3)d\theta_3$$

$$M = -S_2C_3$$

$$dM = -C_2C_3d\theta_2 + S_2S_3d\theta_3$$

$$d_{\theta^5} = C_5(dS_5) - S_5(dC_5) \tag{86}$$

from Eq. (41),

$$S_6 = \{(K)C_5 + [(-D)C_4 + N]S\}a_x +$$

$$+ \{(L)C_5 + [(-E)C_4 + P]S\}a_y +$$

$$+ (M)C_5 + [(-M)C_4 + Q]S\}a_z$$

where

$$N = C_1S_2S_4$$

$$dN = -S_1S_2S_5d\theta_1 + C_1C_2S_4d\theta_2 + C_1S_2C_4d\theta_4$$

$$P = S_1S_2S_4$$

$$dP = C_1S_2S_4d\theta_1 + S_1C_2S_4d\theta_2 + S_1S_2C_4d\theta_4$$

$$Q = -C_2S_4$$

$$dQ = S_2S_4d\theta_2 - C_2C_4d\theta_4$$

Let

$$R = (K)C_5 + [(-D)C_4 + N]S_5$$

$$S = (L)C_5 + [(-E)C_4 + P]S_5$$

and

$$T = (M)C_5 + [(-M)C_4 + Q]S_5$$

$$dR = (dK)C_5 - KS_5d\theta_5 + [(-dD)C_4 + (D)S_4d\theta_4 + dN]S_5 + \\ + [(-D)C_4 + N]C_5d\theta_5\}$$

$$dS = (dL)C_5 - (L)S_5d\theta_5 + [(-dE)C_4 + (E)S_4d\theta_4 + dP]S_5 + \\ [(-E)C_4 + P]C_5d\theta_5\}$$

$$dT = dMC_5 - MS_5d\theta_5 + [(-dM)C_4 + (M)S_4d\theta_4 + dQ]S_5 \\ + [(-M)C_4 + Q]C_5d\theta_5$$

Then

$$S_6 = (R)a_x + (S)a_y + (T)a_z$$

and

$$dS_6 = (dR)a_x + R(da_x) + (dS)a_y + S(da_y) + (dT)a_z + T(da_z)$$

$$C_6 = [(-D)S_4 + (U)]a_x + [(-E)S_4 + (V)]a_y + [(-F)S_4 + (W)]a_z$$

where

$$U = -C_1S_2C_4$$
$$dU = (C_1S_2C_4)d\theta_1 - (C_1C_2C_4)d\theta_2 + (C_1S_2S_4)d\theta_4$$
$$V = -S_1S_2C_4$$
$$dV = (-C_1S_2C_4)d\theta_1 - (S_1C_2C_4)d\theta_2 + (S_1S_2S_4)d\theta_4$$
$$W = C_2C_4$$
$$dW = -S_2C_4d\theta_2 - C_2S_4d\theta_4$$

Let

$$X = [(-D)S_4 + U]$$
$$Y = (-E)S_4 + V$$
$$Z = (-F)S_4 + W$$

then,

$$dX = (-dD)S_4 - (D)C_4d\theta_4 + dU$$
$$dY = (-dE)S_4 - (E)C_4d\theta_4 + dV$$
$$dZ = (-dF)S_4 - (F)C_4d\theta_4 + dW$$

then

$$C_6 = Xa_x + Ya_y + Za_z$$

and

$$dC_6 = (dX)a_x + X(da_x) + (dY)a_y + Y(da_y) + (dZ)a_z + Z(da_z)$$

and

$$d\theta_6 = C_6(dS_6) - S_6(dC_6) \tag{87}$$

## Static Joint Torque Distribution

The general relationship between joint torques and tong static loads will now be derived. These results will be used with the experimental results to evaluate the manipulator load-sharing capabilities and gear reductions.

### Load given in the E-frame

E = end effector (tong) matrix = Trans $(0, -d_6, 0)$
Here the differential coordinate transform that relates forces and torques in the given frame to forces and torques in the $T_6$ frame is simply

$E^{-1}$. So, for

$$^{E}F = \begin{bmatrix} ^{E}f_x & ^{E}f_y & ^{E}f_z & ^{E}M_x & ^{E}M_y & ^{E}M_z \end{bmatrix}^T$$

$$^{T}6f_x = n \cdot f = {}^{E}f_x \tag{88}$$

$$^{T}6f_y = o \cdot f = {}^{E}f_y \tag{89}$$

$$^{T}6f_z = a \cdot f = {}^{E}f_z \tag{90}$$

$$^{E}f \times p = \begin{vmatrix} i & j & k \\ ^{E}f_x & ^{E}f_y & ^{E}f_z \\ 0 & d_6 & 0 \end{vmatrix} = -d_6 \, ^{E}f_z \, i + d_6 \, ^{E}f_x \, k \tag{91}$$

$$^{T}6m_x = n \cdot \left( (^{E} f \times p) + {}^{E}M \right) = {}^{E}m_x - d_6 \, ^{E}f_z \tag{92}$$

$$^{T}6m_y = o \cdot \left(\left(^{E}f \times p\right) + {}^{E}M\right) = {}^{E}m_y \tag{93}$$

$$^{T}6m_z = a \cdot \left(\left(^{E}f \times p\right) + + {}^{E}M\right) = {}^{E}m_z + d_6 {}^{E}f_x \tag{94}$$

where n, o, a, and p are the vectors of the different coordinate transform,

$$E^{-1} = \begin{bmatrix} 1 & 0 & 0 & 0 \\ 0 & 1 & 0 & d_6 \\ 0 & 0 & 1 & 0 \\ 0 & 0 & 0 & 1 \end{bmatrix}$$

So,

$$^{T}6F = \left[{}^{E}f_x \quad {}^{E}f_y \quad {}^{E}f_z \quad \left({}^{E}m_x - d_6 \, {}^{E}f_z\right) \quad {}^{E}m_y \quad \left(d_6 \, {}^{E}f_x + {}^{E}m_z\right)\right] \tag{95}$$

The joint torques required to support this load (static) are given by

$$\tau = J^T \, {}^{T}6F \tag{96}$$

where $J^T$ = the $T_6$ Jacobian transposed.

<u>Load and moments given in base frame</u>. More commonly, loads are given in the manipulator base frame.

Let $X = T_6 E$

Define a coordinate frame G,

$$G = \begin{bmatrix} 1 & 0 & 0 & Xp_x \\ 0 & 1 & 0 & Xp_y \\ 0 & 0 & 1 & Xp_z \\ 0 & 0 & 0 & 1 \end{bmatrix} \tag{97}$$

That is, G is located at the end effector, with the orientation of the base coordinates. The general base coordinate load vector is then

$$^{G}F = [f_x \quad f_y \quad f_z \quad M_x \quad M_y \quad M_z]^T \tag{98}$$

Define a transform Y by

$$GY = X, \text{ or}$$

$$Y = G^{-1}X \tag{99}$$

Note that Y has no translation because G and X are defined to describe the same translation, and the orientation of Y is exactly the orientation of the $T_6$ frame.

$$Y = \begin{bmatrix} x_{n_x} & x_{o_x} & x_{a_x} & 0 \\ x_{n_y} & x_{o_y} & x_{z_y} & 0 \\ x_{n_z} & x_{o_z} & x_{a_z} & 0 \\ 0 & 0 & 0 & 1 \end{bmatrix} \tag{100}$$

$$YE^{-1} = \begin{bmatrix} x_{n_x} & x_{o_x} & x_{a_x} & x_{o_x} d_6 \\ x_{n_y} & x_{o_y} & x_{a_y} & x_{o_y} d_6 \\ x_{n_z} & x_{o_z} & x_{a_z} & x_{o_z} d_6 \\ 0 & 0 & 0 & 1 \end{bmatrix} \tag{101}$$

The base coordinate load vector can now be transformed to $^{T}6F$ by using $YE^{-1}$ as the differential coordinate transform.

$$f \times p = [d_6 (-{}^{x}o_y f_z + {}^{x}o_z f_y)] i + [d_6 ({}^{x}o_z f_x + {}^{x}o_x f_z)]j \quad (102)$$
$$+ d_6(-{}^{x}o_x f_y + {}^{x}o_y f_x) k$$

So,

$$T_{6m_x} = {}^{x}n_x (M_1) + {}^{x}n_y (M_2) + {}^{x}n_z(M_3) \quad (103)$$

where

$$M_1 = d_6(-{}^{x}o_y f_z + {}^{x}o_z f_y) + m_x$$

$$M_2 = d_6(-{}^{x}o_z f_x + {}^{x}o_x f_z) + m_y$$

$$M_3 = d_6(-{}^{x}o_x f_y + {}^{x}o_y f_x) + m_z$$

Similarly,

$$T_{6m_y} = {}^{x}o_x (M_1) + {}^{x}o_y (M_2) + {}^{x}o_z (M_3) \quad (104)$$

$$T_{6m_z} = {}^{x}a_x (M_1) + {}^{x}a_y (M_2) + {}^{x}a_z (M_3) \quad (105)$$

$$T_{6f_x} = {}^{x}n_x f_x + {}^{x}n_y f_y + {}^{x}n_z f_z \quad (106)$$

$$T_{6f_y} = {}^{x}o_x f_x + {}^{x}o_y f_y + {}^{x}o_z f_z \quad (107)$$

$$^{T}6f_z = {}^{x}a_x\, f_x + {}^{x}a_y\, f_y + {}^{x}a_z\, f_z \tag{108}$$

and

$$^{T}6F = \left[ {}^{T}6f_x \quad {}^{T}6f_y \quad {}^{T}6f_z \quad {}^{T}6M_x \quad {}^{T}6M_y \quad {}^{T}6M_z \right]^{T} \tag{109}$$

The joint torque distribution is given by Eq. (96),

$$\tau = J^T\, {}^{T}6F$$

where $J^T = T_6$ Jacobian transposed.

In the case of gravity loading,

$$f_x = \text{weight}$$

$$f_y = f_z = M_x = M_y = M_z = 0$$

[Object assumed to be held at center of gravity (c.g.)]

$$^{x}n_x = {}^{0}T^{6}_{11}$$

$$^{x}n_y = {}^{0}T^{6}_{21}$$

$$^{x}n_z = {}^{0}T^{6}_{31}$$

$$^{x}o_x = {}^{0}T^{6}_{12}$$

$$^{x}o_{y} = {}^{0}T^{6}_{22}$$

$$^{x}o_{z} = {}^{0}T^{6}_{32}$$

$$^{x}a_{x} = {}^{0}T^{6}_{13}$$

$$^{x}a_{y} = {}^{0}T^{6}_{23}$$

$$^{x}a_{z} = {}^{0}T^{6}_{33}$$

<u>Gravity Load on Tong</u>. Assume that the object is picked up at its c.g., then

$$F = [1 \quad 0 \quad 0 \quad 0 \quad 0 \quad 0]^{T} \tag{110}$$

for a normalized load, and

$$^{T}6f_{x} = {}^{x}n_{x} = {}^{0}T^{6}_{11}$$
$$^{T}6f_{y} = {}^{x}o_{x} = {}^{0}T^{6}_{12}$$
$$^{T}6f_{z} = {}^{x}a_{x} = {}^{0}T^{6}_{13}$$

$$^{T}6m_{x} = (-{}^{0}T^{6}_{21} \; {}^{0}T^{6}_{32} + {}^{0}T^{6}_{31} \; {}^{0}T^{6}_{22}6) \; d_{6}$$

$$^{T}6m_{y} = 0$$

$$^{T}6m_{z} = (-{}^{0}T^{6}_{23}\ {}^{0}T^{6}_{32} + {}^{0}T^{6}_{33}\ {}^{0}T^{6}_{22}6)\ d_{6}$$

Note: If an object is not held at its c.g., but is held such that its c.g. lies along the wrist roll axis, simply add to $d_6$ in the above equations the distance from the tong to the c.g.

<u>Forward (horizontal) Load on Tong</u>. In this case,

$$f_x = f_z = m_x = m_y = m_z = o$$

and

$$f_y = 1\ .$$

So,

$$^{T}6f_{x} = {}^{T}6n_{y} = T^{6}_{21}$$

$$^{T}6f_{y} = {}^{T}6o_{y} = T^{6}_{22}$$

$$^{T}6f_{z} = {}^{T}6a_{y} = T^{6}_{23}$$

$$^{T}6m_{x} = d_{6}\ (T_{32}{}^{6}\ T_{11}{}^{6} - T_{31}{}^{6}\ T_{12}{}^{6})$$

$$^{T}6m_{y} = 0$$

$$^{T}6m_{z} = d_{6}\ (+\ T^{6}_{13}\ \ T^{6}_{32} - T^{6}_{33}\ \ T^{6}_{12})$$

<u>Transverse (horizontal) Load on Tong</u>. Here,

$$f_x = F_y = m_x = m_y = m_z = 0$$

$$f_z = 1,$$

so,

$$T_{6f_x} = T_{31}^{6}$$

$$T_{6f_y} = T_{32}^{6}$$

$$T_{6f_z} = T_{33}^{6}$$

$$T_{6m_x} = d_6 \, (T_{21}^{6} \; T_{12}^{6} - T_{11}^{6} \; T_{22}^{6})$$

$$T_{6m_y} = 0$$

$$T_{6m_z} = d_6 \, (T_{23}^{6} \; T_{12}^{6} - T_{13}^{6} \; T_{22}^{6})$$

ORNL/TM-9655
Distribution Category UC-86

INTERNAL DISTRIBUTION

1. S. M. Babcock
2. R. R. Bentz
3. J. O. Blomeke
4. E. C. Bradley
5. W. D. Burch
6. T. W. Burgess
7. J. Y. Chang
8. B. G. Eads
9. M. J. Feldman
10. N. R. Grant
11. W. S. Groenier
12. W. R. Hamel
13. D. C. Hampson
14. A. L. Harkey
15. J. N. Herndon
16. H. T. Kerr
17. S. M. Killough
18. D. P. Kuban
19. D. MacDonald
20. H. L. Martin
21. S. A. Meacham
22. F. R. Mynatt
23. J. E. Richardson
24. M. J. Rohr
25. S. L. Schrock
26. R. S. Stoughton
27. J. G. Stradley
28. B. S. Weil
29. C. R. Weisbin
30. R. S. Wiltshire
31. O. O. Yarbro
32. M. J. Kopp (Advisor)
33. P. F. McCrea (Advisor)
34. P. W. Murrill (Advisor)
35. H. M. Paynter (Advisor)
36. H. E. Trammell (Advisor)
37. Manson Benedict (Consultant)
38-39. Central Research Laboratory
40. ORNL Y-12 Technical Library
41-42. Laboratory Records
43. Laboratory Records, ORNL-RC
44. ORNL Patent Section
45. I&C Publications Office

EXTERNAL DISTRIBUTION

46. Office of Assistance Manager for Energy Research and Development, DOE-ORO, Oak Ridge, TN 37831
47. D. E. Bailey, Director, Division of Fuels and Reprocessing, U.S. Department of Energy, Washington, DC 20545
48. F. P. Baranowski, 1110 Dapple Grey Court, Great Falls, VA 22066
49. S. J. Beard, Vice President, Marketing and Uranium Operations, Exxon Nuclear Company, Inc., 600 108th Avenue, N.E., C-00777, Bellevue, WA 98009
50. Joe Byrd, Savannah River Plant, Aiken, SC 29808-0001
51. D. Grishom, Los Alamos National Laboratory, Post Office Box 1663, Los Alamos, NM 87545
52. J. Draper, Clark-Ambrose, Bldg. 7601, X-10
53. R. Little, Princeton Plasma Physics Laboratory, James Forrestal Campus, P.O. Box 451, Princeton, NJ 08544
54. J. L. McElroy, Pacific Northwest Laboratories, P.O. Box 999, Richland, WA 99352
55. M. J. Ohanian, Associate Dean for Research, College of Engineering, 300 Weil Hall, Univeristy of Florida, Gainesville, FL 32611
56. J. F. Proctor, Senior Technical Specialist, E. I. du Pont de Nemours and Company, Savannah River Laboratory, Aiken, SC 29801

57-158. Given distribution as shown in TIC-4500 under Category UC-86, Consolidated Fuel Reprocessing (Base Technology)